NISTIR 6470

Comparison of FPETool: FIRE SIMULATOR With Data From Full Scale Experiments

Robert L. Vettori
Daniel Madrzykowski

Prepared for:
U. S. General Services Administration
Public Buildings Service

NIST
National Institute of Standards and Technology
Technology Administration, U.S. Department of Commerce

NISTIR 6470

Comparison of FPETool: FIRE SIMULATOR With Data From Full Scale Experiments

Robert L. Vettori
Daniel Madrzykowski
Building and Fire Research Laboratory
National Institute of Standards and Technology
Gaithersburg, MD 20899-8641

February 2000

Prepared for:

U.S. General Services Administration
David J. Barram, Administrator

Public Buildings Service
Robert A. Peck, Commissioner

U.S. Department of Commerce
William M. Daley, Secretary

Technology Administration
Dr. Cheryl L. Shavers, Under Secretary of Commerce for Technology

National Institute of Standards and Technology
Raymond G. Kammer, Director

Table of Contents

LIST OF TABLES

LIST OF FIGURES

Comparison of FPETool: FIRE SIMULATOR With Data From Full Scale Experiments

Robert L. Vettori
Daniel Madrzykowski

ABSTRACT

A comparison of the compartment zone fire model FPETool: FIRE SIMULATOR is made with data from three different full scale experimental compartment fire studies. These three studies represent a variation of room geometry, ventilation factors, thermal physical properties, fuels, fire geometry and fire growth. Depending on the experimental data presented, comparisons were made for the following parameters, ceiling jet velocity, ceiling jet temperature, upper layer temperature, upper layer depth, detector link temperature, time to sprinkler activation, and heat release rate at time of sprinkler activation. Results for predicted sprinkler activation times ranged from 74% to 159% of measured times depending on the RTI chosen for the sprinkler, characteristics of the fire, and fire growth rate. All predicted ceiling jet velocities differed by approximately a factor of two from measured values. Generally, upper layer depth predictions were good only for situations where there was not a large vent from the room. For the full scale experiment conducted in a large room with a high ceiling, predicted link and ceiling jet temperatures had better agreement with measured values if consideration was given to the time required for the transport of the products of combustion from the fire to the link. For experiments which had varying fire growth rates predictions for upper layer temperature increase were better for experiments with the slower fire growth rates.

Key Words: ceiling jets; computer models; fire growth; layer heights; quick response sprinklers; residential sprinkler; sprinklers; sprinkler response; wall fires; zone models;

1.0 INTRODUCTION

Zone fire models are being used to assist in both the design of fire protection systems and in the reconstruction of fires [1-5].[1] The capability to predict the effects of a fire on the environment within a compartment is an important element for fire protection system and life safety analyses. In addition, the ability to predict the activation times of smoke detectors, sprinklers, or other thermal detectors is important since these devices are used to warn occupants of a potential fire, initiate suppression, and summon outside help. For the accident investigator, this capability could assist in the understanding of factors that produce hazardous conditions and to devise ways to mitigate their effects in the future. This paper discusses the performance of the compartment zone fire model FPETool: FIRE SIMULATOR version 3.2 [6,7], henceforth referred to in this paper as FPETool, against experimental data obtained from three different full scale compartment fire test series.

FPETool is a single room, two zone model simulating the effects of pre and post flashover fires within the fire compartment and characterizes the effluent (energy, gases, and fuel) that leave the fire compartment. FPETool is based on the compartment filling model developed by Zukoski [8]. Zukoski developed an analytical model to determine the time required to fill a room with products of combustion from a small fire. The room is assumed to be closed except for small openings at either the floor or ceiling level. The leaks through these openings are assumed to be just large enough so that any pressure change within the room can be neglected. The products of combustion are assumed to occupy an upper layer next to the ceiling and Zukoski's model also predicts the growth or thickness of this upper layer as a function of time.

1.1 Fire Plume Algorithm

FPETool assumes an axisymmetrical or unconfined plume. The plume is considered a point source and is able to entrain air along its entire perimeter. There is no effect on this free entrainment of air by walls or other objects. The relationships for air entrainment into the fire plume used by FPETool were developed by Heskestad [11]. Heskestad's relationships deal with axisymmetric, turbulent fire plumes in which the environment is uncontaminated by fire products and is uniform in temperature. The upward buoyant gas stream of the plume is considered turbulent, except when the source is very small and smoldering. Once an upper layer has formed within the compartment, Heskestad's relationships cease to be valid beyond the elevation where the plume enters this upper layer.

Two predictive relations are used by FPETool for plume entrainment. The first considers an area extending above a limiting elevation within the plume, the second, the area within the plume that is below this limiting elevation. This limiting elevation Z_l , is defined as the elevation within the plume where the mean center line temperature increase ΔT = 500 °C (900 °F). For normal atmospheric conditions, the limiting elevation can be expressed as [11]:

$$z_l = z_o + 0.166\dot{Q}_c^{2/5} \qquad (1)$$

[1]Number in brackets indicate literature references at the end of the paper.

where: z_l = height above the top of combustible where ΔT = 500 °C
z_o = height of virtual origin above or below the top of combustible (m)
$\dot{Q}_c$ = convective heat release rate into the plume (kW)

The virtual origin, z_o in the above equation, is a computational tool rather than a physical one. Since the derivations for the plume relationships assume that the plume is rising from a point source, a correction needs to be made to the real source of the plume. This is done by identifying a virtual origin for the plume. The location of this virtual origin is such that a plume originating from this point source will have identical entrainment characteristics as the real source. The virtual origin can be located above or below the actual surface of the fire. For normal atmospheric conditions and fire sources that do not have substantial in-depth combustion, the prediction for the virtual origin of a fire plume is [12]:

$$z_o = -1.02D + 0.083\dot{Q}^{2/5} \qquad (2)$$

where: D = effective diameter of the fire source (m)
$\dot{Q}$ = total heat release rate of the fire source (kW)

FPETool uses the following method to calculate the effective diameter of the fire source.

$$D = 2\left(\frac{\dot{m}_f}{\dot{m}_f'' \pi}\right)^{1/2} \qquad (3)$$

where: D = the effective diameter of the fire source (m)
$\dot{m}_f$ = mass burning rate (kg/s)
$\dot{m}_f''$ = mass burning rate per unit area (kg/s m^2). FPETool has set this as a default rate based on the mass burning rate of wood needed to produce 1135 kW/m^2.

The limiting elevation z_l, in Eq. 1, closely corresponds to the median visible flame height of the fire. The median flame height is the location above the fire source where the flame is present 50 % of the time. Therefore, it can be seen that the two entrainment relationships used are divided into elevations above the flaming region of the plume and elevations within the flaming region of the plume.

For elevations within the plume that are greater than or equal to z_l or elevations of the plume above the flaming region, the prediction for mass flow rate in the plume is:

$$\dot{m} = 0.071\dot{Q}_c^{1/3}(z - z_o)^{5/3}[1 + 0.026\dot{Q}_c^{2/3}(z - z_o)^{-5/3}] \qquad (4)$$

where: $\dot{m}$ = mass of air entrained (kg/s)
$\dot{Q}_c$ = convective heat release rate into the plume (kW)
z = distance from the top of combustible to bottom of smoke layer (m)

z_o = height of virtual origin above or below the top of combustible (m)

For elevations within the plume less than z_l or what would be considered the flaming region, the mass flow rate in the plume is:

$$\dot{m} = 0.0054\dot{Q}_c \frac{z}{0.166\dot{Q}_c^{2/5} + z_o} \qquad (5)$$

Equation 5 is limited to pool fires or horizontal surface fires. The relationship becomes inaccurate for fire sources with substantial in-depth combustion such as well ventilated wood crib and wood pallet fires, fires involving high storage, and vertical wall or corner fires [11]. A fire with substantial in-depth combustion may have a large portion, greater than 33%, of the volatiles undergoing combustion within or internally of the fuel array by air entering the array [13]. Equation 4 is not limited with respect to the fire source. However, predicting the location of the virtual origin z_o used in Eq. 4, is itself limited to fire sources that do not have substantial in-depth combustion.

1.2 Ceiling Jet Algorithm

The time to sprinkler activation algorithm used in FPETool is based on the sprinkler activation model DETACT-QS developed by Evans and Stroup [14]. DETACT-QS calculates the thermal response of a thermal element located at the ceiling in which the ceiling area is large enough to neglect the effects of smoke layer development. Therefore any heating of the thermal element will be based only on the temperature and velocity of the ceiling jet. No account is made for the effects of a warm gas layer. This methodology may be applied to large spaces such as industrial buildings or for short times after fire ignition when enclosure effects are negligible. The correlations used by DETACT-QS for ceiling jet temperatures and velocities were developed by Alpert [15]. Alpert's correlations assume that the fire is under a smooth, horizontal, unconfined ceiling, and that the fire plume entrains air which is at ambient temperature. The correlations for the maximum temperature of the ceiling jet are divided into two regions.

$$T_{\max} - T_o = \frac{16.9\ \dot{Q}^{2/3}}{H^{5/3}} \quad for \quad \frac{r}{H} \le 0.18 \qquad (7)$$

$$T_{\max} - T_o = \frac{5.38\ (\frac{\dot{Q}}{r})^{2/3}}{H} \quad for \quad \frac{r}{H} > 0.18 \qquad (8)$$

where: $T_{\max}$ = maximum gas temperature in the ceiling jet °C

T_o = initial gas temperature °C

$\dot{Q}$ = total heat release rate of the fire source (kW)

H = distance from the top of the combustible to the ceiling (m)

r = radial distance of the thermal element from the vertical axis of the fire (m)

The correlations for maximum velocity of the ceiling jet are also divided into two regions.

$$v = 0.946 \left(\frac{\dot{Q}}{H}\right)^{1/3} \quad for \quad \frac{r}{H} \leq 0.15 \qquad (9)$$

$$v = \frac{0.195\ \dot{Q}^{1/3}\ H^{1/2}}{r^{5/6}} \quad for \quad \frac{r}{H} > 0.15 \qquad (10)$$

Where: v = maximum gas velocity in the ceiling jet (m/s)

Equations 7 and 9 are independent of radius and are axial plume flow temperatures and velocities calculated at the ceiling height above the fire source. Equations 8 and 10 apply to the region outside of the plume as the flow moves away from the impingement area.

Alpert found that for smooth horizontal ceilings when there is only negligible accumulation of stagnant hot gases underneath, that the maximum gas temperature within the ceiling jet occurs a distance below the ceiling of no more than 1 percent of the distance between the uppermost burning fuel surface and the ceiling. [15] The temperature of the ceiling jet approaches room temperature at 5.5 to 12.5 percent of the fire to ceiling height. The maximum ceiling jet velocity is also found quite close to the ceiling, and the ceiling jet velocity approaches zero at approximately the same distance below the ceiling where the gas temperature approaches room temperature. [15]

In compartment sizes characteristic of office and living spaces, a warm upper layer of gas may accumulate rapidly after ignition. As a warm upper layer develops the fire plume no longer entrains air only from the cool lower layer, but includes warm upper layer entrained gases. In FPETool the sprinkler activation algorithm includes what the effect of entraining these warm upper layer gases has on the ceiling jet temperatures and velocities. The implementation of this warm upper layer gas entrainment algorithm begins when the thickness of the warm upper layer exceeds that of the ceiling jet. Using the correlations that Alpert developed, the thickness of the fully developed ceiling jet considered in FPETool is [16]:

$$0.12\ (H) \qquad (11)$$

where: H = distance from the top of the combustible to the ceiling (m)

In a room fire in which a warm upper gas layer has accumulated above the lower ambient gas forming a two layer environment, the weakly buoyant point source plume flow calculations are just as applicable in the lower layer containing the fire as in a totally uniform ambient environment. However, adjustments are needed to describe the plume flow after penetration into the upper layer. A method developed by Evans [17] is used in FPETool to take into account the effects of entrainment

of the warm upper layer gases. This plume continuation method relates plume flow in a two layer environment to an equivalent flow in a single layer environment at the temperature of the warm upper layer. The adjustments made consist of changing the fire source heat release rate and location of the fire source a distance below the ceiling. The substitute source location and heat release rate are calculated by preserving across the interface between the cool lower and warm upper layers the maximum temperature in the plume and the excess enthalpy flux. Preserving velocity and closely associated plume mass and momentum fluxes are not considered as important as preserving excess temperature and excess energy flux in calculating sprinkler activation times, because thermal detectors primarily respond to temperature rise and not gas velocity [18]. In the equations presented below, the subscripts 1 and 2 will be used to indicate quantities related to the original source and the second or pseudo source respectively. The dimensionless heat release rate of the fire source is evaluated at the interface between the upper and lower layer:

$$\dot{Q}^{*}_{I,1} = \frac{\dot{Q}_{1c}}{[\rho_{\infty} C_{p\infty} T_{\infty} g^{1/2} Z^{5/2}_{I,1}]} \qquad (12)$$

where:
- $\dot{Q}_{1c}$ = convective heat release rate of the fire (kW)
- ρ_{∞} = density of air at ambient temperature (kg/m^3)
- $C_{p\infty}$ = specific heat of air at ambient temperature (kJ/kg°K)
- T_{∞} = ambient temperature of 293 °K
- g = gravitational acceleration (m/s^2)
- $Z_{I,1}$ = height of the layer interface from the top of combustible (m)

The dimensionless heat release rate for the second or pseudo source is:

$$Q^{*}_{I,2} = [(1 + C_T Q^{*2/3}_{I,1})/\xi C_T - 1/C_T]^{3/2} \qquad (13)$$

where:
- C_T = 9.115 [19]
- ξ = ratio of the upper layer temperature to lower layer temperature

The position of the second or pseudo fire source relative to the interface is:

$$Z_{I,2} = [\frac{\xi \dot{Q}^{*}_{I,1} \; C_T}{Q^{*1/3}_{I,2}[(\xi - 1)(\beta^2 + 1) + \xi C_T Q^{*2/3}_{I,2}]}]^{2/5} Z_{I,1} \qquad (14)$$

where:
- β = 0.913 [20]

The dimensional heat release rate is

$$\dot{Q}_{2c} = Q^{*}_{I,2} \; \rho_{\infty,2} \; C_{p\infty} \; T_{\infty,2} \; g^{1/2} \; Z^{5/2}_{I,2} \qquad (16)$$

where: $\dot{Q}_{2c}$ = convective heat release rate of the pseudo fire source (kW)
$\rho_{\infty,2}$ = density of the warm upper layer gas (kg/m^3)
$T_{\infty,2}$ = temperature of warm upper layer gas (°K)

and the position relative to the ceiling is

$$H_2 = H_1 - Z_{I,1} + Z_{I,2} \qquad (17)$$

where: H_2 = height above the pseudo source to the ceiling
H_1 = height above the original source to the ceiling

The values Q_{2c} and H_2 replace Q_{1c} and H_1 in Alpert's algorithm. The result of adding this warm air entrainment algorithm is the prediction of higher ceiling jet temperatures and faster ceiling jet velocities.

FPETool assumes that the detector, smoke or thermal, is located such that it is exposed to both the maximum ceiling jet temperature and ceiling jet velocity.

1.3 Heat Release Rate

For all three experimental series, the heat release rate of the fuel packages was determined by using the principle of oxygen consumption calorimetry [21,22]. The oxygen consumption technique for measuring the rate of heat release is predicated upon the capture of all the combustion gases through a duct where the mass flow rate and oxygen concentration are measured as a function of time. From these measurements, the rate at which oxygen is consumed by the fire in the combustion process can be determined. For most common fuels, the rate of heat release per unit mass of oxygen is approximately (13.1 ± 0.66) MJ/kg of oxygen consumed [23]. In addition to the uncertainty inherent to this method, uncertainties in instrument measurements and fluctuations in the volume of exhaust gases through the duct need to be taken into account to determine the heat release rate measurement. Yeager [31] reports uncertainties from 5% to 60% depending of the flow rate of exhaust gases through the duct. However, he was able to establish an optimal uncertainty of ± 6% for fires with heat release rates as low as 71 kW when the mass flow through the duct was controlled at 2 m^3/s.

1.4 Sprinkler Activation Algorithm

An input required for the sprinkler activation algorithm in FPETool is the Response Time Index (RTI) of the sprinkler [24,25]. The RTI is a characterization of the detector's thermal inertia, a measure of how quickly the thermal element reaches its activation temperature. The smaller the RTI value the more thermally responsive the element is to changes in gas temperature. The model used to calculate the heating of a sprinkler bulb or link is based on several assumptions. First, the sprinkler element is heated purely by forced convection. Second, there are no conduction losses from the sprinkler element to the supporting structure. Finally, the sprinkler element heats uniformly. With these approximations, the heat balance on the sensing element is:

$$\frac{d\ (\Delta T_L)}{dt} = \tau^{-1}\ (\Delta T_g - \Delta T_L) \qquad (18)$$

where: ΔT_L = the excess temperature of the link above its initial temperature (°C)
ΔT_g = the excess temperature of the gas above the initial link temperature (°C)

and τ is a time constant related to the properties of the sensing element and the convective heating of the gas flow to which it is exposed according to:

$$\tau = \frac{m_L\ c_L}{h_c\ A_L} \qquad (19)$$

where: m_L = the mass of the sensing element (kg)
c_L = the specific heat of the sensing element (kJ/kg°K)
h_c = the convective heat transfer coefficient over the sensing element (kW/m^2 °K)
A_L = the area of the sensing element (m^2)

For a given sensing element, the time constant depends only on the convective heat transfer coefficient. Data on convective heating and cooling of objects similar to typical sensing elements show that for conditions expected in the fire environment that [24]

$$h_c \propto u^{1/2} \qquad (20)$$

where: u = velocity of gas flow (m/s)

Consequently the time constant of a given sensing element is proportional to $u^{1/2}$ or equivalently:

$$\tau u^{1/2} = constant \qquad (21)$$

This constant is the RTI of the sprinkler and has units (m-s)^{½} or (ft-s)^{½}. The RTI parameter is nearly constant for a given sprinkler, and together with the sprinkler's operating temperature, is sufficient for predicting sprinkler response for known gas temperatures and gas velocities near the sprinkler as long as conduction losses to the supporting structure are small compared with the convective heating rate.

1.5 Internal Energy Loss

The internal energy loss λ_c is a measure of the combined instantaneous fraction of the total heat release rate lost by the combustion zone, the plume gases, and the hot upper layer gases to the bounding surfaces of the room and its contents. [28] The total rate of energy loss which is characterized by λ_c occurs as a result of a variety of different convective and radiative heat transfer

exchanges between the room's gases and the above mentioned surfaces. Although λ_c is taken as a constant, it is in fact, a time varying parameter. However, in the early stages of a fire in a single room, the value of λ_c is relatively constant and in the range of 0.6 to 0.9. The lower value of 0.6 would relate to high aspect ratio spaces (ratio of ceiling span to room height) with smooth ceilings and with fires positioned far away from the walls. The 0.9 value for λ_c would relate to low aspect ratio spaces, and fire scenarios where the fire position is within a room height from the walls. For the simulations conducted in this paper a value of 0.9 was chosen for λ_c .

2.0 CHEMICAL LABORATORY EXPERIMENTS

The first experimental series modeled was conducted in chemical laboratories [26]. Four experiments were conducted to evaluate the performance of an automatic sprinkler system against a flammable liquid spill fire. A fifth experiment without sprinklers was also conducted. This series was modeled to compare predicted sprinkler activation times, upper layer depth, upper layer temperatures, and ceiling jet temperatures with measurements.

Each experiment was conducted in a different laboratory and the configuration of each laboratory was slightly different. All laboratories were constructed with concrete floors and ceilings with tile block walls. Each had a single open doorway, 2.1 m high x 0.91 m wide (6.9 ft x 3.0 ft) connecting the laboratory to the building corridor and a closed wooden double hung window connecting the laboratory to the outside. All laboratories were approximately 5.48 m (18 ft) deep, 3.2 m (10.5 ft) high, and varied in width between 3.2 m and 3.7 m (10.5 ft and 12 ft). A typical plan view of one of the chemical laboratories is shown in figure 1. The FPETool inputs for each of the five simulations is shown in table 1.

The fuel package consisted of a 134.3 kg (296 lb) steel laboratory bench with a stone laboratory bench top. Above the bench was a 24.0 kg (53 lb) open wooden shelving unit. On top of the laboratory bench and in the shelving unit were 50.8 kg (112 lb) of paper, files and other miscellaneous supplies. Four liters of acetone were used as the initial fuel ignited. Three liters were placed in a 0.76 m x 1.23 m (30 in x 48 in) steel pan on the floor and one liter in a 0.46 m x 0.61 m (18 in x 24 in) steel pan on the bench top. The heat release rate inputs for this fuel package are listed in table 2. A graph of this heat release curve is shown in figure 2.

Temperature measurements were taken with 0.05 mm (0.02 in) diameter chromel-alumel thermocouples. While the absolute uncertainty in thermocouple measurements as reported by the manufacturer is ± 2.2 °C (± 4.0 °F), at the start of an experiment, the thermocouples used in the analysis registered ambient temperature to within ± 3.0 °C (± 5.4 °F). The method used to determine either the start time of the experiment or the sprinkler actuation time were not mentioned. These timing uncertainties may be on the order of ± 1 s each.

Of the four experiments which utilized sprinklers, one utilized a standard upright sprinkler, two utilized quick response pendent sprinklers and one utilized a quick response sidewall sprinkler. In the original report for this experimental series, no RTI values were reported, only the sprinkler activation temperatures. For a standard fusible link sprinkler, the typical RTI values range from 193 $(m\text{-}s)^{½}$ to 331 $(m\text{-}s)^{½}$ (350 $(ft\text{-}s)^{½}$ to 600 $(ft\text{-}s)^{½}$), while for quick response sprinklers RTI values range

from 25 (m-s)^{½} to 55 (m-s)^{½} (45 (ft-s)^{½} to 100 (ft-s)^{½}). For this analysis several values of RTIs' were used for each experiment to determine the sensitivity of the simulation to this parameter.

Since the radiative fraction χ_R of acetone is 28% and that of some natural materials such as wood and paper in the range of 38% to 41% [27] the radiative fraction was approximated to be 35%.

2.1 Comparisons - Sprinkler Activation Times

The first experiment, table 3, utilized the standard upright sprinkler with an activation temperature of 74 °C (165 °F) located 0.61 m (1.5 ft) radially from the center of the floor pan, figure 3. The r/H value is 0.19 which places the sprinkler at the edge of the plume. The sprinkler deflectors were located 0.24 m (9.5 in) below the ceiling. A value of 250 (m-s)^{½} (452 (ft-s)^{½}) was originally chosen for the RTI of the sprinkler. The time to activation predicted by FPETool of 34 s is a difference of 5 s from the measured time of 39 s. Two additional simulations were performed one with a high and one with a low value for the RTI. This was done in order to bracket the response of the sprinkler to this environment as a function of the sprinkler RTI. By changing the RTI value to 300 (m-s)^{½} (544 (ft-s)^{½}), and leaving all other inputs the same, FPETool predicted an activation time of 37 s. For the low value, the RTI was chosen as 200 (m-s)^{½} (362 (ft-s)^{½}) and the predicted activation time was 32 s.

For both experiment 2 and experiment 3, table 4, a 71 °C (160 °F) quick response pendent sprinkler was utilized. In both experiments the sprinklers were located 0.61 m (1.5 ft) radially from the center of the floor pan, figure 3. As in the previous experiment this places them at the edge of the plume. In experiment 2 the sprinkler deflectors were located 0.28 m (11 in) below the ceiling, and in experiment 3 the sprinkler deflectors were located 0.33 m (13 in) below the ceiling. With the value of 40 (m-s)^{½} (75 (ft-s)^{½}) originally chosen for the RTI, FPETool predicted an activation time of 17 s. The reported times for experiments 2 and 3 were 16 s and 18 s respectively. Again, in order to bracket the response of the sprinkler to this environment as a function of the sprinkler RTI, a value of 25 (m-s)^{½} (45 (ft-s)^{½}) was used for the low RTI and a value of 55 (m-s)^{½} (100 (ft-s)^{½}) was used for the high RTI. The results were predicted activation times of 15 s and 19 s for experiment 2 and 14 s and 19 s for experiment 3.

Experiment 4, table 5, utilized a 71 °C (160 °F) quick response sidewall sprinkler located 3.66 m (12 ft) radially from the center of the floor pan, figure 4. The sprinkler deflectors was located 0.20 m (8 in) below the ceiling. Since the sprinkler algorithm used in FPETool assumes the sprinkler is positioned on a flat horizontal unobstructed ceiling, the effects of placing the sprinkler in a sidewall position is considered by assuming a reduction in the ceiling jet velocity. FPETool calculates what the ceiling jet velocity would be at the location of the sprinkler, as if it were placed on the ceiling, and then reduces it by a velocity reduction factor. The default value for FPETool is a 50% reduction in the ceiling jet velocity. There were no referenced papers in the FPETool technical reference manual indicating how the value of 50% was derived. Additionally, there were no papers found in the literature describing a method for the prediction of the activation time of a side wall sprinkler in the context of a zone model. No effect on the ceiling jet temperature is considered in the model. For the original RTI value of 40 (m-s)^{½} (72 (ft-s)^{½}) and a velocity reduction factor of 50%, FPETool

predicted a sprinkler activation time of 31 s compared to a measured time of 26 s. With a ceiling height of 3.2 m (10.5 ft), the thickness of the ceiling jet is approximately 0.38 m (15 in). Since the sprinkler is 0.20 m (8 in) below the ceiling it is still considered within the ceiling jet. By allowing the velocity reduction factor to be 0, which gives the same results as placing the sprinkler on the ceiling i.e., not in a sidewall position, the predicted activation time by FPETool is 27 s. By varying the RTI of the sprinkler along with the velocity reduction factor the predictions by FPETool can be bracketed for this environment as a function of both the RTI and velocity reduction factor.

2.2 Comparisons - Upper Layer Temperature and Upper Layer Depth

Data from experiment 5 was used to compare predicted with measured results for upper layer temperature and upper layer depth development. This experiment did not have sprinklers and the room was allowed to burn until manually extinguished. In the experimental set up a thermocouple array was placed in the corner of each burn room with thermocouples placed (48, 109, 170, 231, 292) cm ((19, 43, 67, 91,115) in) below the ceiling. In order to determine the depth of the layer based on the reported temperature data a method developed by Cooper et al [29] named the N Percent Rule is used. To use the N Percent Rule, at a specified time in the experiment, compute a reference upper layer temperature based on the maximum temperature change of the thermocouple at the highest elevation.

$$\Delta T_{ref}(t) = \max\left[T(z_{top}, t)\right] - T_{amb}(z_{top}) \qquad (29)$$

where: $\Delta T_{ref}(t)$ = referenced upper layer temperature at time t (°C)
$T(z_{top}, t)$ = temperature at top most thermocouple at time t (°C)
z_{top} = the elevation of the top most thermocouple (m)
$T_{amb}(z_{top})$ = ambient temperature at top most thermocouple at time 0 (°C)

Then by the N Percent rule, the interface is defined as passing the elevation $z_i(t)$ at that time t when z_i first satisfies

$$T(z_i, t) - T_{amb}(z_i) = \frac{N\ \Delta T_{ref}(t)}{100} \qquad (30)$$

where: $T(z_i, t)$ = temperature of thermocouple at elevation z_i at time t (°C)
$T_{amb}(z_i)$ = ambient temperature of thermocouple at elevation z_i (°C)

Cooper concluded that allowing N = 10 would provide a reasonable basis for an experimentally determined interface elevation history.

Temperatures for each thermocouple were obtained from the data files. A vertically averaged temperature increase $\overline{\Delta T}$ is estimated from

$$\overline{\Delta T}(t) = \frac{1}{H}\int_0^H [T(z,t) - T_{amb}(z)]\ dz \qquad (31)$$

$$\overline{\Delta T}(t) \approx \frac{1}{H}\sum_{n=1}^{x} [T(z_n,\ t) - T_{amb}(z_n)]\ \Delta z_n \qquad (32)$$

where: $\overline{\Delta T}(t)$ = vertically averaged temperature increase at time t (°C)
H = floor to ceiling height of the compartment (m)
$T(z_n,t)$ = temperature of the nth thermocouple in the array (°C)
$T_{amb}(z_n)$ = ambient temperature of the nth thermocouple in the array (°C)
Δz_n = the vertical zone of influence associated with this thermocouple (m)

By using the N Percent Rule, a determination was made as to which thermocouples were to be considered in the upper layer. Then each one was assigned a zone of influence depending on its vertical distance from the thermocouple above and below it. Comparisons of measured versus predicted upper layer temperature are presented in figure 5, and comparisons of measured versus predicted upper layer depth are presented in figure 6.

2.3 Comparisons - Heat Release Rate at Sprinkler Activation

Another comparison that can be made, and possibly more important since it may give a more detailed picture of the impact of the fire on the environment, is to compare the heat release rate of the fire at measured sprinkler activation to the heat release rate at predicted sprinkler activation. For rapidly growing fires such as these a relatively short time interval can translate into a significant increase of the heat release rate of the fire. Table 6 gives this comparison. Column two of table 6 is the measured heat release rate of the fire at sprinkler activation. Column three is the predicted range of heat release rates based on the RTI of the sprinkler used on the model.

2.4 Discussions and Conclusions

Predictions by FPETool for experiment number 1 of the chemical laboratories series showed faster activation times than actually measured. In order for FPETool to predict an activation time of 39 s, a RTI of 339 (m-s)^{½} (615 (ft-s)^{½}) has to be used. This assumes all other inputs remain constant. A value of 339 (m-s)^{½} (615 (ft-s)^{½}) is only slightly higher than the range of values recommended by FPETool for this type of sprinkler.

For experiments 2 and 3 of the chemical laboratories series the predicted activation times are in excellent agreement with the measured values. The choice of RTI in this case is not as critical since the range of suggested values is rather narrow when compared to the range offered for the standard sprinkler.

For these first 3 experiments, it must be noted that none of the sprinklers were within 1% of the distance from the top of the combustible to the ceiling. The distance that FPETool assumes. For this series the height was taken as the distance from the floor to ceiling since the initial fire was a flammable liquid on the floor of the laboratory. However all three were within 12% of this value which places them within the confines of the ceiling jet. For these experiments 12% of the floor to ceiling height is 0.38 m (15 in). Additionally, and more likely the case, the proximity to the center of the fire places the sprinklers close to the edge of the plume. Alpert gives a range of the ceiling jet thickness of 5% to 12%. The value of 5% is more appropriate near the plume.

For experiment number 4 of the chemical laboratory series, the sidewall sprinkler experiment, there is a wide range of predicted times depending on which scenario is used. As in the previous three experiments, FPETool was exercised using 3 different RTI values. Using the default value for velocity reduction of 50% adds 3 to 4 s onto the activation times.

A possible explanation for the relatively good agreement between the measured and predicted values of the sprinkler activation times is that the fire growth was at such a rapid rate. Figure 2 shows the heat release rate curve of the fuel package used in the chemical laboratory experiments. As can be seen the fire has an output of 1 MW at approximately 30 s. This provides an environment for the sprinkler similar to that found in the plunge test.

The upper layer temperature increase and upper layer depth development both follow that predicted by FPETool, figures 5 and 6. There is only a small period of time, approximately 150 s into the experiment, that the measured upper layer depth drops to a level 2.92 m from the ceiling. It should be remembered that these two graphs were developed from data obtained from one thermocouple array placed in the corner of the room, figure 1.

The heat release rate at the measured time of sprinkler activation for the standard sprinkler, experiment 1, is double that of the quick response sprinklers, experiments 2 and 3. The quick response side wall sprinkler which was located 3.66 m from the fire activated faster than the standard sprinkler located 0.61 m from the fire. The difference in heat release rate at time of sprinkler activation for these two experiments is approximately 400 kW. Heat release rate is not predicted by FPETool, it is an input supplied by the user. Column 3 of table 6 gives the range of heat release rates at predicted sprinkler activation times. Depending on the RTI used and in the case of the sidewall sprinkler, the value of the velocity reduction factor, a wide range of predicted sprinkler activation times is obtained. This translates into a range of heat release rates for these predicted activation times. For experiment 1, the range of heat release rates is approximately 150 kW, for experiments 2 and 3, 180 kW and 230 kW respectively. For experiment 4, which had the greatest range of predicted sprinkler activation times, the range of heat release rates is approximately 390 kW.

3.0 AIRCRAFT HANGER EXPERIMENTS

The second experimental series modeled was conducted in an aircraft hanger [30]. The experiments were conducted as part of the acceptance of the fire detection system within the hanger. This series was modeled to compare ceiling jet temperatures, detector link temperatures at various radial distances from the fire, and upper layer depth.

Two experiments were conducted in a hanger which measured 37.2 m x 40.2 m (122 ft x 132 ft) with a ceiling height of 14 m (46 ft). Since the results of these two experiments were similar only data from one of the experiments was reported. The hanger had concrete block walls to a height of 11.0 m (36.5 ft) with the remaining upper walls of steel panel construction. The flat ceiling was composed of corrugated steel panels supported on 254 mm (10 in) deep steel I beams installed on 2.0 m (6.6 ft) trusses. The fuel package for this experimental series was industrial grade isopropyl alcohol placed in steel pans that formed a square measuring 1.8 m x 1.8 m (6 ft x 6 ft). The pans were supported on bricks approximately 125 mm (5 in) above the floor. Enough alcohol was placed in the pans to allow the experiment to run for 60 s, at which time the fire was extinguished. The FPETool inputs are listed in table 7. The heat release rate input for this fuel package is given in table 8.

There were no sprinklers used in this experimental series. Instead, thermocouples attached to 9.75 mm (0.384 in) diameter x 2.3 mm (0.092 in) thick brass disks simulated the heat responsive element of a sprinkler. The RTI measured for the brass disks was 57.7 $(m\text{-}s)^{½}$ (101 $(ft\text{-}s)^{½}$). Since there is no activation temperature for a brass disk, a device activation temperature of 999°C was used in the FPETool inputs. Brass disks were located a distance of 380 mm (15 in) below the ceiling at radial distances of (0, 2.7, 5.5, 8.2, 11.0) m ((0, 9, 18, 27, 36) ft) from the center of the fire. Comparisons are made of the measured thermal device temperature with that predicted by the model. The only difference between the computer model simulations is the radial distance from the center of the fire source the simulated sprinkler link is located. In addition, 0.05 mm (0.02 in) diameter chromel-alumel thermocouples were located next to each brass disk to measure the temperature of the ceiling jet at that location. Temperatures obtained from the thermocouples were used to measure the ceiling jet temperatures and temperatures obtained from the brass disks to simulate temperatures of sprinkler links.

3.1 Comparisons - Ceiling Jet and Disk Temperatures

Comparisons of the measured versus predicted temperatures for the brass disks and ceiling jet are presented in figures 7 through 11 for the five radial distances. Table 9 shows the average measured excess ceiling jet temperature, the standard deviation of these measured temperatures, and the average excess ceiling jet temperature predicted by FPETool. The average measured excess ceiling jet temperature applies to the portion of the experiment where the ceiling jet temperature has become steady state. The standard deviation was obtained from this portion of the data. The average excess ceiling jet temperature predicted by FPETool is taken from the portion after steady state, but before the initiation of the warm air entrainment model. Before the initiation of the warm air entrainment model FPETool over predicts the excess ceiling jet temperature from between one and three standard deviations. At the 2.7 m (9 ft) location the difference is over 4 standard deviations. Once the warm air entrainment model is initiated the over prediction by FPETool is greater.

3.2 Comparisons - Upper Layer Depth

The depth of the upper layer is based on the response of two thermocouples located 11 m (36 ft) from the fire. The first was positioned 1.8 m (6 ft) below the ceiling, the second 3.4 m (11 ft) below the ceiling. The thermocouple located 1.8 m (6 ft) started to respond to an increase in temperature at approximately 36 s into the experiment, FPETool predicted that the layer would not reach this level until 46 s. The second thermocouple located 3.4 m (11 ft) did not respond to an increase in

temperature during the experiment and FPETool also predicted that the upper layer would not reach this level within the 60 s experiment time.

3.3 Discussions and Conclusions

For these hanger experiments the degree to which the predicted values by FPETool agree with those measured also depends on how far out radially the measurement is taken. The measured gas and disk temperatures shown in figures 7 through 11 show an increasing time offset with increasing radial distance from the centerline of the fire. Thermocouples at 0.0 m and 2.7 m (9 ft) initially respond at the same time. This is due to the plume expanding to a radius that includes the 2.7 m thermocouple before striking the ceiling. The r/H value at the 2.7 m position is 0.19 which places the thermocouple at the edge of the plume. The offset time for the (5.5, 8.2, 11.0) m ((18, 27, 36) ft) thermocouples is approximately 8 s, 12 s, and 18 s respectively.

A reason for this discrepancy between measured and predicted values is FPETool, like many zone models does not take into account transport time for the products of combustion to travel to a specified location. Any change in the heat release of the fire immediately effects the upper layer and does so throughout the upper layer. This can be seen graphically in figures 7 and 11 where FPETool predicts that the thermocouples and disks respond instantaneously. The transport time usually does not have a significant effect on the predictive outcome from FPETool when used in rooms that are typical of residential or office spaces. However, as can be seen here when the distances become great the transport time for the products of combustion need to be taken into consideration.

At 42 s into the simulations, FPETool predicts that the layer has dropped down 12 percent of the distance from the top of the combustible to the ceiling. At this point FPETool uses Evans' correlation to take into account what the effect of entraining these additional warm gases has on the ceiling jet temperatures. This can be seen in the sudden increase in the excess temperatures in figures 8 through 11. In figure 7 there is a decrease, albeit small, in the plume temperature at 42 s.

For these simulations, FPETool predicted that the upper layer would descend 2.4 m (94 in) below the ceiling. This is between two thermocouples, one at 1.8 m (6 ft) below the ceiling and the second 3.4 m (11 ft) below the ceiling. The distance between these two thermocouples is 1.6 m (5 ft). This distance represents 11% of the floor to ceiling height. Since the first thermocouple responded and the second did not, all that can be said is that the upper layer descended between 1.8 m (6 ft) and 3.4 m (11 ft) below the ceiling. It would seem reasonable, for this configuration, that FPETool predicted the upper layer depth within 11% of the floor to ceiling height.

4.0 RESIDENTIAL SPRINKLER EXPERIMENTS

The third experimental series modeled [32] was conducted in a room 9.2 m x 5.6 m (30 ft x 18 ft) with a ceiling height of 2.4 m (8 ft), figure 12. The walls and ceiling were constructed of a wood frame covered with 12.7 mm (0.5 in) gypsum board. The floor was concrete. A hollow steel door measuring 2.1 m high x 0.91 m wide (6.9 ft x 3.0 ft) opened to the outside. The air gap under the door measured 25 mm (1 in). This door was closed for all experiments. The only vent consisted of a stairway which measured 2.7 m x 0.9 m (8.9 ft x 3 ft) leading to an upper floor that had the same dimensions as the fire compartment. There was no vent from this upper floor. Since FPETool does

not allow vents to be located on the ceiling, this vent was modeled as having a height of 2.4 m (8 ft) which places the top of the vent at the ceiling, a width of 2.7 m (8.9 ft) which is the length of the original opening to the upper floor, and a sill height of 1.5 m (5 ft), which makes the opening height of this vent 0.9 m (3 ft).

Four instrumentation arrays were located within the room as shown in figure 12. Each of the instrumentation arrays had 0.51 mm (0.02 in) nominal diameter type K thermocouples located (0, 25, 50, 75, 100, 125, 150, 250, 350, 450, 550, 900) mm ((0, 1.0, 2.0, 3.0, 3.9, 4.9, 5.9, 9.8, 13.8, 17.7, 21.7, 35.4) in) below the ceiling, figure 13. Additionally, gas velocity measurements were recorded at instrumentation arrays one and two using bi directional probes [33]. The bi-directional probes were located (25, 75, 125, 250) mm ((1, 3, 4.9, 9.8) in) below the ceiling, figure 13. The standard uncertainty for the velocity measurements is ± 0.1 m/s (± 0.3 ft/s) based on the manufacturer's data for the differential pressure transducers. At the start of each test the readings from the velocity probes were assumed to be zero. There were no gas velocity measurements taken at sprinklers three and four.

At each of the four instrumentation locations a quick response residential pendent sprinkler was installed on the ceiling in accordance with the 1993 edition of the National Fire Protection Association (NFPA) 13D, Sprinkler Systems in One and Two Family Dwellings and Manufactured Homes [34]. The sprinklers used throughout these experiments were commercially available quick response residential pendent sprinklers. The sprinklers had glass bulb elements with an activation temperature of 68 ± 2.4 °C (154 ± 5.4 °F). The response time index (RTI) for the sprinklers was 55.8 (m-s)^{½} (100 (ft-s)^{½}), as determined by an independent testing laboratory [35]. When mounted the sprinklers were fully exposed and the center of the glass bulb element was 25 mm (1 in) below the gypsum ceiling. The sprinkler system was pressurized with air to approximately 100 kPa (15 psi). Each sprinkler was connected to a pressure switch that was electronically connected to a timer. The pressure switches were set at 5 kPa (1 psi) so that upon sprinkler activation the drop in pressure would automatically stop the corresponding timer. This provided an activation time accurate to ± 0.1 s.

The FPETool inputs for this experimental series are listed in table 10.

The fire source in this experimental series consisted of a rectangular methane gas burner with a piloted ignition. The burner had dimensions of 0.7 m x 1.0 m (28 in x 40 in) and was 0.31 m (1 ft) high. A technical grade of methane was used, which was certified by the supplier to contain at least 98% methane. The flow of methane to the burner was controlled by a computer. The computer was programmed to monitor the flow of methane through four mass flow controllers arranged in parallel. With this configuration the heat release rate curve produced by the burner is one that follows the fire growth rates used in the 1993 edition of the NFPA 72 National Fire Alarm Code Appendix B [36]. The fast, medium and slow fires described by this NFPA standard are based on a wide variety of fires that grow with the square of time and are sometimes referred to as t-squared (t^2) fires. A mathematical representation for these curves is as follows:

$$\dot{Q} = \alpha t^2 \qquad (34)$$

where: $\dot{Q}$ = heat release rate (kW)

α = coefficient (kW/s^2)

t = time (s)

Figure 14 demonstrates the repeatability obtained with the burner during calibration tests. The three theoretical fire growth curves used in this experimental series are overlaid with data obtained from the respective burner calibration tests. For each fire growth rate, two calibration tests were performed. The heat release inputs used for the fast fire growth are listed in table 11. For the medium and slow fire growths the heat release rate inputs are listed in tables 12 and 13 respectively. A value of 14% was used to model the radiative fraction for methane gas [27]. Internal heat loss λ_c was set at 0.9.

4.1 Location of Fire

In addition to varying the heat release rate of the fire, the burner was placed in three different locations within the room. These locations were as follows; in the open or away from any wall (detached experiment), against a wall (wall experiment), and in a corner (corner experiment). The effect of placing the burner against a wall or in a corner of the room is to restrict the entrainment of air into the plume [20,37]. When the burner is placed away from a wall or what would be considered in the open, cool room air is entrained into the plume from all directions. By placing the burner adjacent to one or more walls, the area over which this cool room air can be entrained into the plume is reduced. One result of this reduction in entrainment is higher flame heights. Since the fuel requires the same amount of air to complete the oxidation process a greater distance is now needed for the fuel vapors to mix with the smaller quantity of air that is entering the plume. With the higher flame height there is also less distance from the tip of the flame to the bottom of the warm upper layer for the plume to entrain cool air than in the case for the burner placed in the open. The higher plume temperatures that result from the reduced cool air entrainment cause similar increases in the upper layer temperatures.

Zukoski [20] placed a vertical wall across the diameter of a circular burner which caused it to be reduced to a semi-circular geometry figure. The effect of placing the wall over a diameter of the burner, blocking off half of the burner, was to reduce entrainment to 0.57 of the original value obtained when the burner was placed in the center of the room, a reduction of 43%. The rate of entrainment for a fire is related to the heat release rate as:

$$\dot{m}_{plume} \propto \dot{Q}_C^{1/3} \qquad (36)$$

where $\dot{m}_{plume}$ = mass entrainment into the plume (kg/s)

$\dot{Q}_C$ = convective heat release rate of fire (kW)

By placing the fire against a wall, the entrainment is now limited to one half the perimeter of the fire. For a wall fire, a pseudo heat release rate of two times the actual heat release is used to represent the

effect of the wall on entrainment. The entrainment would be expected to increase by a factor of $(2)^{1/3}$ or:

$$\dot{m}_{plume} \propto (2\dot{Q}_C)^{1/3} \qquad (37)$$

Since the entrainment only occurs over half the perimeter of the pseudo fire the actual entrainment rate would be:

$$\dot{m}_{plume} \propto 0.5(2\dot{Q}_C)^{1/3} = 0.63\dot{Q}_C^{1/3} \qquad (38)$$

This value is close to the measured value of 0.57 reported by Zukoski.

By applying the same argument to a fire in the corner in which the entrainment will occur over one fourth of the perimeter, this corner geometry fire entrainment rate compared to a center geometry fire would be:

$$\dot{m}_{plume} \propto 0.25(4\dot{Q}_C)^{1/3} = 0.40\dot{Q}_C^{1/3} \qquad (39)$$

Additionally the temperature difference within a plume is related to the entrainment rate as follows:

$$\Delta T_{plume} \propto \frac{\dot{Q}_C}{\dot{m}_{plume}} \qquad (40)$$

For a given heat release rate $\dot{Q}_c$, the change in temperature over ambient in the plume varies inversely with the entrainment of air into the plume. For a wall fire:

$$\frac{\dot{m}_{plume_{center}}}{\dot{m}_{plume_{wall}}} = \frac{1}{0.63} = 1.6 \qquad (41)$$

which suggests that the average plume temperature rise within the plume will increase by a factor of 1.6 over that of a plume in the open at the same height.

For the corner case:

$$\frac{\dot{m}_{plume_{center}}}{\dot{m}_{plume_{corner}}} = \frac{1}{0.4} = 2.5 \qquad (42)$$

which suggests that the average plume temperature rise within the plume will increase by a factor of 2.5 over that of a plume in the open at the same height. To account for this effect on entrainment and the subsequent rise in plume temperatures, Alpert [37] suggests doubling the heat release rate for a wall fire geometry and quadrupling the heat release rate for a corner fire geometry when calculating the rise in plume temperature.

Another effect that reduced entrainment rates have on corner and wall fire geometries is the warm upper layer is moved upward in the room. This in turn allows the entrainment of lower layer air, albeit at a reduced rate, to occur over a greater distance. Therefore, the excess temperature of the plume as it enters the warm upper layer should be less than the factors calculated in Eqs. 37 and 38. Mowrer [38] calculated a mass balance between the plume and the doorway mass fluxes which permits the layer height, and consequently the compartment mass fluxes to be determined. By plotting this mass balance between the plume and doorway mass fluxes it was found that the layer height interface moves up for the wall and corner geometries as compared with the center fire geometry. From this Mowrer suggests that the temperature increase in the plume be multiplied by a factor of 1.3 for fires placed along walls and 1.7 for fires placed in corners. Since plume theory relates the temperature rise above the fire source as:

$$\Delta T \propto \dot{Q}^{2/3} \qquad (43)$$

then

$$\frac{\Delta T_{wall}}{\Delta T_{center}} = \frac{\dot{Q}_{wall}^{2/3}}{\dot{Q}_{center}^{2/3}} \qquad (44)$$

The ratio of temperatures differences between the center fire and the wall fire is 1.3. Thus

$$\dot{Q}_{wall} = 1.3^{3/2}\ \dot{Q}_{center} = 1.5\ \dot{Q}_{center} \qquad (45)$$

Therefore a fire along the wall is equivalent with respect to temperature difference to a fire about 1.5 times as large in the center of the room. By using the value of 1.7 for the ratio of temperature difference a fire placed in a corner is equivalent with respect to temperature difference to a fire about 2.2 times as large in the center of the room.

4.2 Comparisons - Sprinkler Activation Times

Tables 14 and 15 give sprinkler activation times with the burner detached or placed away from any wall and the vent to the upper floor opened and closed respectively For each heat release rate slow, medium, and fast, three experiments were performed. The activation time for each experiment is shown. Next to the activation times is a simple average of the three experiments. Two FPETool simulations were performed, one with the default value for the fraction of radiative heat loss or χ_R = 0.35 and one with χ_R = 0.14. The predicted activation times are listed along with the percent difference from the average of the three experiments.

Tables 16 and 17 give sprinkler activation times for the burner placed against a wall and in the corner respectively. In all cases the vent to the upper floor was open. For each heat release rate slow, medium, and fast, three experiments were performed. The activation time for each experiment is shown. Next to the activation times is a simple average of the three experiments. Two FPETool simulations were performed for each scenario. For the wall scenario, one in which the heat release rate was multiplied by a factor of 2 and one in which the heat release rate was multiplied by a factor of 1.5. For the corner scenario, one in which the heat release rate was multiplied by a factor of 4 and one in which the heat release rate was multiplied by a factor of 2.2. For both scenarios, the value for the fraction of radiative heat loss or χ_R was set at 0.14. The predicted activation times are listed along with the percent difference from the average of the three experiments. No experiments were conducted with the burner placed against a wall or in the corner and the vent to the upper floor closed.

4.3 Comparisons - Upper Layer Temperature and Upper Layer Depth

Using the N Percent Rule, the upper layer temperatures and upper layer depths were calculated. Results for upper layer temperatures are presented in figures 15 through 20 for the detached burner scenarios. Plotted along with the measured values are two predicted values from FPETool. The first utilized a radiative heat loss fraction or χ_R of 0.35, the default value, and the second a radiative heat loss fraction or χ_R of 0.14. For the experiments where the burner was placed against a wall the measured values are compared with the heat release rate multiplied by a factor of 2 and 1.5. In this case the radiative heat loss fraction or χ_R was 0.14. The wall scenario are presented in figures 21 through 23. For the experiments where the burner was placed in a corner of the room, the measured values are compared with the heat release rate multiplied by a factor of 4 and 2.2. In this case the radiative heat loss fraction or χ_R was 0.14. The corner scenario are presented in figures 24 through 26.

The upper layer development are presented in figures 27 through 32 for the detached burner scenarios. Two measured depths were obtained for the upper layer, the first using N = 10 and the second using N = 20. Plotted along with these two measured values are two predicted values from FPETool. The first utilized a radiative heat loss fraction or χ_R of 0.35, the default value, and the second a radiative heat loss fraction or χ_R of 0.14. For the experiments where the burner was placed against a wall the two measured depths are compared with both the center heat release rate multiplied by a factor of 2 and 1.5. In both cases the radiative heat loss fraction χ_R was 0.14. The wall scenario are presented in figures 33 through 35. For the experiments where the burner was placed in the corner of the room the two measured depths are compared with the heat release rate multiplied by a factor of 4 and 2.2. In both case the radiative heat loss fraction χ_R was 0.14. The corner scenario are presented in figures 36 through 38.

4.4 Comparisons - Ceiling Jet Velocities and Temperatures

Results for ceiling jet velocities are presented in figures 39 through 44 for the detached burner scenarios. Plotted along with the measured values are two predicted values from FPETool. The first utilized a radiative heat loss fraction χ_R of 0.35, the default value, and the second a radiative heat loss fraction χ_R of 0.14. For the experiments where the burner was placed against a wall the measured values are compared with the heat release rate multiplied by a factor of 2 and 1.5. In both

cases the radiative heat loss fraction χ_R was 0.14. The wall scenario are presented in figures 45 through 47. For the experiments where the burner was placed in the corner of the room, the measured values are compared with the heat release rate multiplied by a factor of 4 and 2.2. In both cases the radiative heat loss fraction χ_R was 0.14. The corner scenario are presented in figures 48 through 50.

Results for the ceiling jet temperatures are presented in figures 51 through 56 for the detached burner scenario. Plotted along with the measured values are two predicted values from FPETool. The first utilized a radiative heat loss fraction χ_R of 0.35, the default value, and the second a radiative heat loss fraction χ_R of 0.14. For the experiments where the burner was placed against a wall the measured values are compared with the heat release rate multiplied by a factor of 2 and 1.5. In both cases the radiative heat loss fraction χ_R was 0.14. The wall scenario are presented in figures 57 through 59. For the experiments where the burner was placed in the corner of the room, the measured values are compared with the heat release rate multiplied by a factor of 4 and 2.2. In both cases the radiative heat loss fraction χ_R was 0.14. The corner scenario are presented in figures 60 through 62.

4.5 Comparisons - Heat Release Rate at Sprinkler Activation

As in the chemical laboratory experiments a comparison is made of the heat release rate of the fire at measured sprinkler activation to the heat release rate at predicted sprinkler activation. Tables 18 and 19 provide this for the detached burner scenario with the vent opened and closed respectively. The format for these tables follows closely the one used to compare sprinkler activation. The measured heat release rate at sprinkler activation is shown for each experiment. Next to the heat release rates is a simple average of the three experiments. The heat release rate at the time of predicted sprinkler activation is listed along with the percent difference from the average of the three experiments.

For the scenario where the burner is placed against the wall, table 20 shows the results when the input heat release rate for FPETool is doubled in order to take into account the effect of the wall on entrainment. The measured heat release rate at sprinkler activation is shown for each experiment. Next to the heat release rates is a simple average of the three experiments. The heat release rate at the time of predicted activation is listed along with the percent difference from the average of the three experiments. Table 21 shows the results when the input heat release rate for FPETool is multiplied by 1.5 in order to take into account the effect of the wall on entrainment.

For the scenario where the burner is placed in the corner, table 22 shows the results when the input heat release rate for FPETool is quadrupled in order to take into account the effect of the corner geometry on entrainment. The measured heat release rate at sprinkler activation is shown for each experiment. Next to the heat release rates is a simple average of the three experiments. The heat release rate at the time of predicted activation is listed along with the percent difference from the average of the three experiments. Table 22 shows the results when the input heat release rate for FPETool is multiplied by 2.2 in order to take into account the effect of the corner geometry on entrainment.

4.6 Discussion and Conclusions

For the detached burner experiments the use of a χ_R of 0.14 as the fraction of radiative heat loss provided better agreement with experimental results. By using a χ_R of 0.35 for the fraction of radiative heat loss, FPETool over predicted activation times by 28% to 59%. By using a χ_R of 0.14 the model still over predicted activation times, but by a range of 10% to 39%. In this configuration the effect of the vent or stairs to the upper floor being opened or closed was examined and it was found not to have an appreciable effect on the measured or predicted activation times of the sprinkler.

Placing the burner against the wall had no appreciable effect on measured activation times. Therefore in this situation, multiplying the heat release rate by any factor in an attempt to take into account any increase in ceiling jet temperatures gave, as expected, faster predicted activation times. When the burner against the wall, a short side of the burner was placed against the wall figure 12. The original perimeter of the burner was 3.4 m (11 ft). By placing the short side of the burner against the wall the perimeter is only reduced by 0.7 m (28 in), a reduction of only 21%. In this configuration, air was being entrained over 79% of the burner perimeter.

Placing the burner in the corner did have an effect on the measured activation times. In this configuration, the perimeter over which air can be entrained was reduced by 50%. The method of quadrupling the heat release rate in order to take into account wall effects under predicted activation times for all fire growth rates by a range of 9% to 26%. By using Mowrer's correlation the model over predicted activation times by a range of 3% to 24%.

For upper layer temperature increase with the burner in the detached position, the use of χ_R of either 0.14 or 0.35 lie within the data scatter, figures 15 through 20. As with sprinkler activation times, placing the burner against a wall did not have an appreciable effect on the upper layer temperature increase, figures 21 through 23.

The upper layer development for the detached burner experiments, figures 27 through 32, was also insensitive to the value of χ_R chosen. For the three scenarios in which the vent was open, FPETool predicted a layer that asymptotically approached 1.8 m, while the measured values showed that the layer continued toward the floor. For the three scenarios in which the vent was closed, FPETool did predict that the layer in the room continued toward the floor as was measured. Upper layer development was also insensitive to which method was used to take into account the effect of walls when the burner was placed against a wall or in a corner, figures 33 through 38. Mowrer's and Alpert's correlations gave similar predictions.

Gas velocity predictions for the detached burner experiments, figures 39 through 44, were also insensitive to the value of χ_R chosen. Gas velocity predictions were also insensitive as to which method was used to take into account the effect of walls when the burner was placed against a wall or in a corner, figures 45 through 50. Mowrer's and Alpert's correlations gave similar predictions. For all 6 scenarios, the measured gas velocity was consistently higher than that predicted by a factor of 2.

Ceiling jet temperature increase predictions for the detached burner experiments, figures 51 through 55 had better agreement when using χ_R = 0.14 instead of 0.35 for the slow and medium fires. However, both under predicted the increase in ceiling jet temperature. For the fast fire growth

scenario the use of χ_R of 0.14 or 0.35 produced similar results, as both were within the data scatter. Placing the burner against a wall did not have an appreciable effect on the measured ceiling jet temperature. Multiplying the heat release rate by a factor in an attempt to take into account any increase in ceiling jet temperature simply brought the predictions more in line with the measured values.

The heat release rate at sprinkler activation again shows the importance of fire growth rate. Take for example the scenario in which the burner is detached from any walls and the vent to the upper floor is open. This is depicted in tables 14 and 18. For the slow fire growth rate the difference in predicted sprinkler activation times is 23 s depending on which χ_R is chosen, table 14. However, the difference in the heat release rate at predicted sprinkler activation is only 25 kW. Compare this when the fast fire growth rate is used. Here the difference in predicted sprinkler activation times is 7 s and the difference in heat release rate is 80 kW.

5.0 CONCLUSIONS

The applicability of FPETool to these three building spaces and fire geometries has been examined. FPETool can provide useful predictions of fire generated environments in a single room such as those described in this paper. Predictive capabilities of FPETool were compared against equivalent or nearly equivalent measurements from the three experimental series. For the variables deemed of interest, FPETool provides predictions which range in quality from within a few percent to double the measured values. Presentation of the differences between FPETool predictions and the experimental data are intentionally simple. Experimental uncertainties in full scale fire experiments are difficult to determine since individual tests do not allow for the assessment of reproducibility of the experimental results. Of these three experimental series, only the one dealing with residential sprinklers had repeat tests.

The fires in these experiments can be characterized from those that grow with the square of time, t-squared fires, to those that reach steady state in a matter of seconds. Heat release rates from these fires varied significantly. From 100 to 200 kW for the residential sprinkler experiments to 2 MW for the chemical laboratory experiments and up to 3.6 MW for the hanger experiment fire. Compartment geometries and ventilation factors also varied.

It must be noted that the physical make up of the compartment being modeled does not always agree with the assumptions in FPETool. For example only the sprinklers in the residential sprinkler experiments meet the criteria of being under a smooth unobstructed ceiling and within 1% of the fire to ceiling height. In this set of experiments only when the burner was in the detached position does it meet the requirement by FPETool that the fire be away from a wall. When the burner is placed against a wall or in a corner adjustments where made in the heat release rate to take into account the effect walls have on entrainment. This is not part of FPETool, but is an assumption that the modeler makes.

Additionally, it was shown that when using FPETool to model a large space such has the hanger experiment, that consideration needs to be taken for the time required for the products of combustion

to leave the combustion zone, travel to the ceiling and then out radially to the sensor. This is shown clearly in figures 7 through 11 where the predicted temperatures of the link and ceiling jet agree well with measured values. Only the time to reach these temperatures is significantly different. An exception to this is figure 8 where the predicted temperatures is significantly greater than measured. This may have been due to the proximity of the sensor to the plume. The ceiling jet is thinnest where it strikes the ceiling and gradually thickens as it expands radially. FPETool assumes that the ceiling jet is a constant thickness. This sensor may have been just below the ceiling jet.

Fire models such as FPETool estimate major fire generated effects. Due to the complex nature of fire, mathematical prediction models, which FPETool is, are often simplified and based on a number of assumptions. Knowledge is necessary of the limitations, approximations, and possible errors associated with the assumptions and equations used in any computer model. The engineer has an obligation to use this knowledge. This evaluation report is intended to be used in conjunction with the models' user manual and/or technical reference guide.

6.0 REFERENCES

1. Stroup, D. W., Analyzing Fire Safety Through Computer Modeling and Product Testing. General Services Administration, Washington DC, Interscience Communications Limited. Fires and Materials. 2nd International Conference, September 23-24, 1993 Arlington Virginia pp 7-12.
2. Bonisch, W. D., Computer Fire Modeling Analysis of Smoke Control System Performance in an Arena. Society of Fire Protection Engineers, Proceedings of Performance Based Fire Safety Engineers, November 15-17, 1993, Phoenix, AZ pp 75-83.
3. Custer, R. L. P., Computer Modeling in Fire Reconstruction and Failure Analysis. Custer Powell, Inc., Wrentham, MA, Society of Fire Protection Engineers and Worcester Polytechnic Institute. Computer Applications in Fire Protection. Proceedings. June 28-29, 1993, Worcester, MA, pp 69-74.
4. Bukowski, R.W., Analysis of the Happyland Social Club Fire with Hazard I. Journal of Fire Protection Engineering, Vol. 4, No. 4, 117-131, 1992.
5. Bukowski, R.W., Modeling a Backdraft: The Fire at 62 Watts Street. NFPA Journal, Vol. 89, No. 6, 85-89, 1995.
6. Nelson, H. E., FPETool: Fire Protection Engineering Tools for Hazard Estimation. NISTIR Report 4380, National Institute of Standards and Technology; October 1990.
7. Deal, S., Technical Reference Guide for FPETool Version 3.2. NISTIR 5486, National Institute of Standards and Technology; August 1994.
8. Zukoski, E. E., Development of a Stratified Ceiling Layer in the Early Stages of a Closed-Room Fire, Fire and Materials, Vol. 2, No., 2 1978.
11. Heskestad, Gunnar, Engineering Relations for Fire Plumes, Fire Safety Journal, Vol. 7, 1984, p 25-32.
12. Heskestad, Gunnar, Virtual Origins of Fire Plumes, Fire Safety Journal, Vol 5, 1983, p 109-114.
13. Heskestad, G., Fire Plumes, Section 2 Chapter 2 Society of Fire Protection Engineers Handbook of Fire Protection Engineering, Second Edition, Boston MA., National Fire Protection Association.

14 Evans, D. D., and Stroup, D. W., Methods to Calculate the Response Time of Heat and Smoke Detectors Installed Below Large Unobstructed Ceilings. Fire Technology, Vol. 22, No. 1, 54-65, February 1986.
15. Alpert, R. L., Calculation of Response Time of Ceiling-Mounted Fire Detectors. Fire Technology, Vol. 8, No. 3, 181-195, August 1972.
16 Madrzykowski, D., The Effect of Recessed Sprinkler Installation on Sprinkler Activation Time and Prediction. Master's Thesis, University of Maryland, Department of Fire Protection Engineering, College Park, Maryland, November 1993
17. Evans, D. D., Calculating Sprinkler Actuation Time in Compartments. Fire Safety Journal, Vol. 9, No. 2, 147-155 1985.
18. Evans, D. D., Thermal Actuation of Extinguishing Systems NBSIR 83-2807. National Institute of Standards and Technology, March 1984, Gaithersburg, Maryland, 20899.
19 Yokoi, S., The Use of Models in Fire Research, Publication No. 786, National Academy of Sciences, National Research Council: Washington D.C., 1961, p 186-206.
20 Zukoski, E. E., Kubota, T., and Cetegen, B., Entrainment in Fire Plumes. Fire Safety Journal, Vol. 3, 107-121 1980.
21. Parker, W. J., Calculations of the Heat Release Rate by Oxygen consumption For Various Applications. Journal of Fire Sciences, Vol. 2, No, 2, 380-395, September/October 1994.
22. Janssens, M. L., Measuring Rate of Heat Release by Oxygen Consumption. Fire Technology, Vol. 27, No. 3, 234-249, August 1991.
23. Huggett, C., Estimation of Rate of Heat Release by Means of Oxygen Consumption Measurements. Fire and Materials, Vol. 4, No. 2, 1980.
24. Heskestad, G., and Smith, H. F., Investigation of a New Sprinkler Sensitivity Approval Test: The Plunge Test. Technical Report, Factory Mutual Research Corporation, FMRC Serial 22485, RC76-T-50, December 1976.
25. Heskestad, G., and Bill, R. G., Quantification of Thermal Responsiveness of Automatic Sprinklers Including Conduction Effects. Fire Safety Journal, Vol. 14, No. 1 and 2, 113-125, July 1, 1988.
26. Walton, W. D., Quick Response Sprinkler in Chemical Laboratories: Fire Test Results. NISTIR 89-4200, National Institute of Standards and Technology, December 1989.
27. Tewarson, A., Generation of Heat and Chemical Compounds in Fires. Society of Fire Protection Engineers Handbook, 2nd Edition.
28. Cooper, L. Y., Estimating Safe Available Egress Times From Fires, NBSIR 80-2172. National Institute of Standards and Technology (formerly National Bureau of Standards), 1982.
29. Cooper, L. Y., Harkleroad, M., Quintiere, J. Q., Rinkinen, W., An Experimental Study of Upper Hot Layer Stratification in Full Scale Multi Room Fire Scenarios. Journal of Heat Transfer, November 1982, Vol. 104, p 741-749.
30. Walton, W. D., and Notarianni, K. A., Comparison of Ceiling Jet Temperatures Measured in an Aircraft Hanger Test Fire With Temperatures Predicted by the DETACT-QS and LAVENT Computer Models. NISTIR 4947, National Institute of Standards and Technology, January 1993.
31. Yeager, R. W., Uncertainty Analysis of Energy Release Rate Measurement for Room Fires. Journal of Fire Sciences, Vol. 4, No. 4, July August 1986.

32. Vettori, R. L., Effect of an Obstructed Ceiling on the Activation Time of a Residential Sprinkler. NISTIR 6253, November 1998, National Institute of Standards and Technology, Gaithersburg, MD 20899.
33. McCaffery, B.J., Heskestad, G., A Robust Bidirectional Low-Velocity Probe For Flame And Fire Application. Combustion and Flame, Vol. 26, No. 1, 127-127, February 1976.
34. National Fire Protection Association, National Fire Protection Association 13D Sprinkler Systems in One and Two Family Dwellings and Manufactured Homes 1993 Edition, National Fire Protection Association, Quincy, MA 02269.
35. Underwriters Laboratory Inc., Determination of the Response Time Index (RTI) and Conductivity © Factor. Project Number 96NK9527 April 1996.
36. National Fire Protection Association, "National Fire Protection Association 72 Standard National Fire Alarm Code Appendix B 1993 Edition, National Fire Protection Association, Quincy, MA 02269.
37. Alpert, R. L., and Ward, E. G., Evaluating Unsprinklered Fire Hazards. Factory Mutual Research Corporation, Norwood, MA, SFPE TR 83-02, FMRC J. I. 01836.20, August 1982.
38. Mowrer, F. A., Williamson, R. B., Estimating Room Temperatures From Fires Along Walls and in Corners. Fire Technology, Vol. 23, No. 2, 133-145, May 1987.

Table 1 - Input for FPETool simulations - chemical laboratory experiments

INPUT PARAMETER		Simulation 1	Simulation 2	Simulation 3	Simulation 4	Simulation 5
Minimum oxygen level	21 (°C)	10.0	10.0	10.0	10.0	10.0
	600 (°C)	2.0	2.0	2.0	2.0	2.0
Heat transfer factor	radiant fraction	0.35	0.35	0.35	0.35	0.35
	max energy loss internal	0.90	0.90	0.90	0.90	0.90
Sprinkler						
distance from center of fire (m)		0.61	0.61	0.61	3.66	n/a
RTI (m-sec)$^{-5}$		250	40	40	40	n/a
activation temperature (°C)		74	71	71	71	999
sidewall velocity reduction factor (%)		n/a	n/a	n/a	50	n/a
Door opening						
height (m)		2.11	2.11	2.11	2.11	2.11
width (m)		0.91	0.91	0.91	0.91	0.91
height above sill (m)		0.0	0.0	0.0	0.0	0.0
Fire height (m)		0	0	0	0	0
Room dimensions						
ceiling height (m)		3.20	3.20	3.20	3.20	3.20
length (m)		5.48	5.48	5.48	5.48	5.48
width (m)		3.66	3.66	3.27	3.20	3.66
Ceiling material		concrete	concrete	concrete	concrete	concrete
thickness (mm)		100	100	100	100	100
thermal conductivity (kW/m-K)		0.0016	0.0016	0.0016	0.0016	0.0016
density (kg/m^3)		2400	2400	2400	2400	2400
specific heat (kJ/kg-K)		0.75	0.75	0.75	0.75	0.75
kρc		2.88	2.88	2.88	2.88	2.88
Wall materials		concrete	concrete	concrete	concrete	concrete
thickness (mm)		100	100	100	100	100
thermal conductivity (kW/m-K)		0.0016	0.0016	0.0016	0.0016	0.0016
density (kg/m^3)		2400	2400	2400	2400	2400
specific heat (kJ/kg-K)		0.75	0.75	0.75	0.75	0.75
kρc		2.88	2.88	2.88	2.88	2.88

Table 2 - Heat release rate input - chemical laboratory simulations

Time (s)	Heat Release Rate (kW)
0	0
10	234
20	698
30	1039
40	1334
50	1553
60	1834
70	2002
80	1117
90	992
100	985
110	1067
120	949
130	915
140	907
150	876
160	792
170	769
180	718
190	610
200	554
210	506
220	485
230	431
240	709
250	630
260	508
270	500
280	442
290	395
300	319

Table 3 - Activation time summary for simulation 1 - chemical laboratory experiments

Type and activation temperature of sprinkler used in experiment	Measured activation time (s)	Predicted activation time (s)		
		RTI=200(m-s)^{½}	RTI=250(m-s)^{½}	RTI=300(m-s)^{½}
Standard Upright 74°C	39	32	34	37

Table 4 - Activation time summary for simulations 2 and 3 - chemical laboratory experiments

Type and activation temperature of sprinkler used in experiment	Measured activation time (s)	Predicted activation time (s)		
		RTI=25(m-s)^{½}	RTI=40(m-s)^{½}	RTI=55(m-s)^{½}
Quick Response 71 °C	Exp 2 = 18 Exp 3 = 16	15 14	17 17	19 19

Table 5 - Activation time summary for simulation 4 - chemical laboratory experiments

Quick Response Side Wall Sprinkler - Activation Temperature of 71°C Measured activation time 26 s		
Response Time Index (m-s)^{½}	Velocity Reduction Factor (%)	Time to Sprinkler Activation FPETool (s)
25	0	23
25	50	26
40	0	27
40	50	31
55	0	31
55	50	35

Table 6 - Heat release rate at time of sprinkler activation

Experiment Number	Heat release rate at time of measured sprinkler activation (kW)	Heat release rate for range of predicted sprinkler activation times. (kW)
1	1300	1100 to 1250
2	600	470 to 650
3	510	420 to 650
4	900	800 to 1190

Table 7 - Input for FPETool simulations - aircraft hanger experiments

INPUT PARAMETERS		Simulation 1	Simulation 2	Simulation 3	Simulation 4	Simulation 5
Minimum oxygen level	21 (°C)	10.0	10.0	10.0	10.0	10.0
	600 (°C	2.0	2.0	2.0	2.0	2.0
Heat transfer factor	radiant fraction	0.30	0.30	0.30	0.30	0.30
	max energy loss internal	0.90	0.90	0.90	0.90	0.90
Sprinkler						
distance from center of fire (m)		0.0	2.7	5.5	8.2	11.0
RTI (m-sec)$^{-5}$		57.7	57.7	57.7	57.7	57.7
activation temperature (°C)		999	999	999	999	999
Door opening		na	na	na	na	na
height (m)						
width (m)						
height above sill (m)						
Fire height (m)		0.125	0.125	0.125	0.125	0.125
Room dimensions						
ceiling height (m)		14.0	14.0	14.0	14.0	14.0
length (m)		40.2	40.2	40.2	40.2	40.2
width (m)		37.2	37.2	37.2	37.2	37.2
Ceiling material		steel	steel	steel	steel	steel
thickness (mm)		100	100	100	100	100
thermal conductivity (kW/m-K)		0.458	0.458	0.458	0.458	0.458
density (kg/m^3)		7850	7850	7850	7850	7850
specific heat (kJ/kg-K)		0.473	0.473	0.473	0.473	0.473
kρc		170.05	170.05	170.05	170.05	170.05
materials		steel	steel	steel	steel	steel
thickness (mm)		25	25	25	25	25
thermal conductivity (kW/m-K)		0.458	0.458	Wall 0.458	0.458	0.458
density (kg/m^3)		7850	7850	7850	7850	7850
specific heat (kJ/kg-K)		0.473	0.473	0.473	0.473	0.473
kρc		170.05	170.05	170.05	170.05	170.05

Table 8 - Heat release rate input - aircraft hanger simulations

Time (s)	Heat Release Rate (kW)
0	0
5	385
10	1750
15	3650
60	3650

Table 9 - Excess ceiling jet temperature comparisons - hanger experiments

Radial distance (m)	Average measured excess ceiling jet temperature (˚C)	Standard deviation of measured excess ceiling jet temperature	Average excess ceiling jet temperature FPETool (˚C)
0.0	44	6	51
2.7	31	4	48
5.5	28	2	30
8.2	20	1	23
11.0	16	1	19

Table 10 - Input for FPETool simulations - residential sprinkler experiments

INPUT PARAMETERS		DETACHED VENT OPEN	WALL VENT OPEN	CORNER VENT OPEN	DETACHED VENT CLOSED
Minimum Oxygen level	21 (°C)	10.0	10.0	10.0	10.0
	600 (°C)	2.0	2.0	2.0	2.0
Heat transfer factor	radiant fraction	0.14	0.14	0.14	0.14
	max energy loss internal	0.90	0.90	0.90	0.90
Sprinkler					
distance from center of fire (m)		2.2	2.4	2.1	2.2
RTI (m-sec)$^{-5}$		55.8	55.8	55.8	55.8
activation temperature (°C)		68	68	68	68
Door opening					na
height (m)		2.4	2.4	2.4	
width (m)		2.7	2.7	2.7	
height above sill (m)		1.5	1.5	1.5	
Fire height (m)		0.3	0.3	0.3	0.3
Room dimensions					
ceiling height (m)		2.4	2.4	2.4	2.4
length (m)		9.2	9.2	9.2	9.2
width (m)		5.6	5.6	5.6	5.6
Ceiling material		gypsum board	gypsum board	gypsum board	gypsum board
thickness (mm)		12.7	12.7	12.7	12.7
thermal conductivity (kW/m-K)		0.0017	0.0017	0.0017	0.0017
density (kg/m^3)		960	960	960	960
specific heat (kJ/kg-K)		1.1	1.1	1.1	1.1
kρc		0.18	0.18	0.18	0.18
Wall materials		gypsum board	gypsum board	gypsum board	gypsum board
thickness (mm)		12.7	12.7	12.7	12.7
thermal conductivity (kW/m-K)		0.0017	0.0017	0.0017	0.0017
density (kg/m^3)		960	960	960	960
specific heat (kJ/kg-K)		1.1	1.1	1.1	1.1
kρc		0.18	0.18	0.18	0.18

Table 11 - Heat release rate input - fast fire - residential sprinkler simulations

Time (s)	Heat Release Rate (kW)
0	0
5	58
10	75
15	110
20	127
25	163
30	173
35	192
40	196
45	216
50	271
55	309

Time (s)	Heat Release Rate (kW)
60	379

Table 12 - Heat release rate input - medium fire - residential sprinkler simulations

Time (s)	Heat Release Rate (kW)		Time (s)	Heat Release Rate (kW)
0	0		65	117
5	10		70	124
10	20		75	134
15	25		80	143
20	34		85	153
25	42		90	162
30	51		95	170
35	59		100	174
40	66		105	181
45	77		110	192
50	83		115	210
55	94		120	239
60	104			

Table 13 - Heat release rate input - slow fire - residential sprinkler simulations

Time (s)	Heat Release Rate (kW)		Time (s)	Heat Release Rate (kW)
0	0		95	75
5	6		100	78
10	9		105	80
15	13		110	85
20	16		115	87
25	20		120	94
30	23		125	97
35	26		130	100
40	30		135	105
45	33		140	109
50	35		145	112
55	41		150	115
60	42		155	121
65	50		160	124
70	52		165	130
75	56		170	137
80	62		175	143
85	65		180	148
90	69			

Table 14 - Activation time summary - burner detached - vent open - residential sprinkler

Fire growth rate	Time to sprinkler activation (s)							
	Exp # 1	Exp # 2	Exp # 3	Average	FPETool prediction			
					χ_R = 35	% diff	χ_R =	% diff
Slow	100	117	116	111	177	59	154	39
Medium	88	67	78	78	111	42	97	24
Fast	46	43	41	43	59	37	52	21

Table 15 - Activation time summary - burner detached - vent closed - residential sprinkler.

Fire growth rate	Time to sprinkler activation (s)							
	Exp # 1	Exp # 2	Exp # 3	Average	FPETool prediction			
					χ_R = 35	% diff	χ_R =	% diff
Slow	134	127	127	129	165	28	142	10
Medium	74	75	74	74	106	43	92	24
Fast	39	44	40	41	57	39	50	22

Table 16 - Activation time summary - burner against wall - vent open - residential sprinkler.

Fire growth rate	Time to sprinkler activation (s)							
	Exp # 1	Exp # 2	Exp # 3	Average	FPETool prediction			
					HRR x 2	% diff	HRR x 1.5	% diff
Slow	129	116	124	123	108	12	126	2
Medium	70	71	68	70	70	0	81	16
Fast	42	40	39	40	36	11	43	8

Table 17 - Activation time summary - burner in corner - vent open - residential sprinkler.

Fire growth rate	Time to sprinkler activation (s)							
	Exp # 1	Exp # 2	Exp # 3	Average	FPETool prediction			
					HRR x 4	% diff	HRR x 2.2	% diff
Slow	99	84	84	89	72	19	98	10
Medium	54	47	54	52	47	10	64	23
Fast	35	29	29	31	23	26	32	3

Table 18 - Heat release rate at time of sprinkler activation. Burner detached - vent open - residential sprinkler.

Fire growth rate	Heat release rate at sprinkler activation (kW)							
	Exp # 1	Exp # 2	Exp # 3	Average	FPETool			
					χ_R = 35	% diff	χ_R =	% diff
Slow	80	90	90	85	145	70	120	41
Medium	160	120	140	140	195	39	175	25
Fast	225	210	200	215	365	70	285	33

Table 19 - Heat release rate at time of sprinkler activation. Burner detached - vent closed - residential sprinkler.

Fire growth rate	Heat release rate at sprinkler activation (kW)							
	Exp # 1	Exp # 2	Exp # 3	Average	FPETool			
					χ_R = 35	% diff	χ_R =	% diff
Slow	105	100	100	100	130	30	110	10
Medium	130	135	130	130	185	42	165	27
Fast	195	210	195	200	335	68	270	35

Table 20 - Heat release rate at time of sprinkler activation. Burner against wall - vent open - residential sprinkler. Assuming heat release rate input for FPETool is doubled due to effect of wall on plume entrainment.

Fire growth rate	Heat release rate at sprinkler activation (kW)					
	Exp # 1	Exp # 2	Exp # 3	Average	FPETool	
					HRR X 2	% difference
Slow	100	90	95	95	85	11
Medium	125	125	120	125	125	0
Fast	205	195	195	200	195	3

Table 21 - Heat release rate at time of sprinkler activation. Burner against wall - vent open - residential sprinkler. Assuming heat release rate input for FPETool is multiplied by 1.5 due to effect of wall on plume entrainment.

Fire growth rate	Heat release rate at sprinkler activation (kW)					
	Exp # 1	Exp # 2	Exp # 3	Average	FPETool	
					HRR x 1.5	% difference
Slow	100	90	95	95	100	5
Medium	125	125	120	125	145	16
Fast	205	195	195	200	210	5

Table 22 - Heat release rate at time of sprinkler activation. Burner in corner - vent open - residential sprinkler. Assuming heat release rate input for FPETool is quadrupled due to effect of corner walls on plume entrainment

Fire growth rate	Heat release rate at sprinkler activation (kW)					
	Exp # 1	Exp # 2	Exp # 3	Average	FPETool	
					HRR x 4	% difference
Slow	80	65	65	70	55	21
Medium	90	80	90	85	80	6
Fast	190	170	170	175	150	14

Table 23 - Heat release rate at time of sprinkler activation. Burner in corner - vent open - residential sprinkler. Assuming heat release rate input for FPETool is multiplied by 2.2 due to effect of corner walls on plume entrainment

Fire growth rate	Heat release rate at sprinkler activation (kW)					
	Exp # 1	Exp # 2	Exp # 3	Average	FPETool	
					HRR x 2.2	% difference
Slow	80	65	65	70	75	7
Medium	90	80	90	85	115	35
Fast	190	170	170	175	180	3

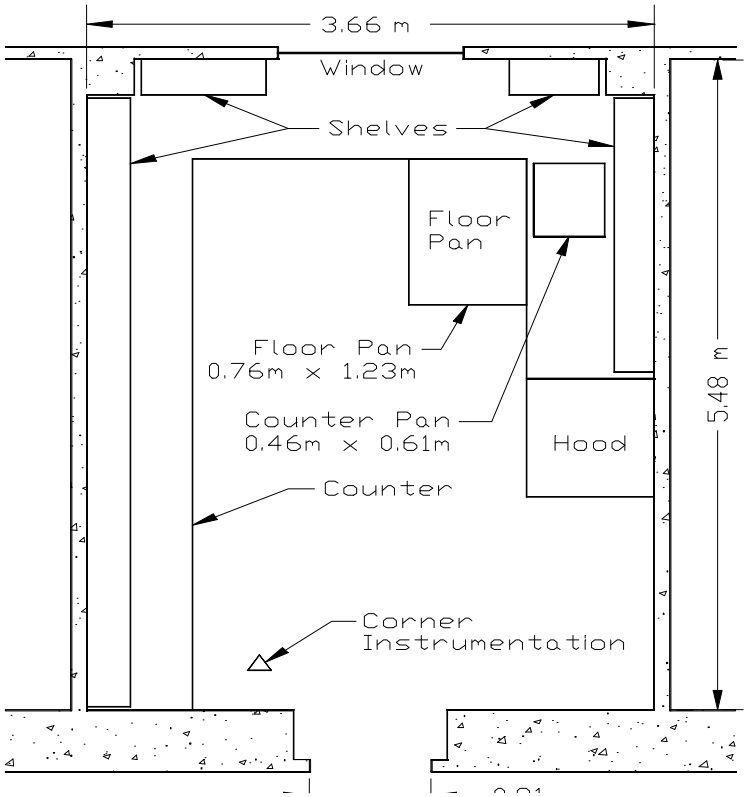

Figure 1 - Plan view for a typical chemical laboratory

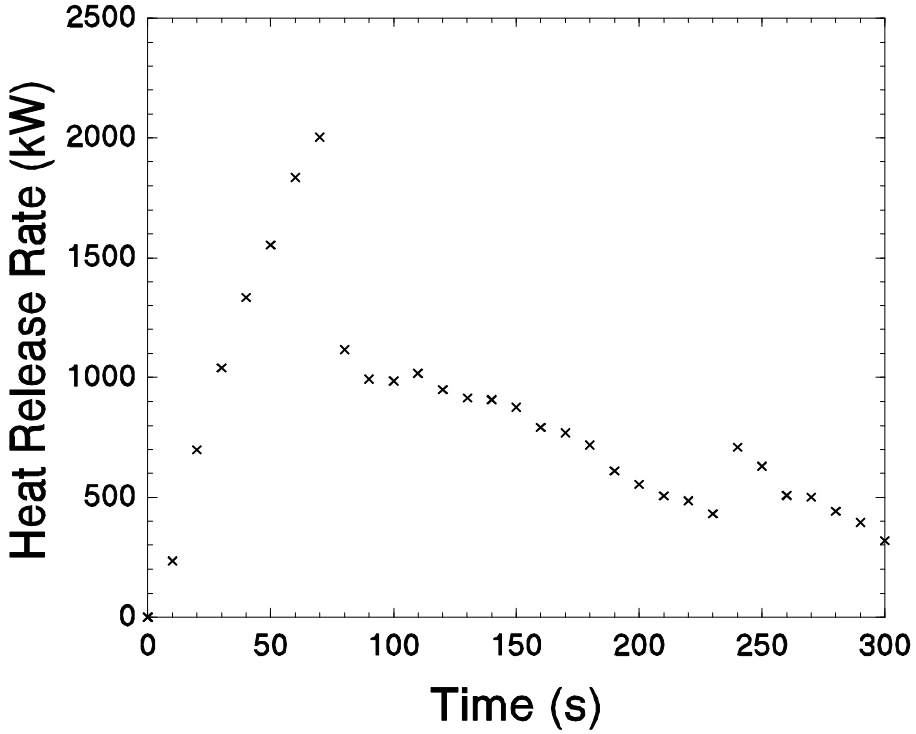

Figure 2 - Heat release rate for chemical laboratory experiments

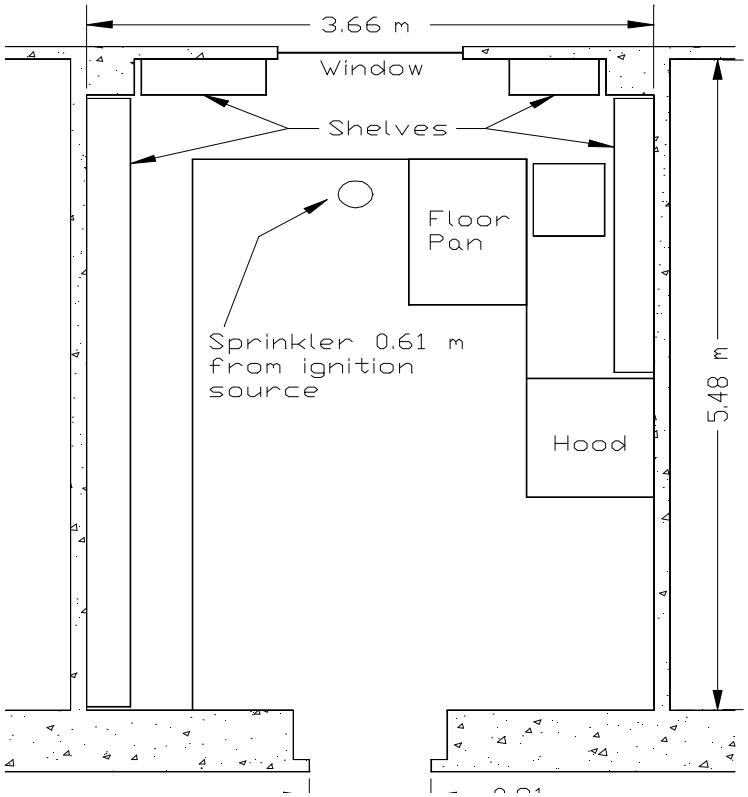

Figure 3 - Approximate sprinkler location for experiments 1, 2, and 3

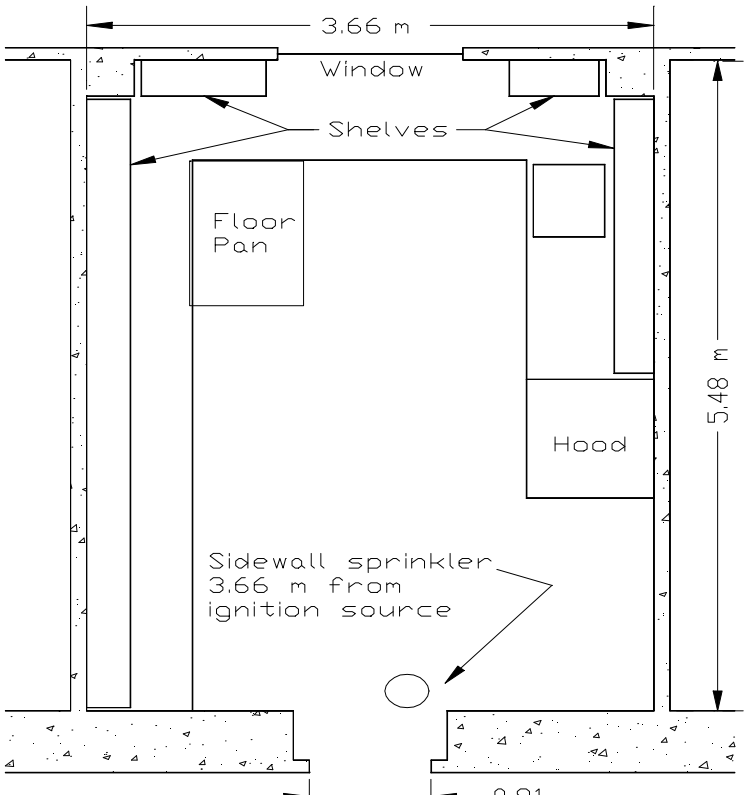

Figure 4 - Approximate sprinkler location for experiment number 4

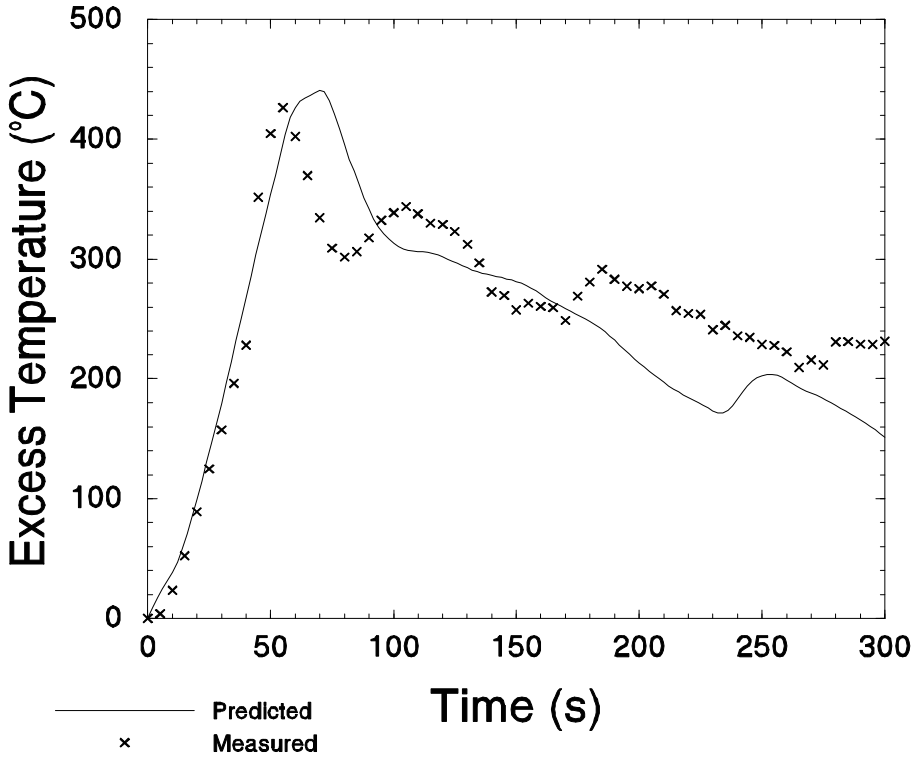

Figure 5 - Upper layer temperature - chemical laboratory experiments

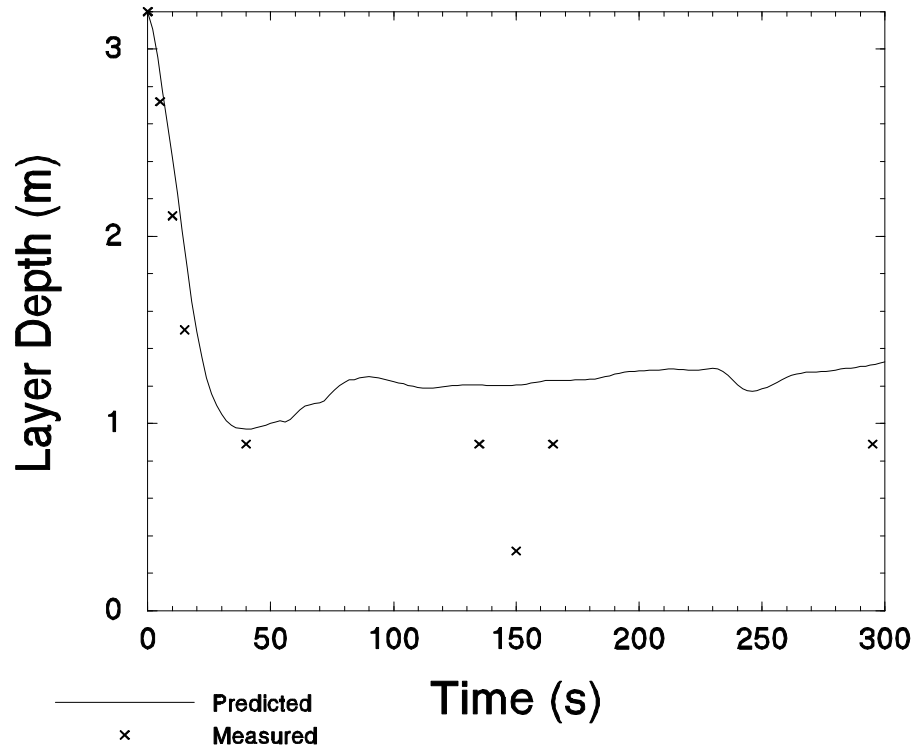

Figure 6 - Upper layer depth development - chemical laboratory experiments

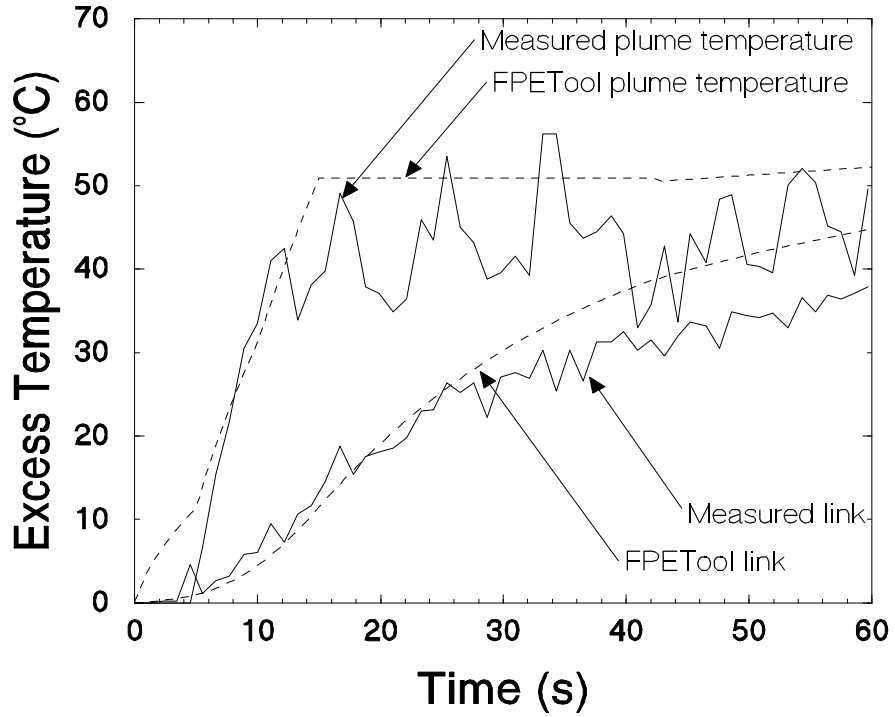

Figure 7 - Measured and predicted temperature increase for plume and detector link at 0.0 m - aircraft hanger experiments

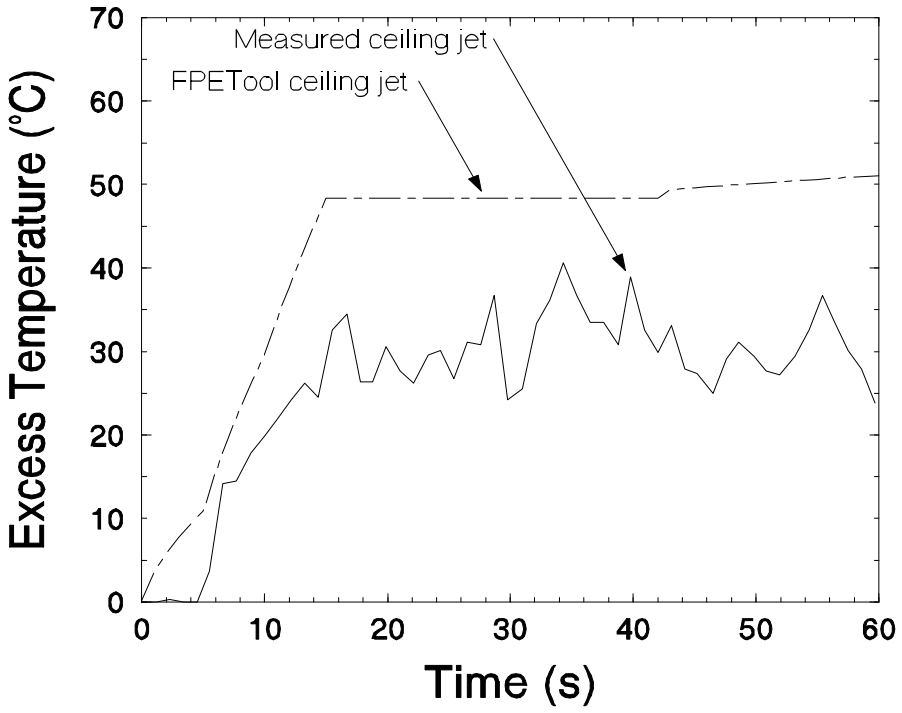

Figure 8 - Measured and predicted temperature increase for ceiling jet at 2.7 m - aircraft hanger experiments. Detector link not shown due to instrument malfunction

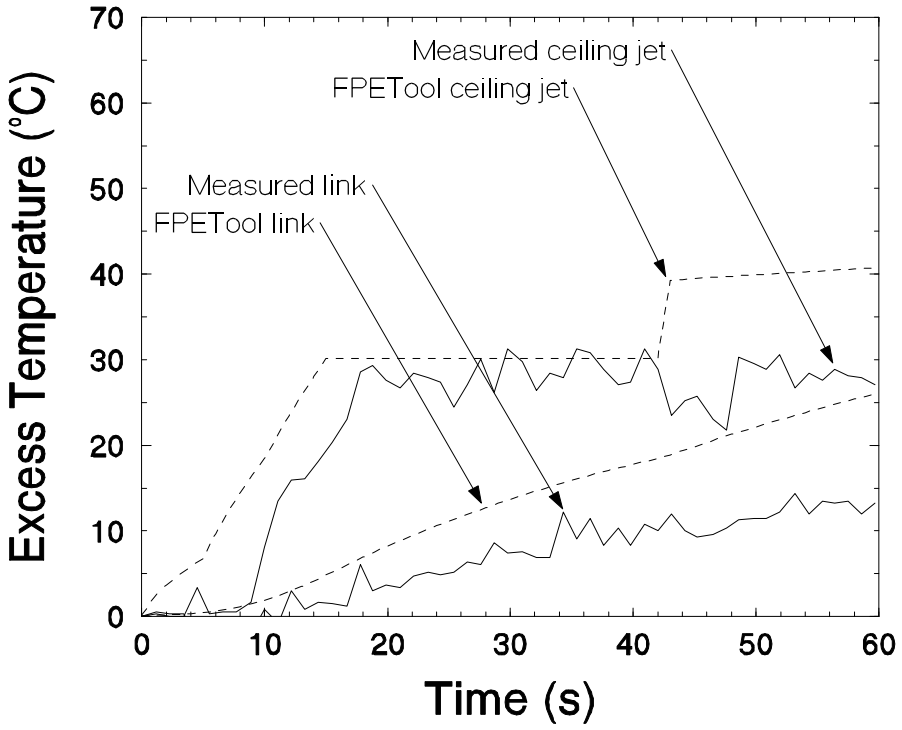

Figure 9 - Measured and predicted temperature increase for ceiling jet and detector link at 5.5 m - aircraft hanger experiments

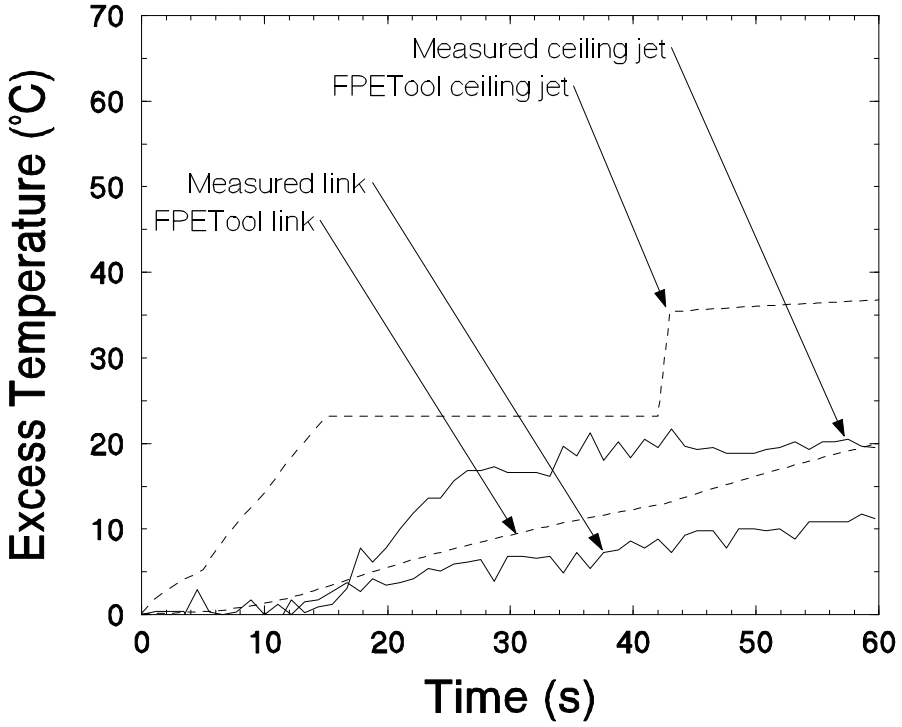

Figure 10 - Measured and predicted temperature increase for ceiling jet and detector link at 8.2 m - aircraft hanger experiments

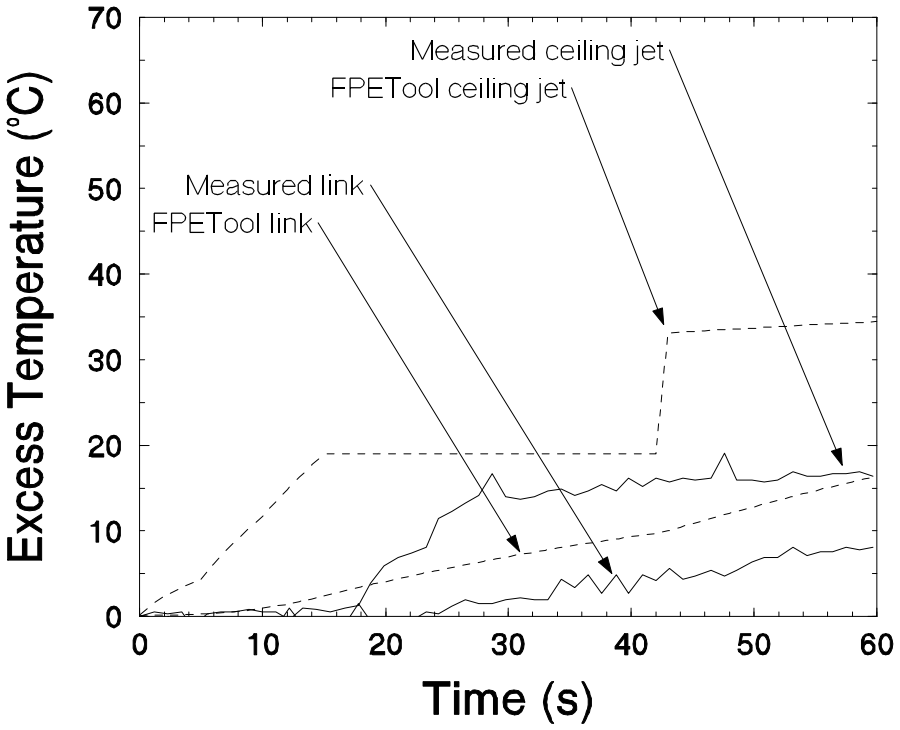

Figure 11 - Measured and predicted temperature increase for ceiling jet and detector link at 11.0 m - aircraft hanger experiments

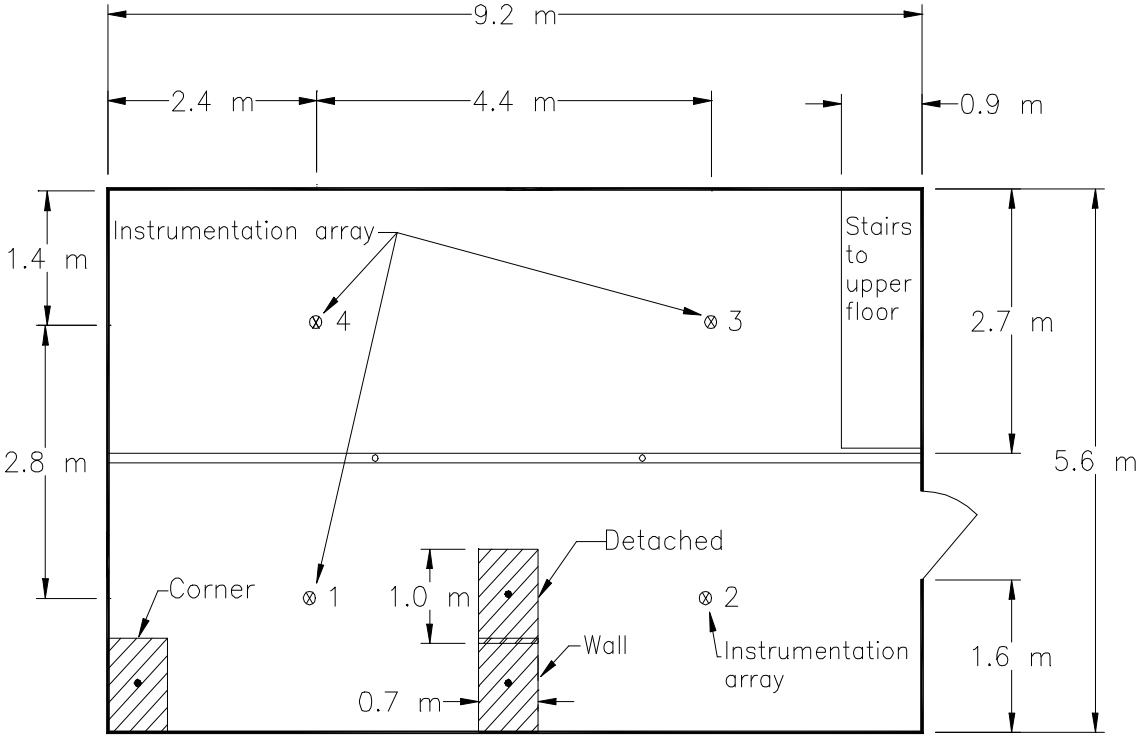

Figure 12 - Plan view - burner locations - residential sprinkler experiments

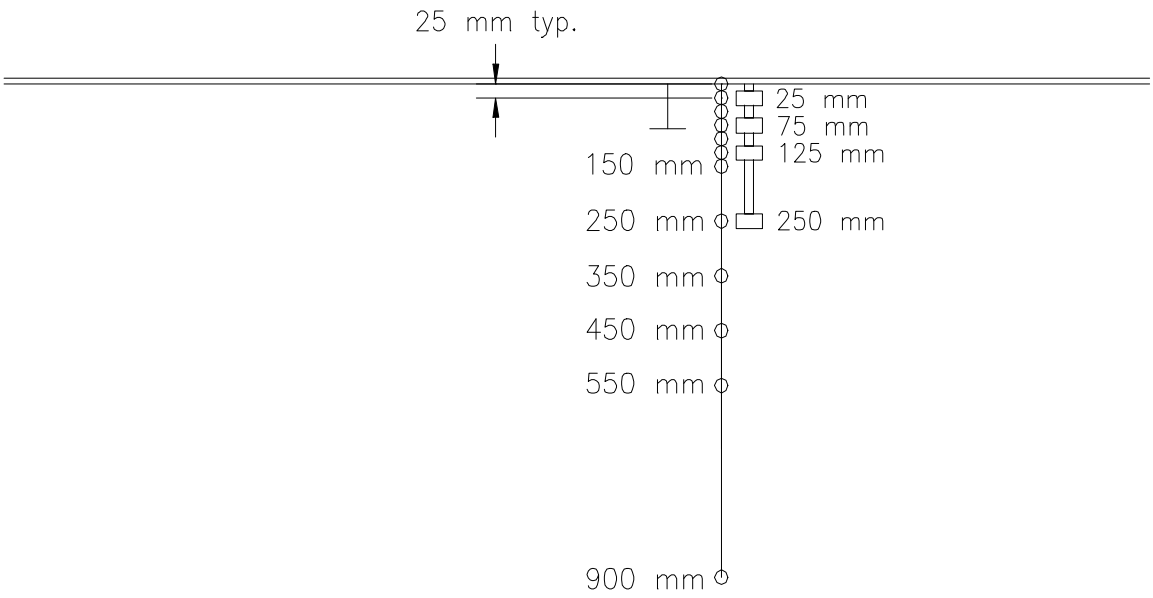

Figure 13 - Instrumentation set up for arrays 1 and 2

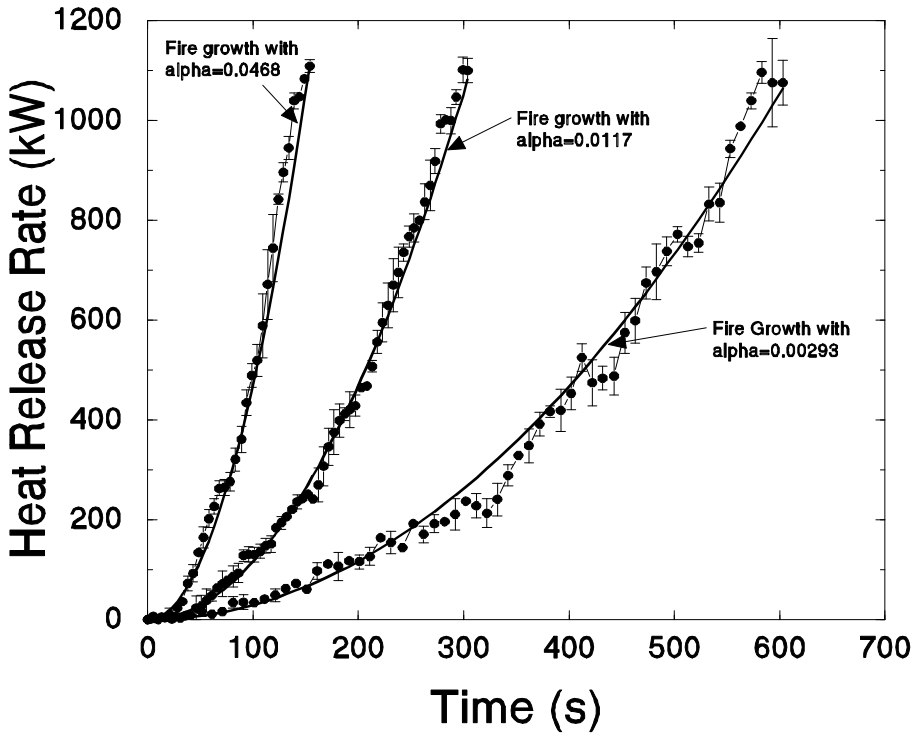

Figure 14 - Heat release rates for fast, medium, and slow fires. NFPA 72, 1993 edition

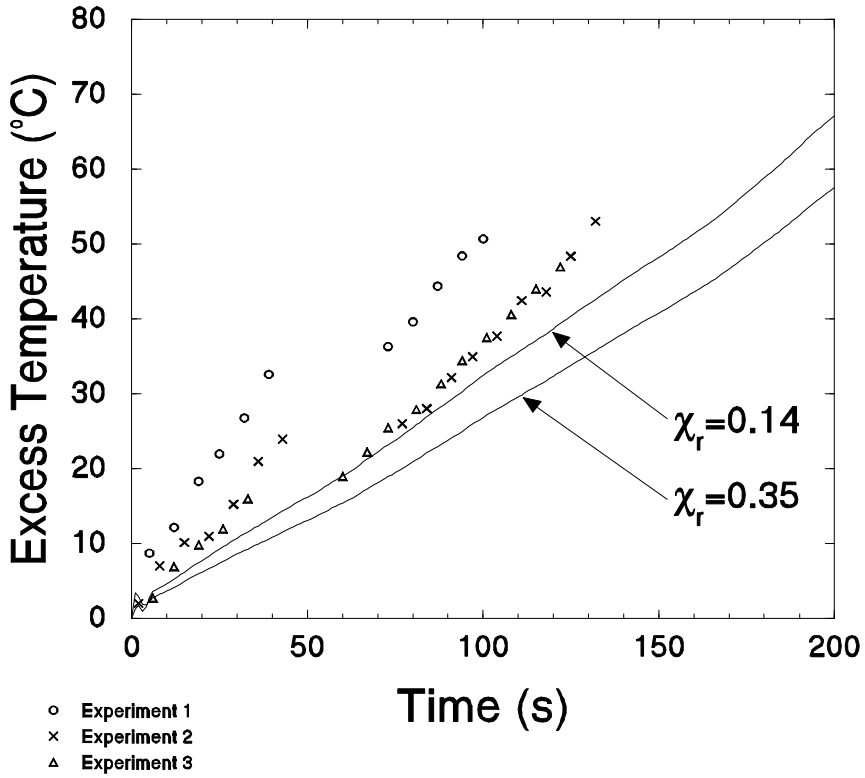

Figure 15 - Upper layer temperature increase - slow fire - detached burner - vent open

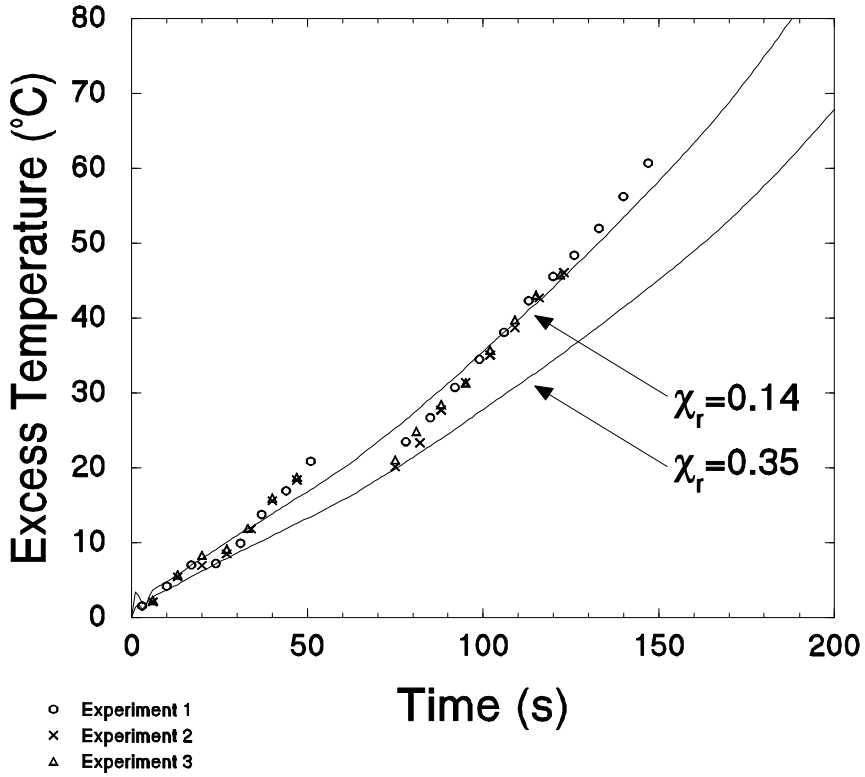

Figure 16 - Upper layer temperature increase - slow fire - detached burner - vent closed

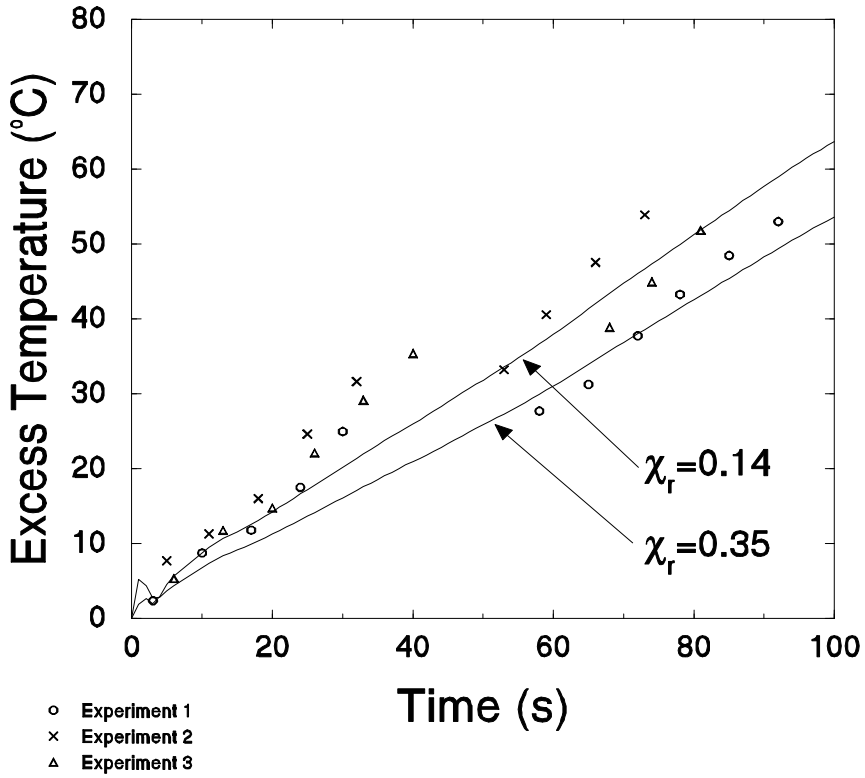

Figure 17 - Upper layer temperature increase - medium fire - detached burner - vent open

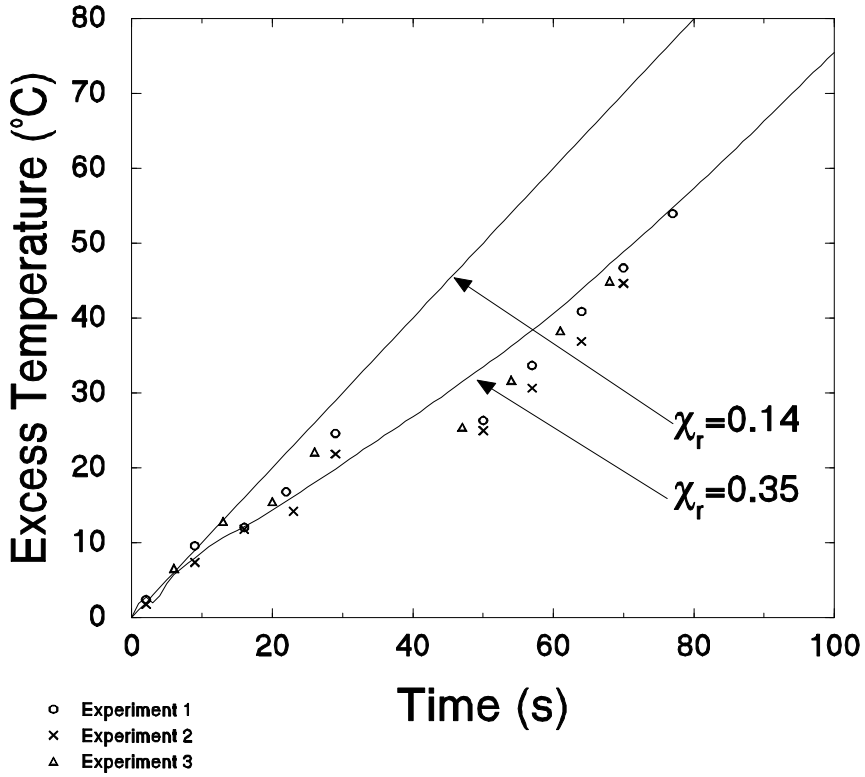

Figure 18 - Upper layer temperature increase - medium fire - detached burner - vent closed

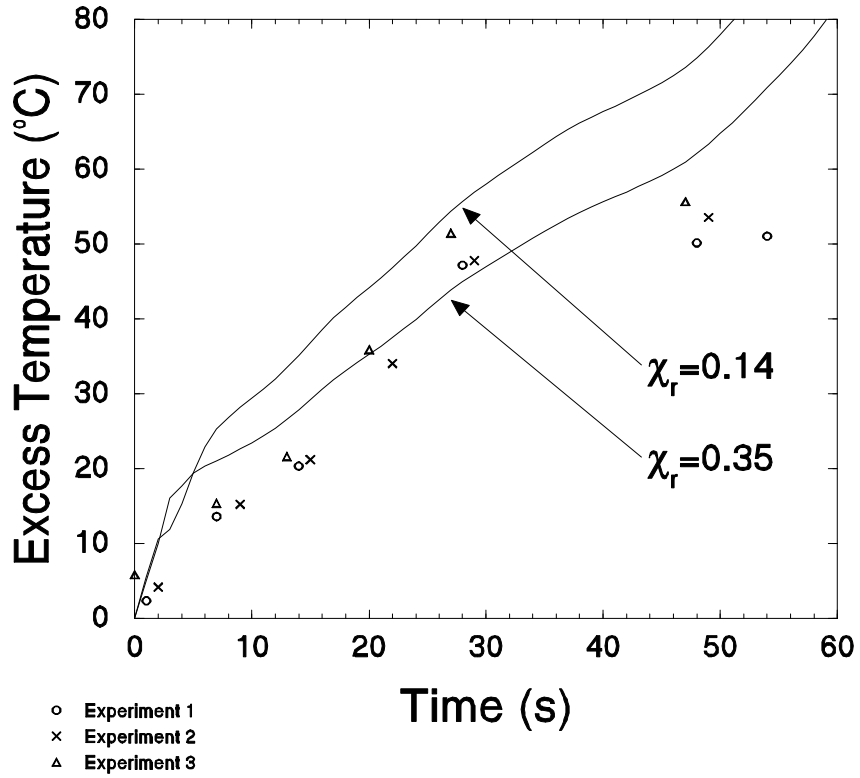

Figure 19 - Upper layer temperature increase - fast fire - detached burner - vent open

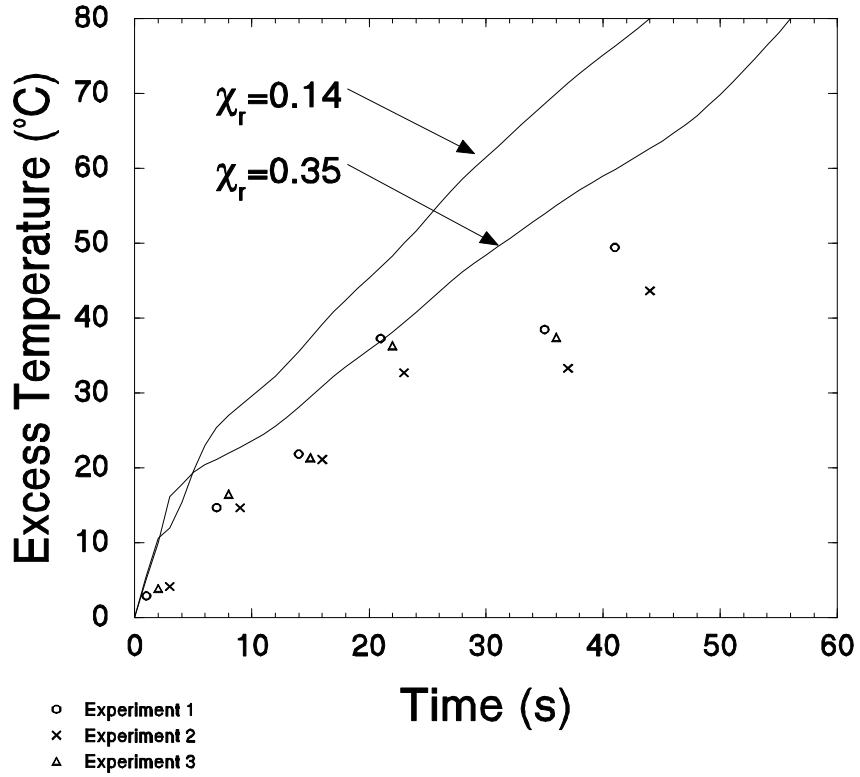

Figure 20 - Upper layer temperature increase - fast fire - detached burner - vent closed

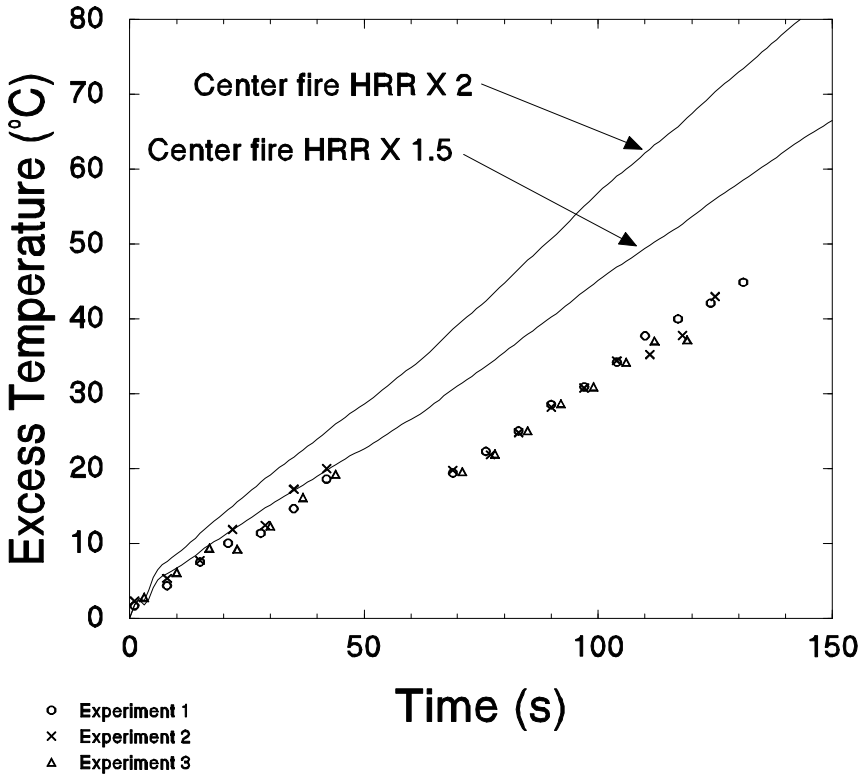

Figure 21 - Upper layer temperature increase - slow fire - burner against wall - vent open

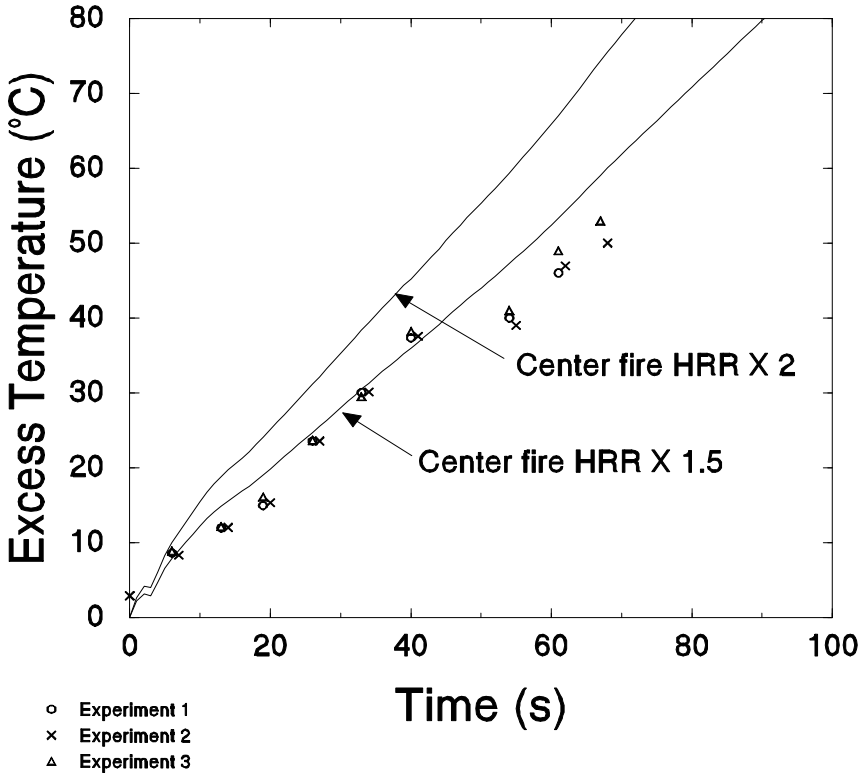

Figure 22 - Upper layer temperature increase - medium fire - burner against wall - vent open

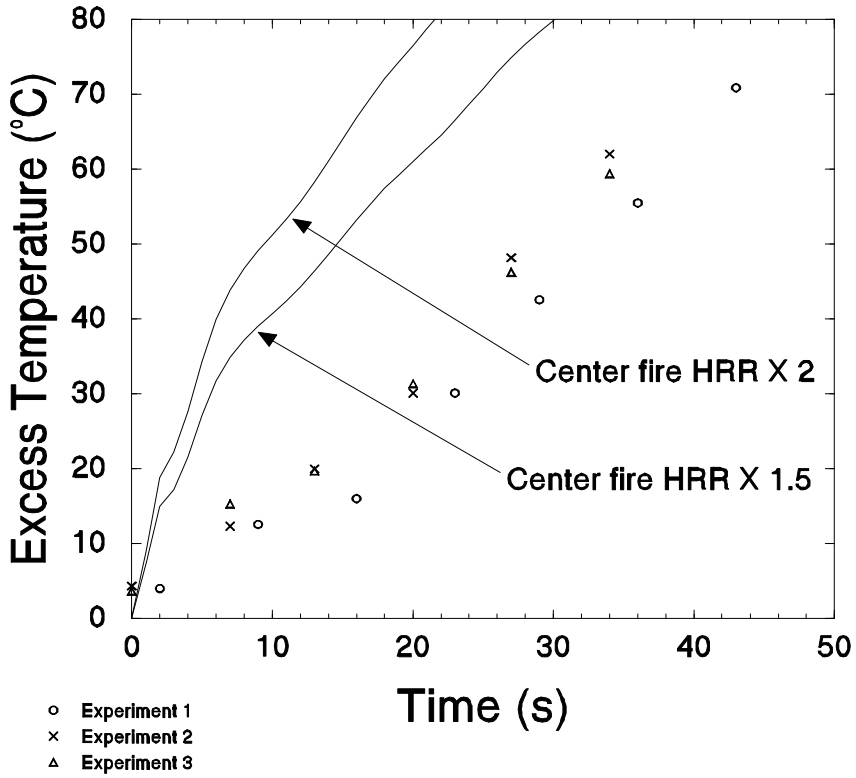

Figure 23 - Upper layer temperature increase - fast fire - burner against wall - vent open

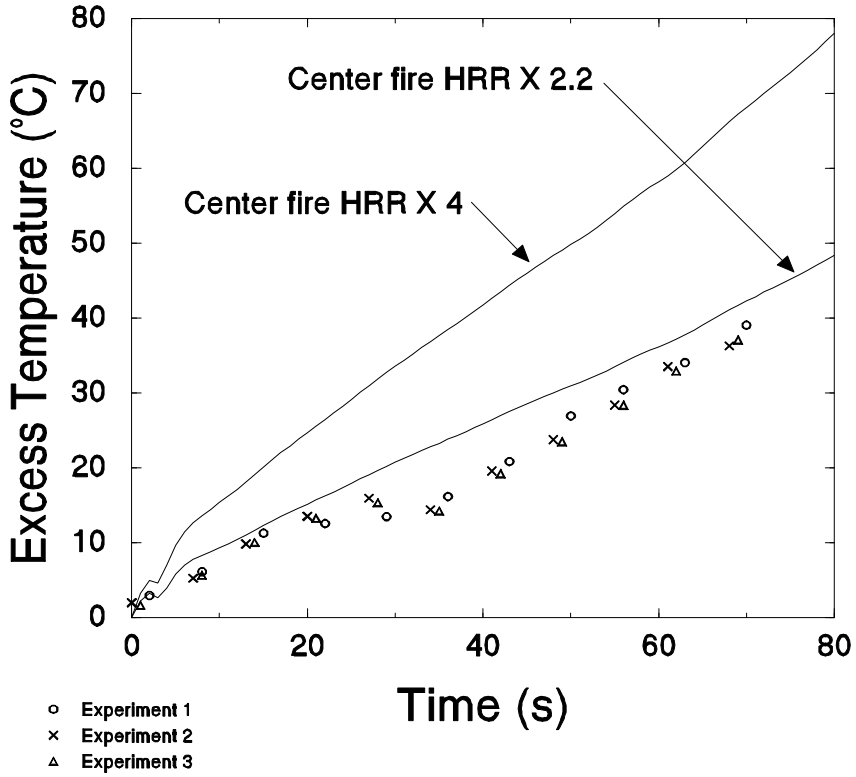

Figure 24 - Upper layer temperature increase - slow fire - burner in corner - vent open

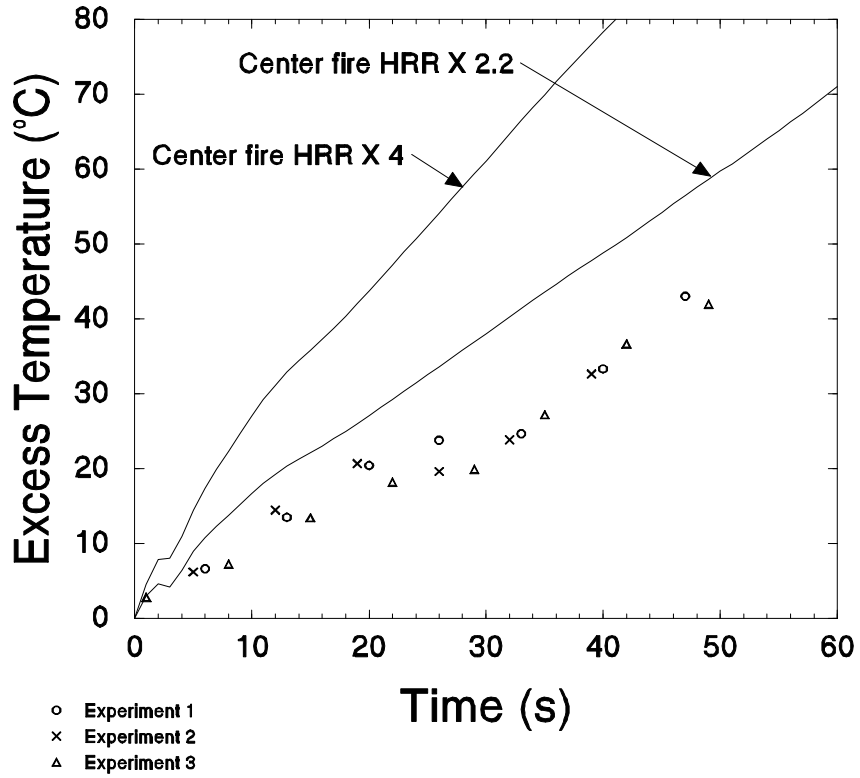

Figure 25 - Upper layer temperature increase - medium fire - burner in corner - vent open

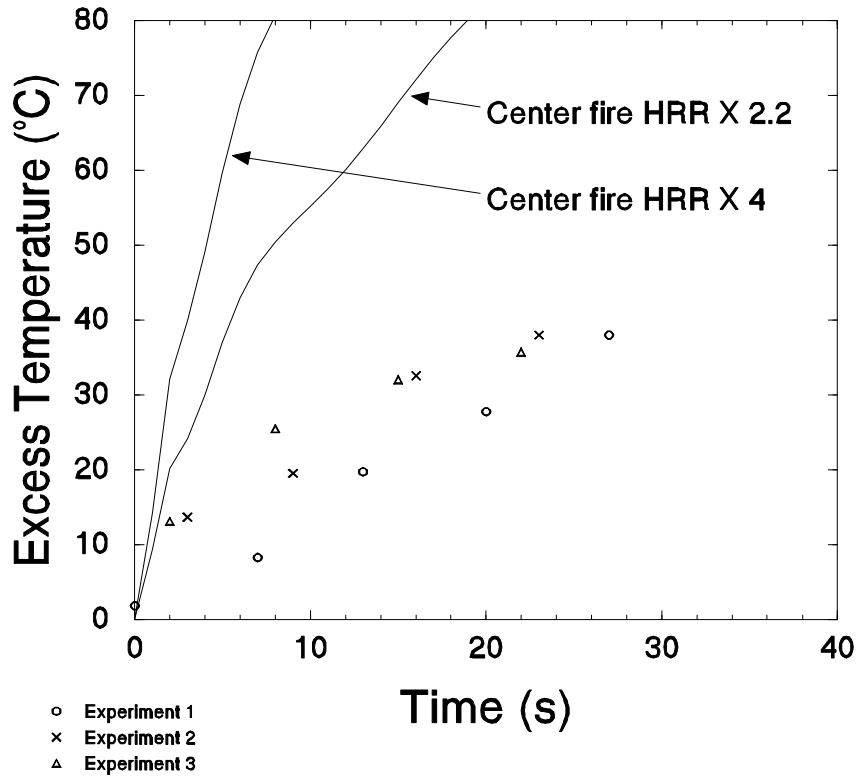

Figure 26 - Upper layer temperature increase - fast fire - burner in corner - vent open

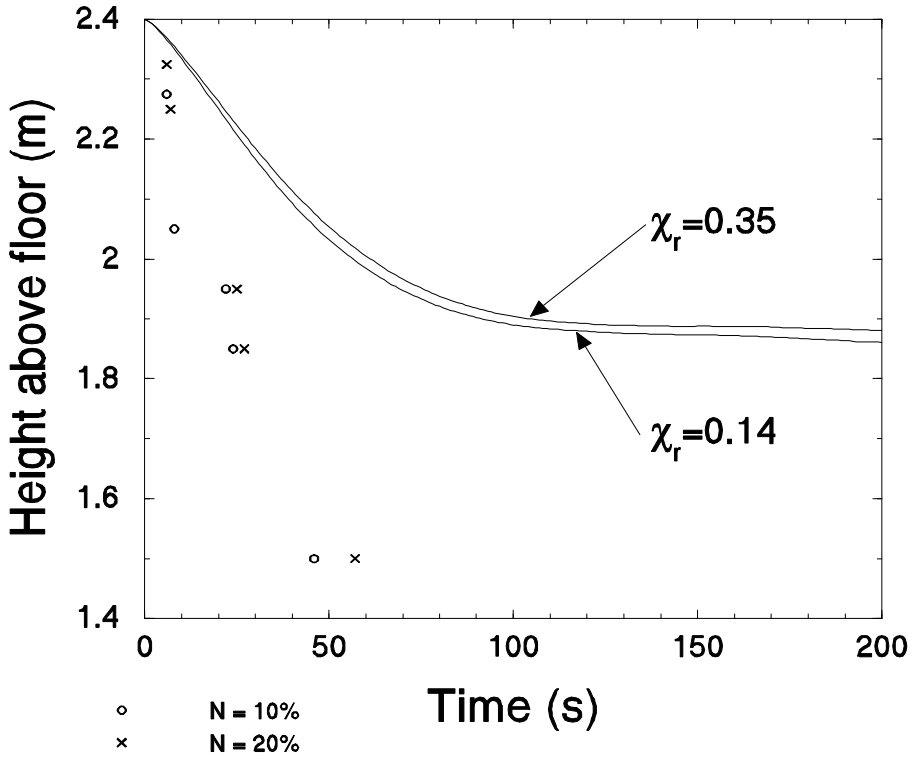

Figure 27 - Upper layer development - slow fire - detached burner - vent open

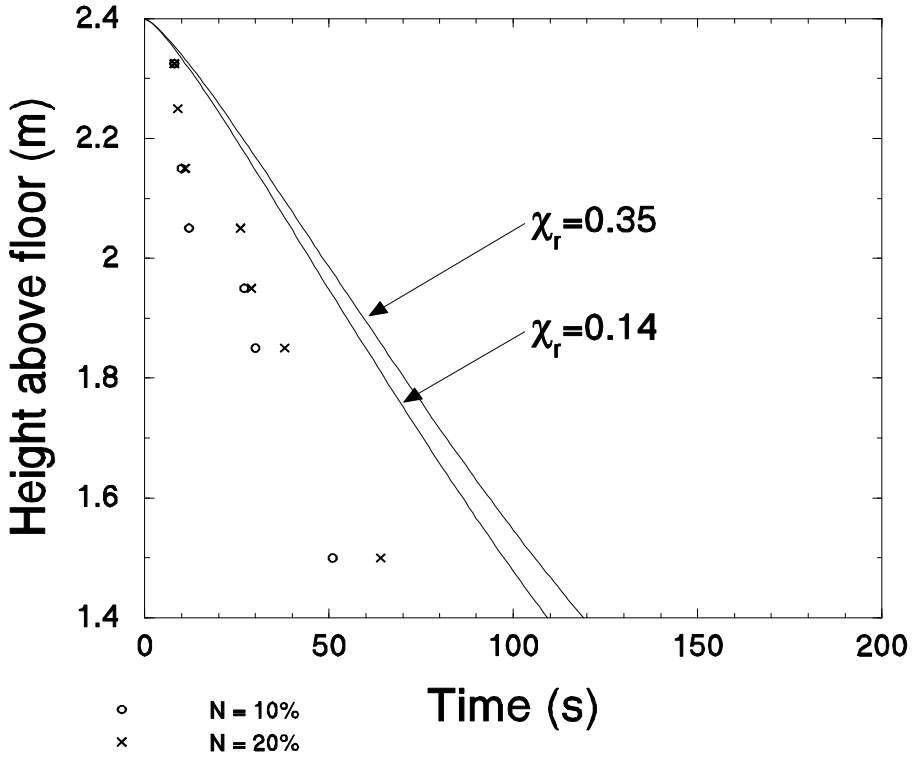

Figure 28 - Upper layer development - slow fire - detached burner - vent closed

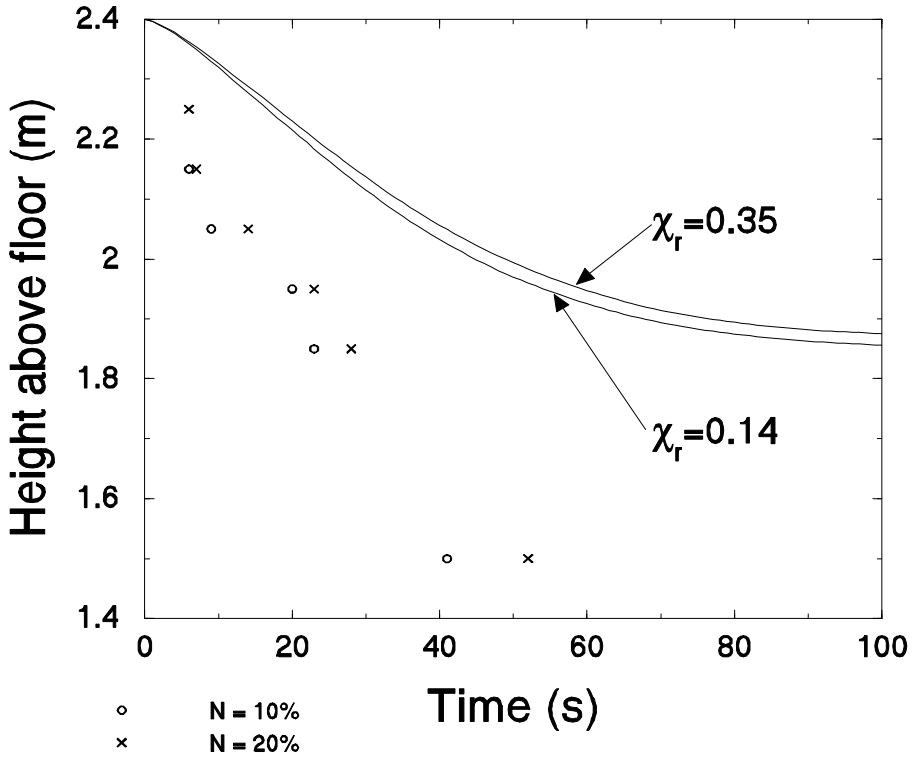

Figure 29 - Upper layer development - medium fire - detached burner - vent open

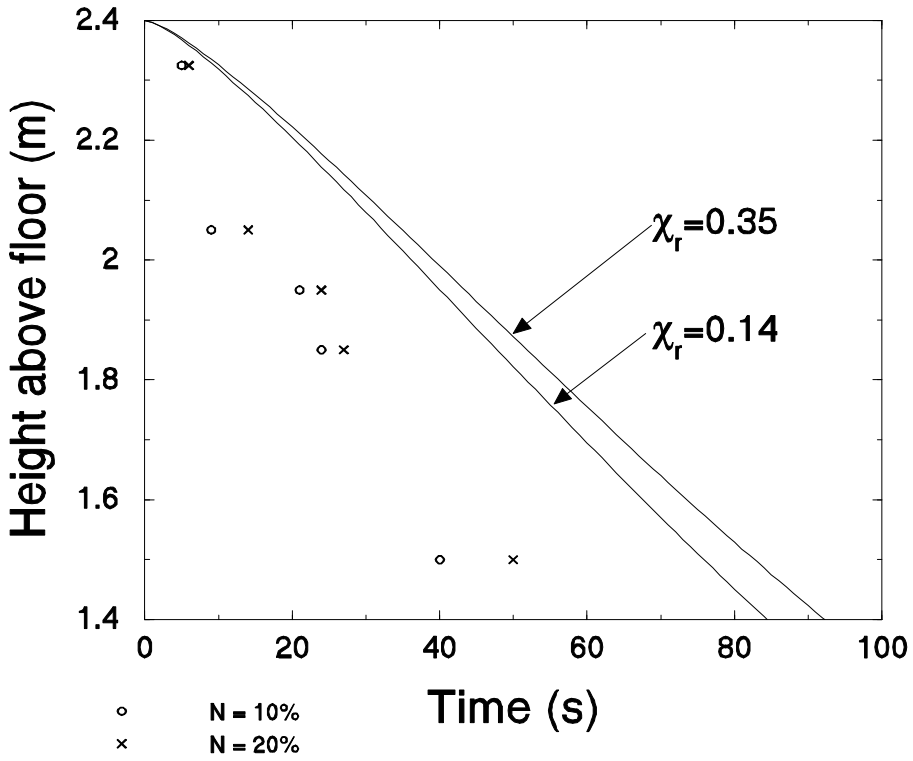

Figure 30 - Upper layer development - medium fire - burner detached - vent closed

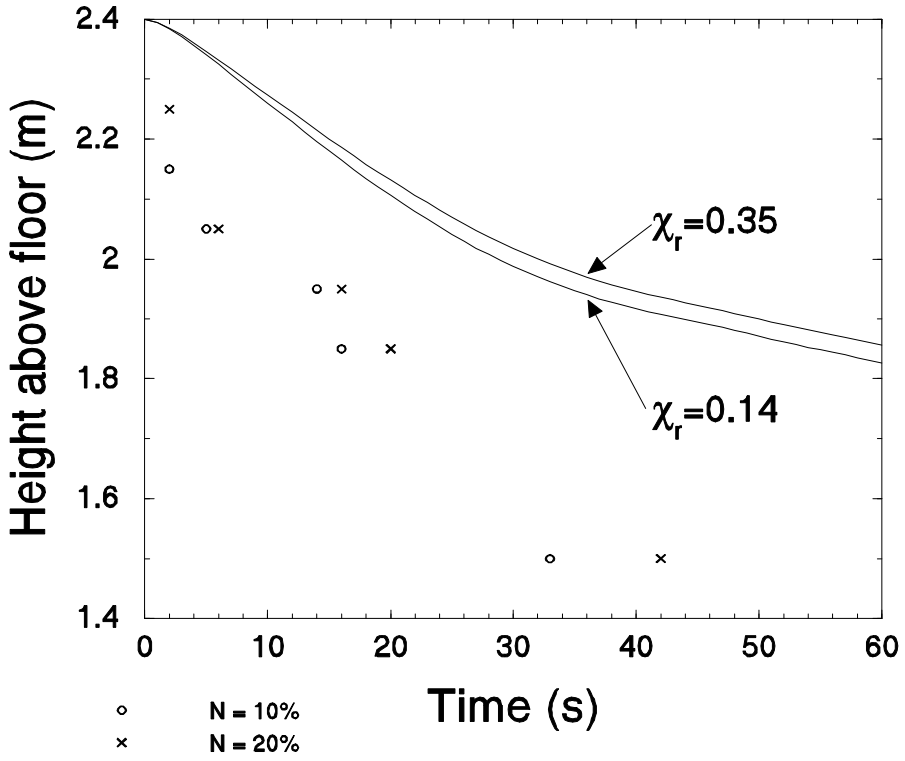

Figure 31 - Upper layer development - fast fire - burner detached - vent open

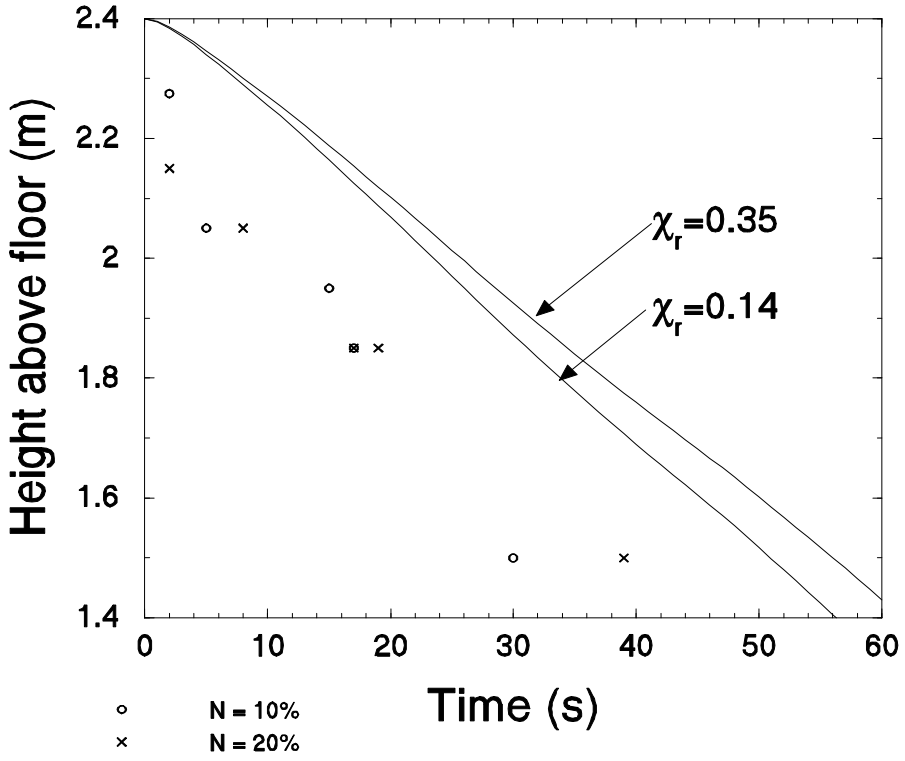

Figure 32 - Upper layer development - fast fire - burner detached - vent closed

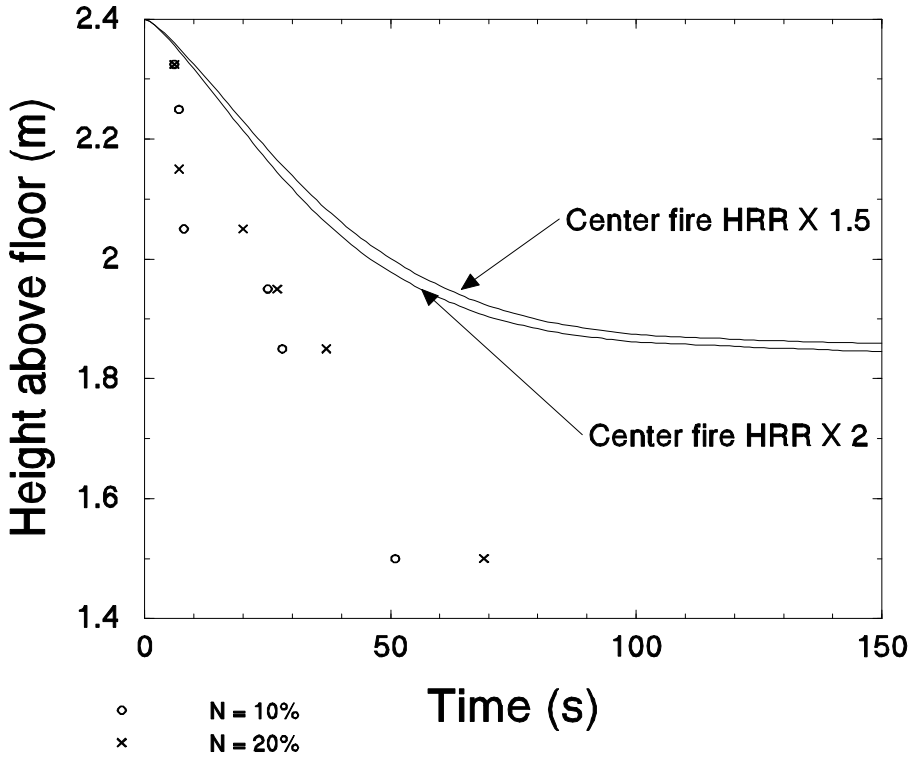

Figure 33 - Upper layer development - slow fire - burner against wall - vent open

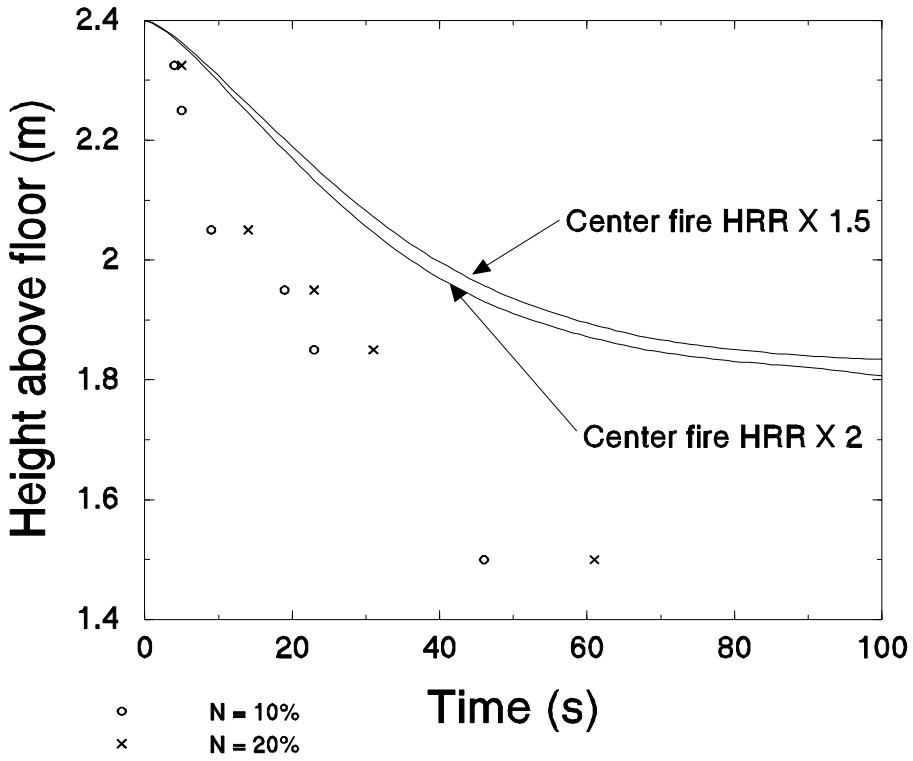

Figure 34 - Upper layer development - medium fire - burner against wall - vent open

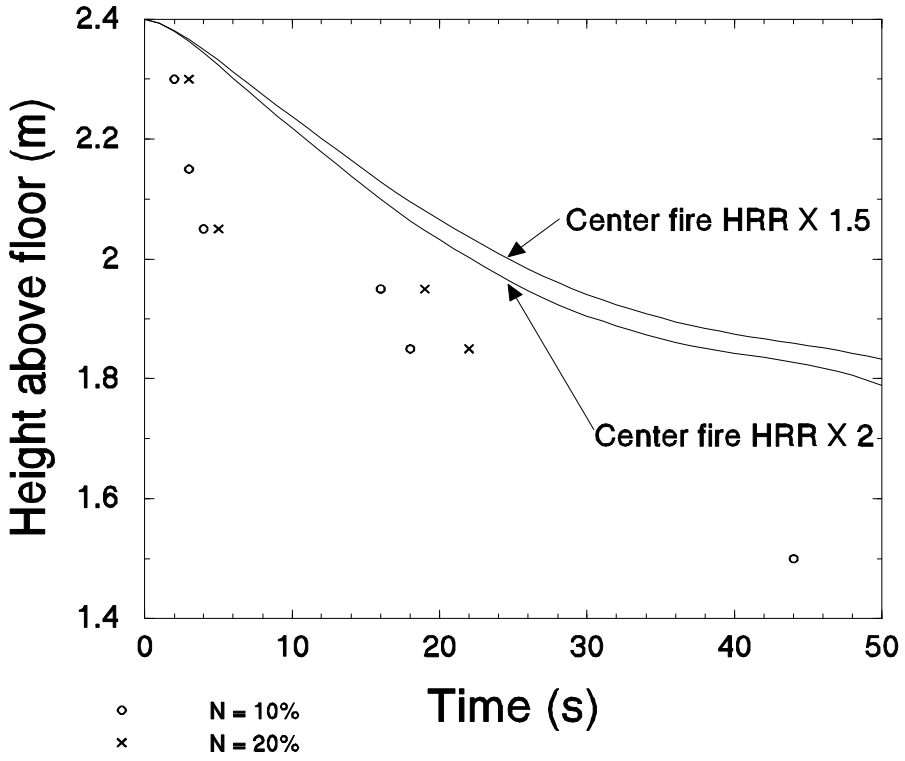

Figure 35 - Upper layer development - fast fire - burner against wall - vent open

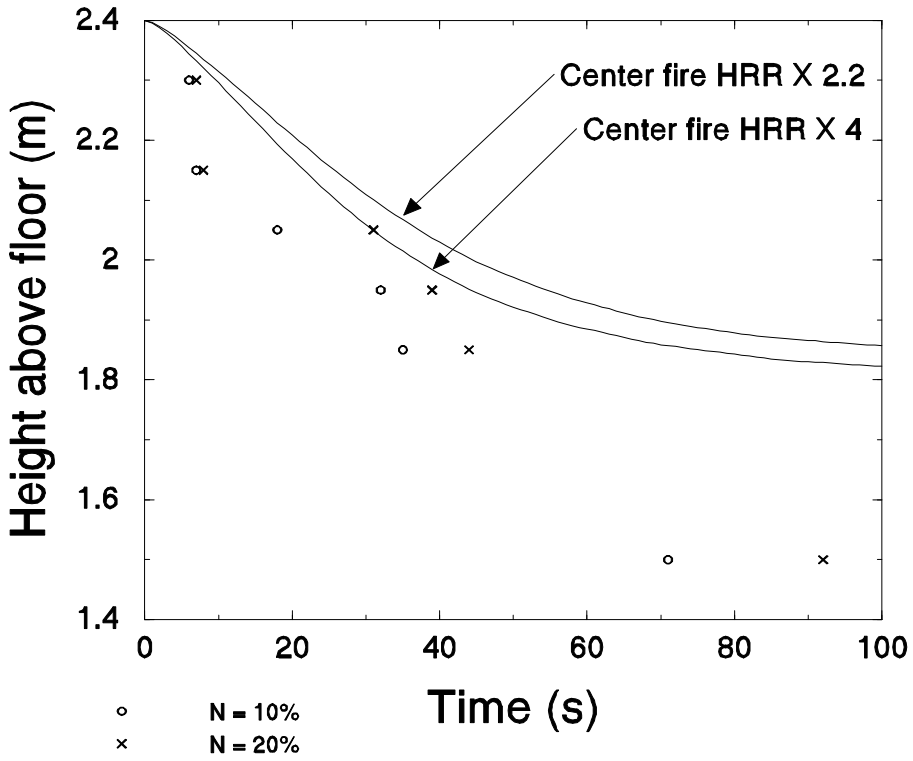

Figure 36 - Upper layer development - slow fire - burner in corner - vent open

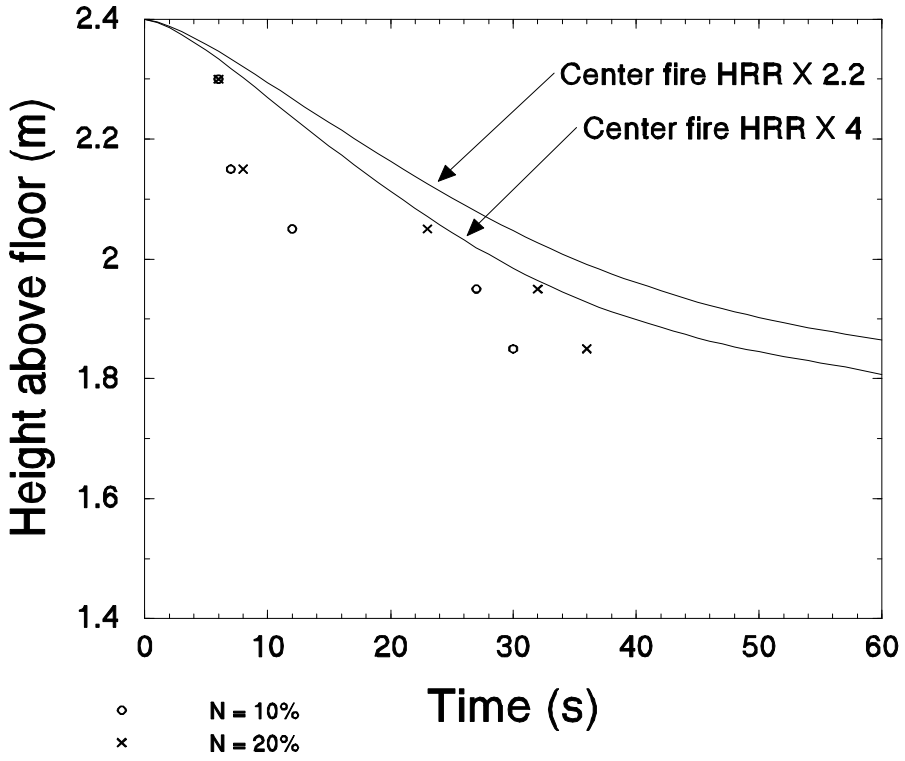

Figure 37 - Upper layer development - medium fire - burner in corner - vent open

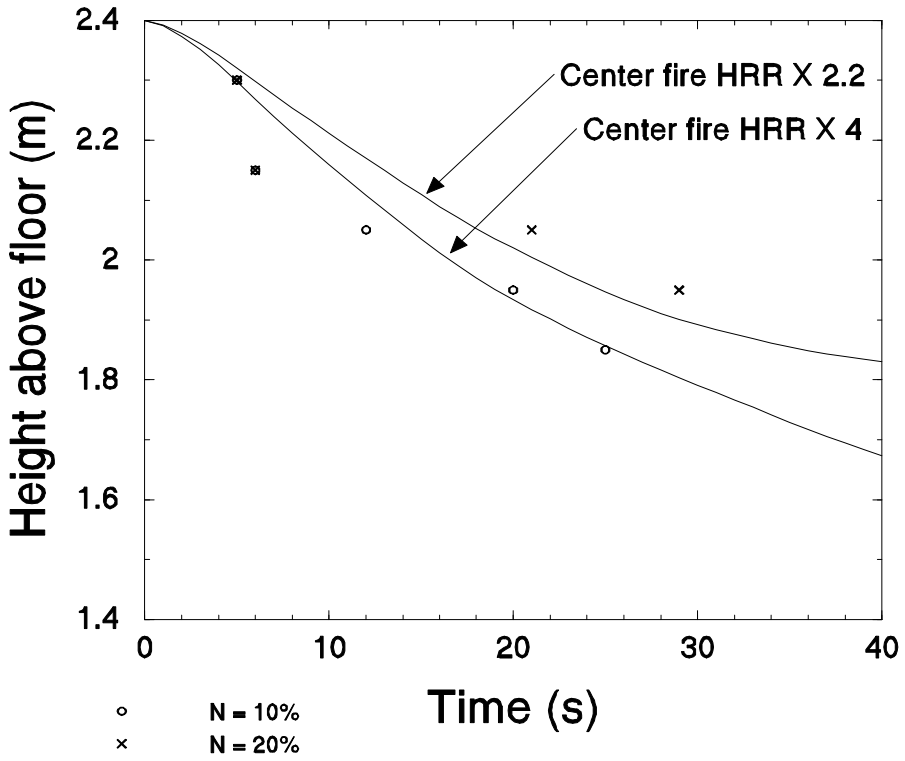

Figure 38 - Upper layer development - fast fire - burner in corner - vent open

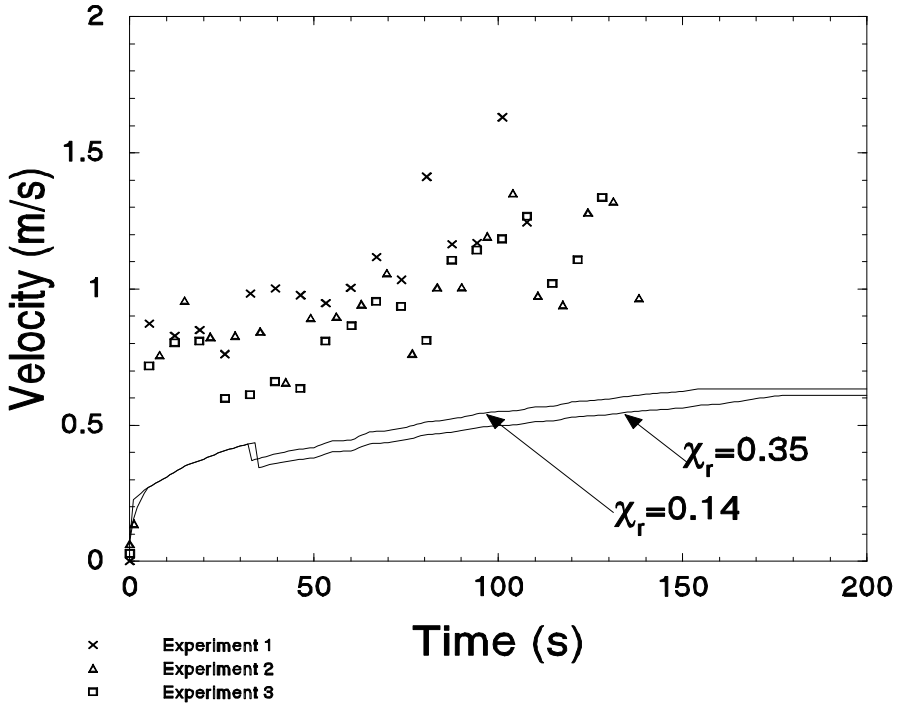

Figure 39 - Velocity measurements - slow fire - detached burner - vent open

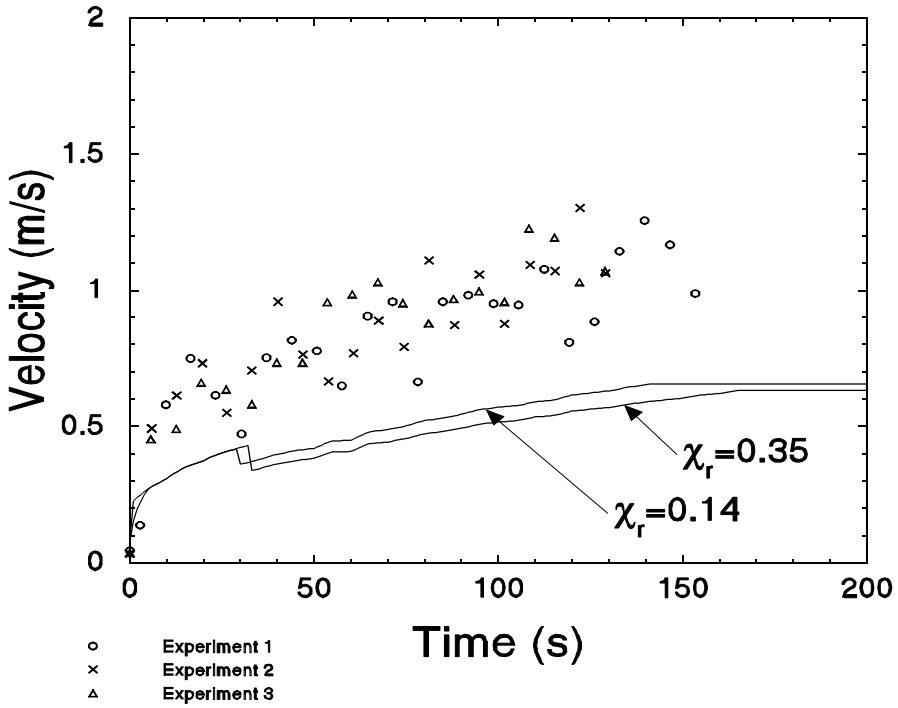

Figure 40 - Velocity measurements - slow fire - detached burner - vent closed

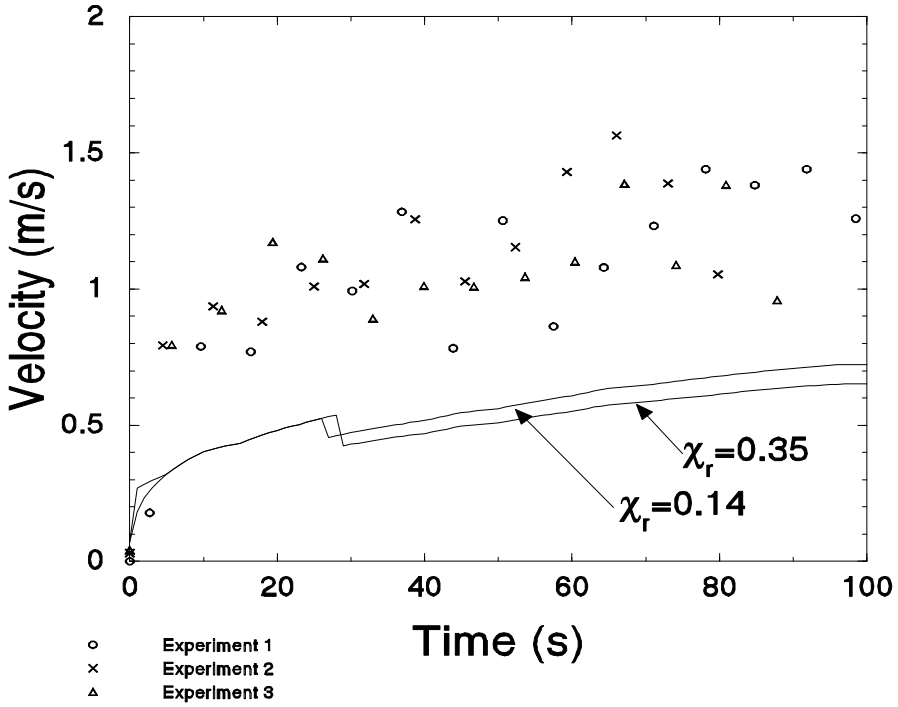

Figure 41 - Velocity measurements - medium fire - detached burner - vent open

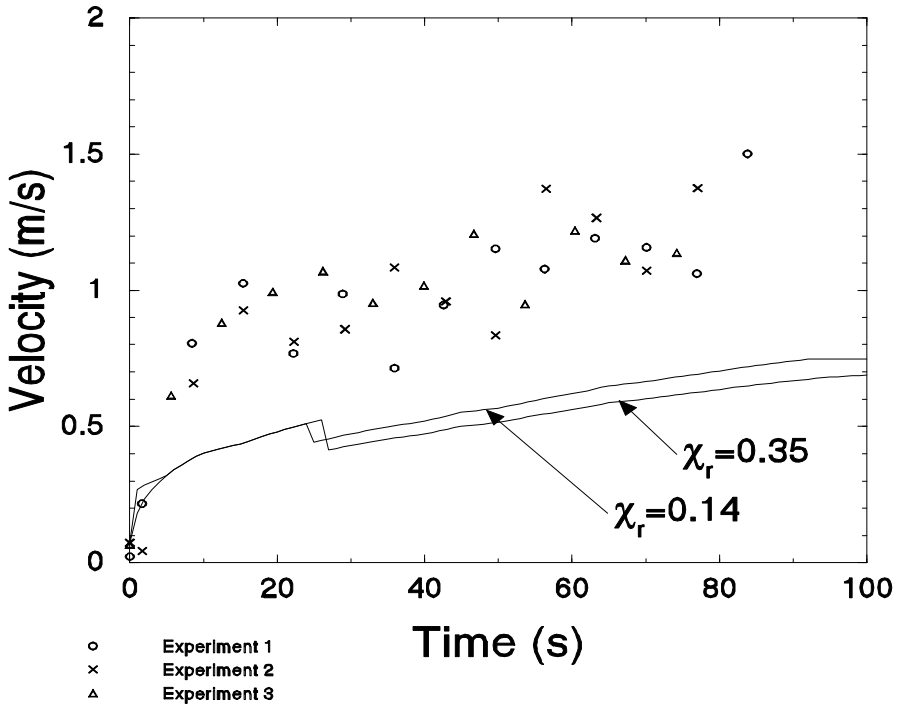

Figure 42 - Velocity measurements - medium fire - detached burner - vent closed

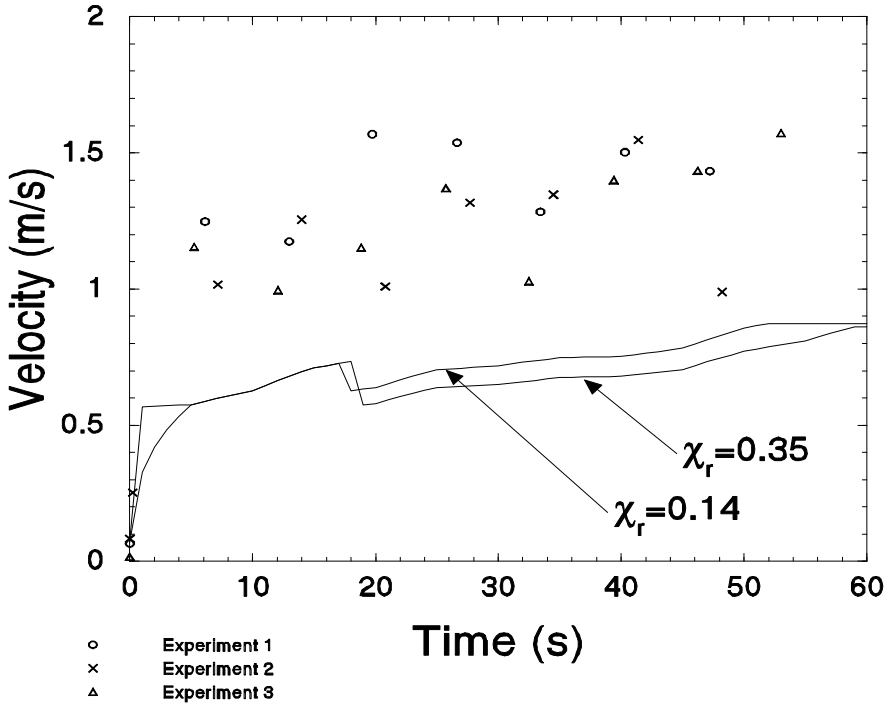

Figure 43 - Velocity measurements - fast fire - detached burner - vent open

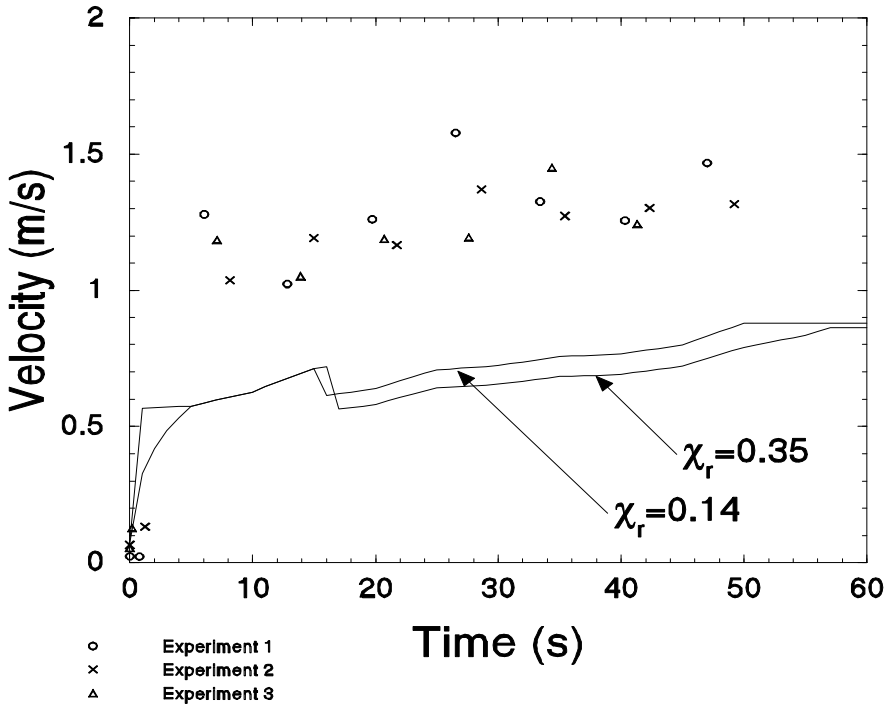

Figure 44 - Velocity measurements - fast fire - detached burner - vent closed

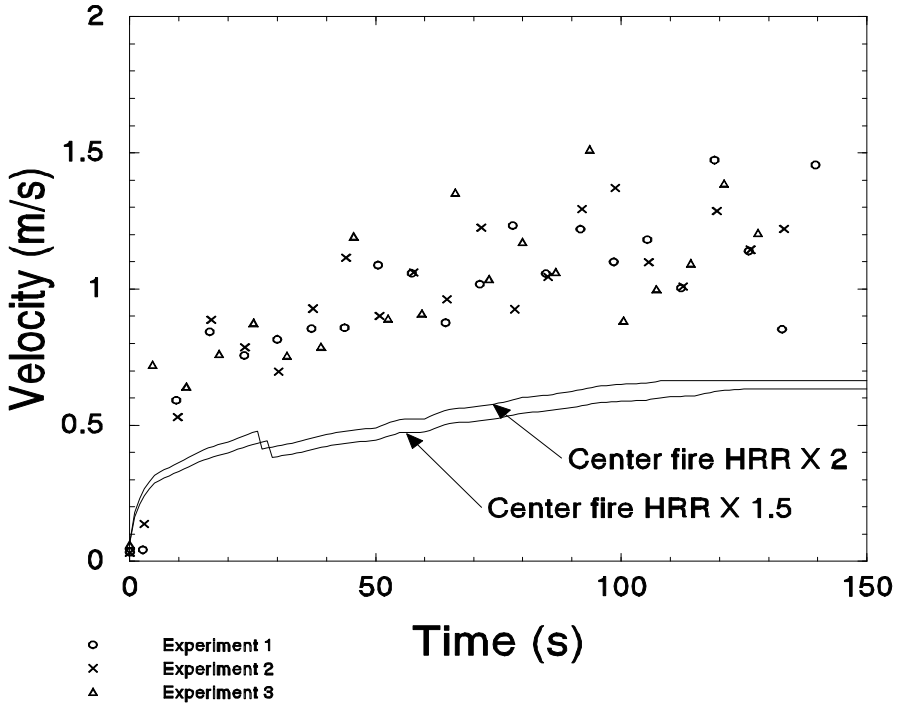

Figure 45 - Velocity measurements - slow fire - burner against wall - vent open

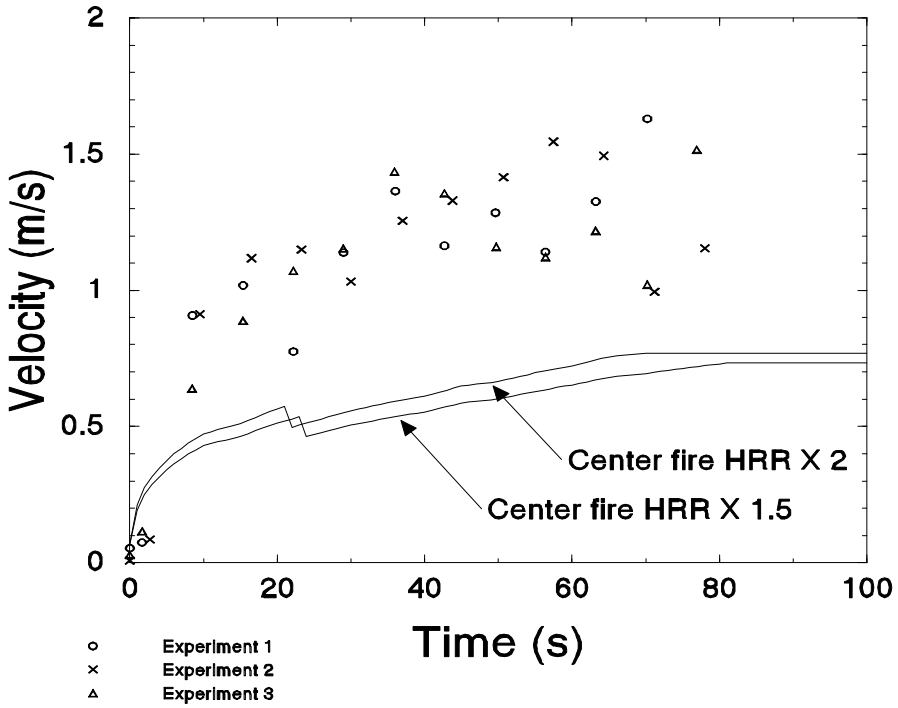

Figure 46 - Velocity measurements - medium fire - burner against wall - vent open

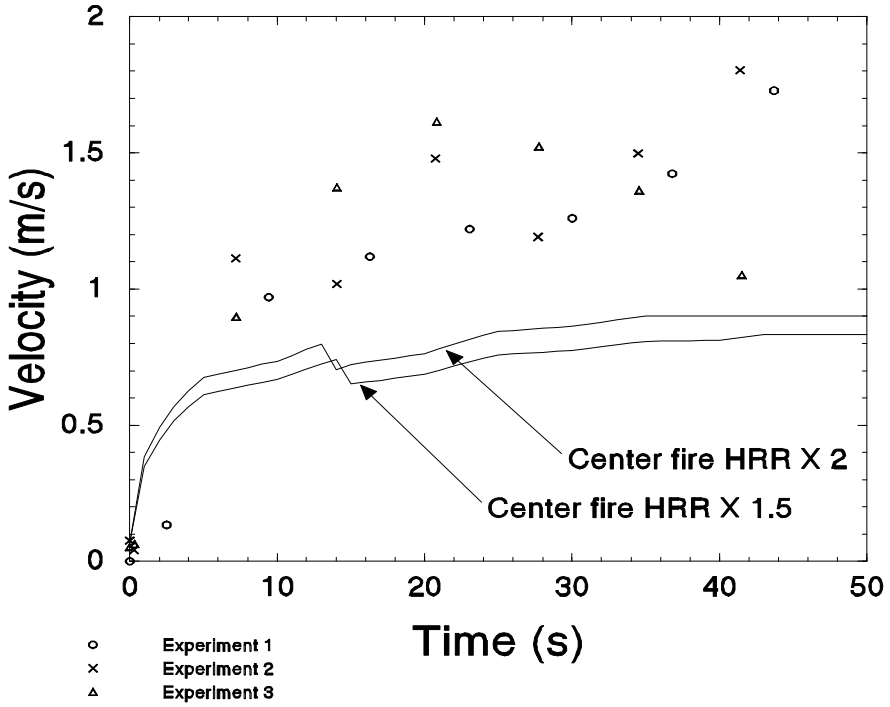

Figure 47 - Velocity measurements - fast fire - burner against wall - vent open

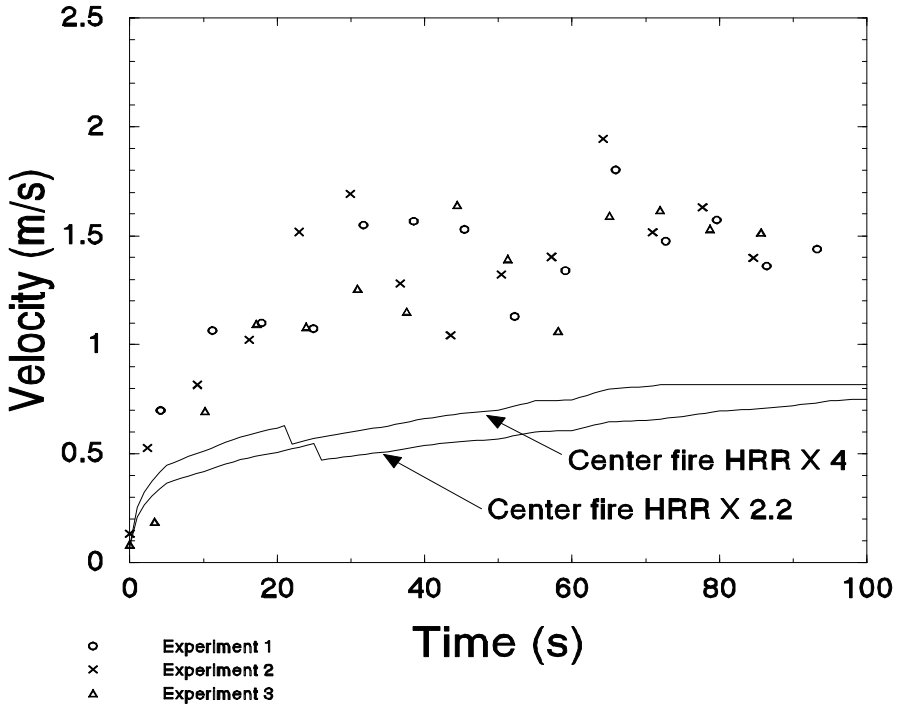

Figure 48 - Velocity measurements - slow fire - burner in corner - vent open

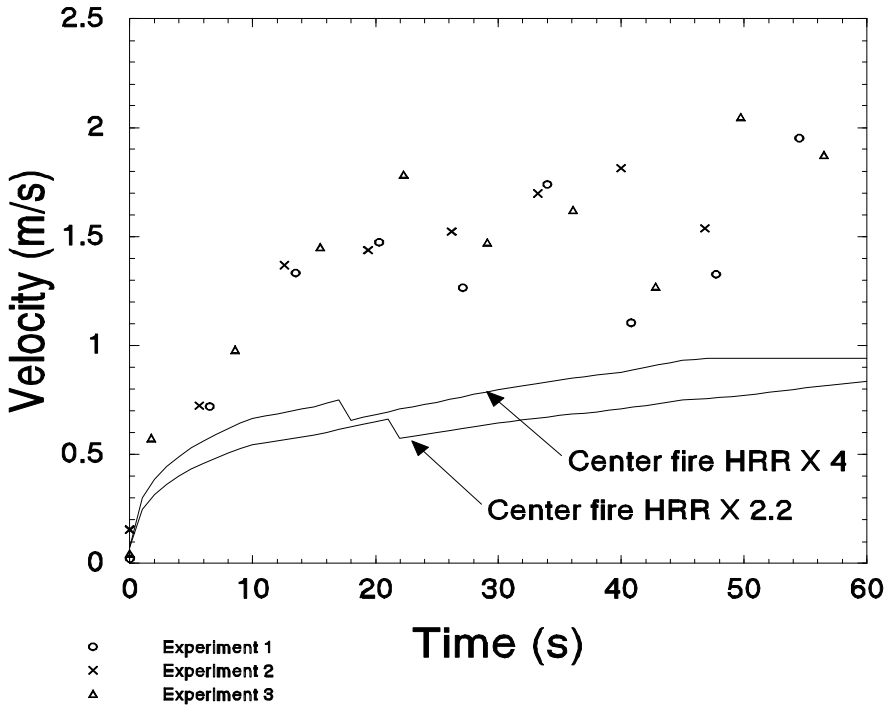

Figure 49 - Velocity measurements - medium fire - burner in corner - vent open

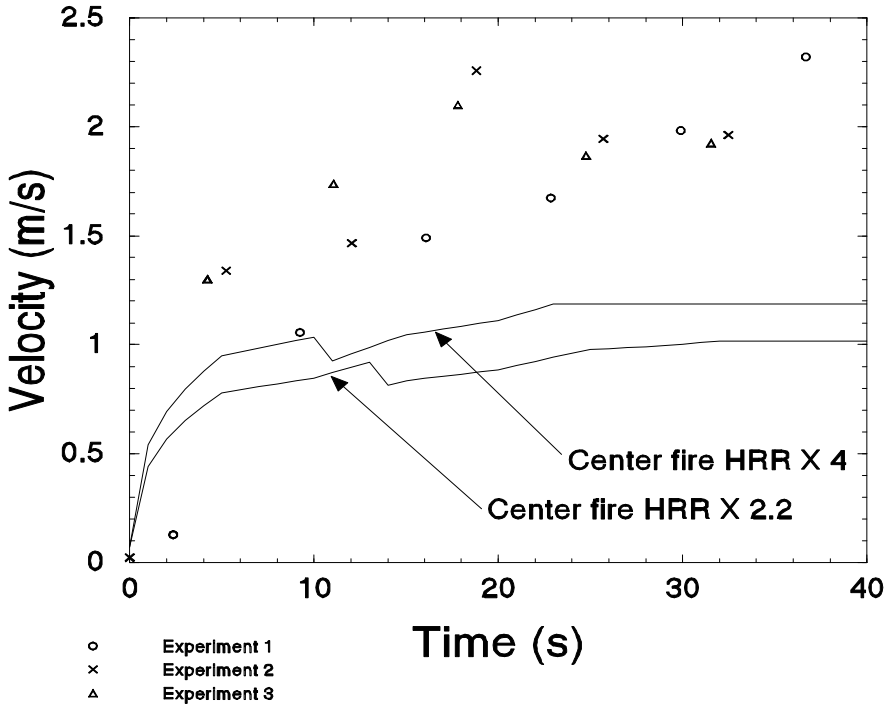

Figure 50 - Velocity measurements - fast fire - burner in corner - vent open

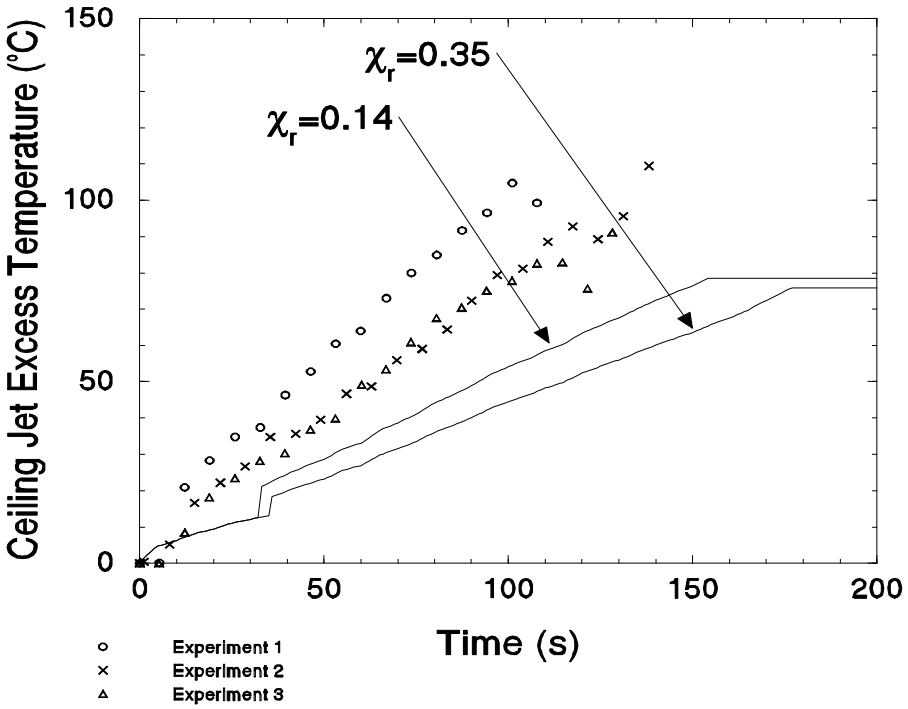

Figure 51 - Ceiling jet temperature increase - slow fire - detached burner - vent open

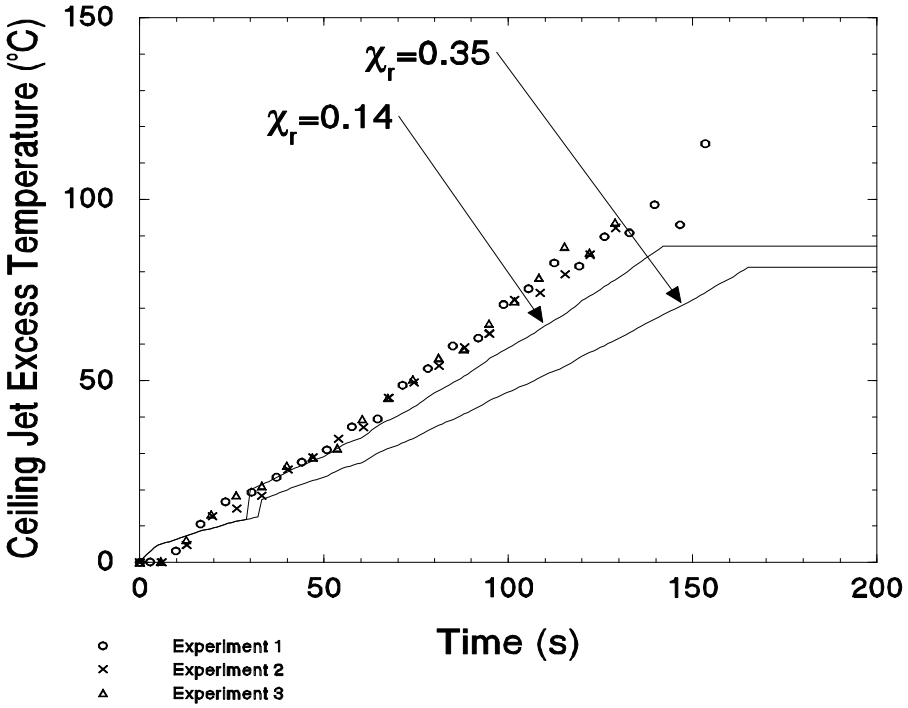

Figure 52 - Ceiling jet temperature increase - slow fire - detached burner - vent closed

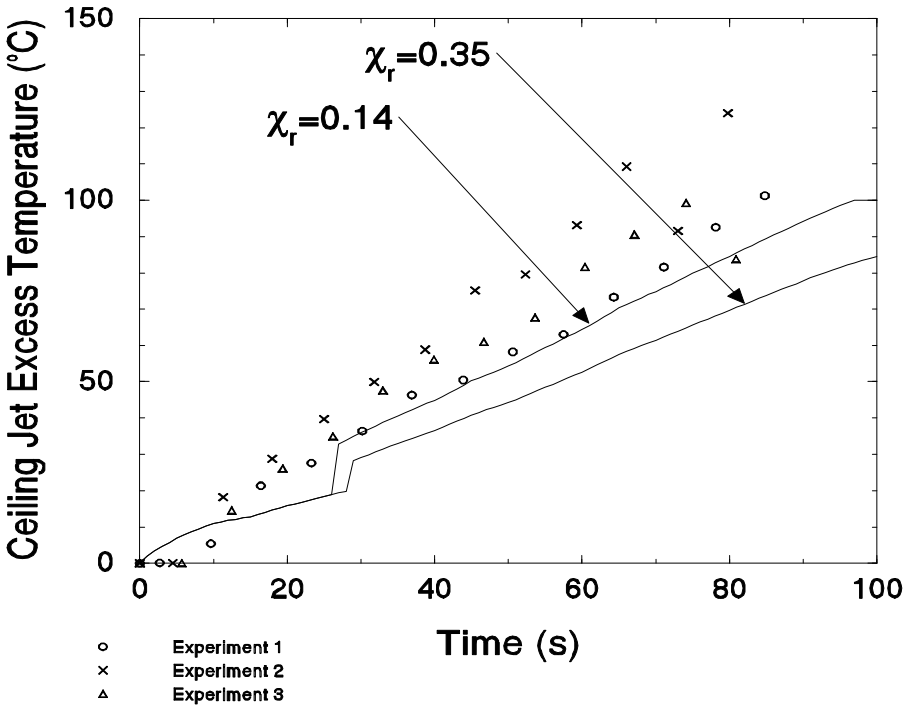

Figure 53 - Ceiling jet temperature increase - medium fire - detached burner - vent open

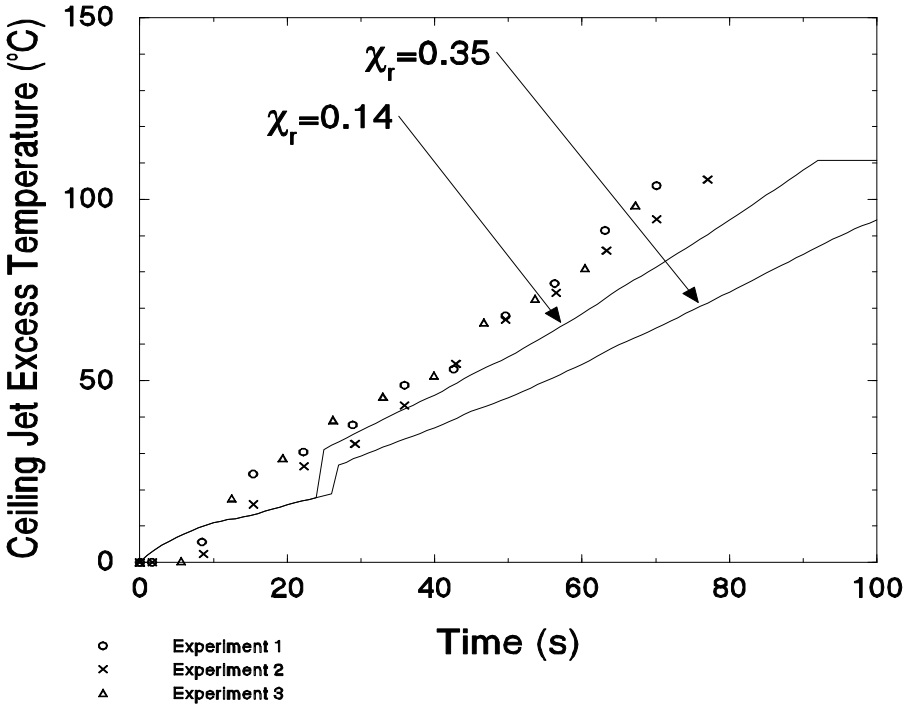

Figure 54 - Ceiling jet temperature increase - medium fire - detached burner - vent closed

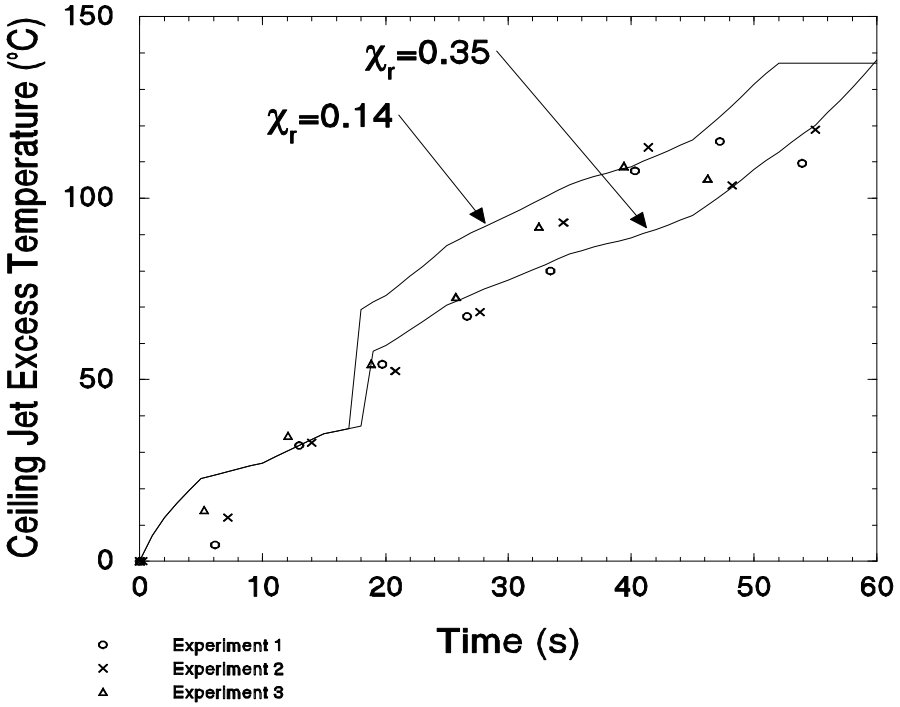

Figure 55 - Ceiling jet temperature increase - fast fire - detached burner - vent open

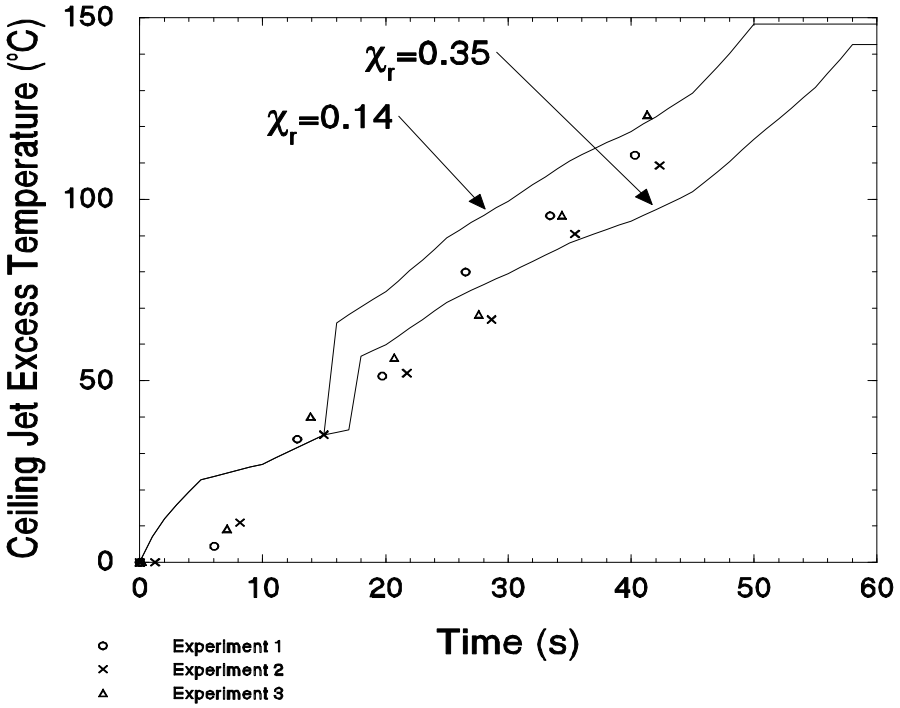

Figure 56 - Ceiling jet temperature increase - fast fire - detached burner - vent closed

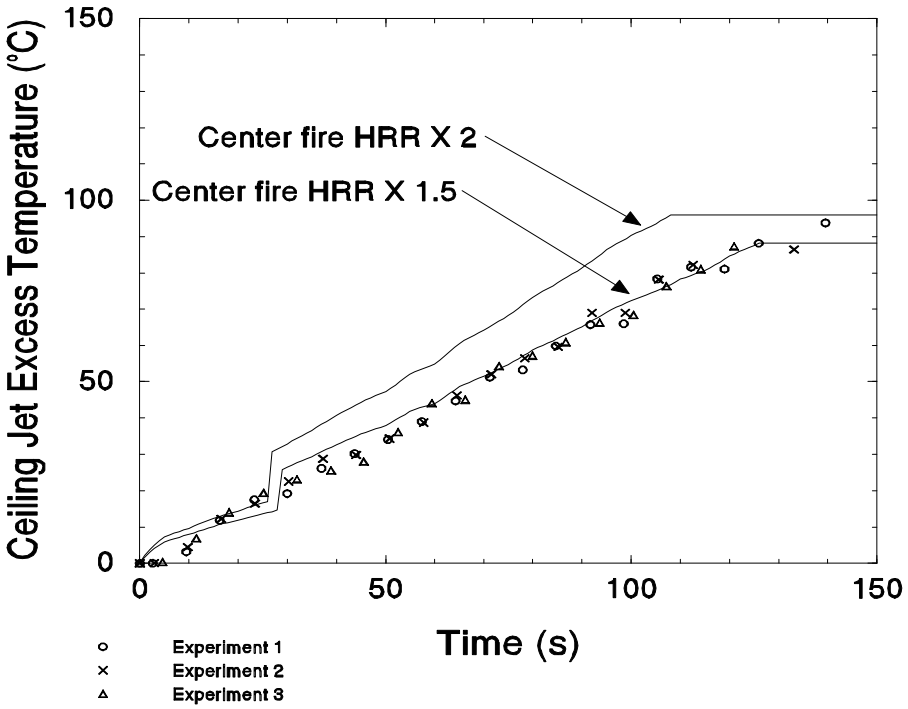

Figure 57 - Ceiling jet temperature increase - slow fire - burner against wall - vent open

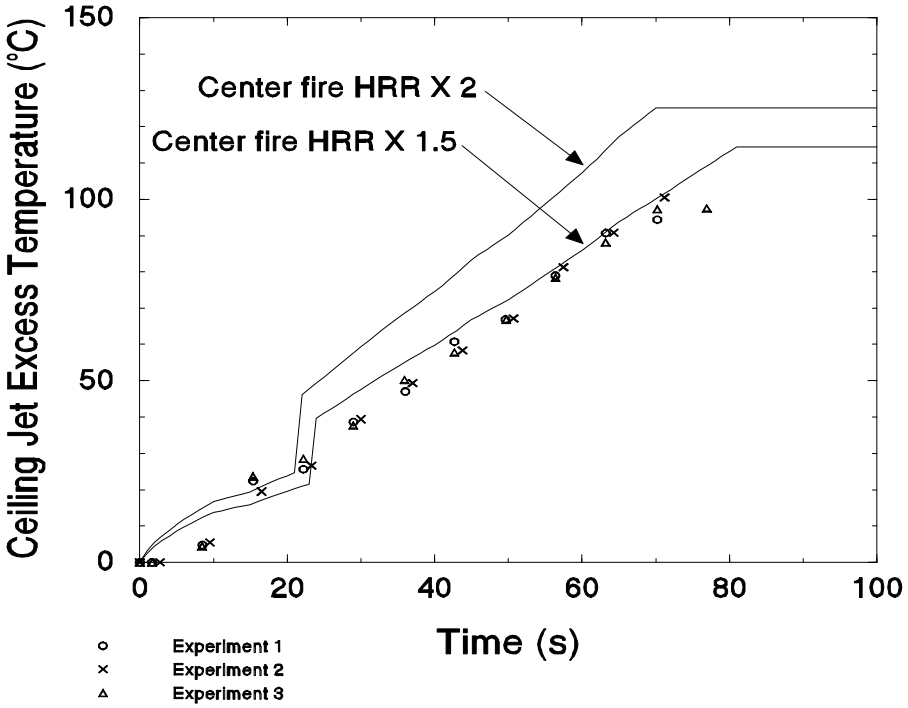

Figure 58 - Ceiling jet temperature increase - medium fire - burner against wall - vent open

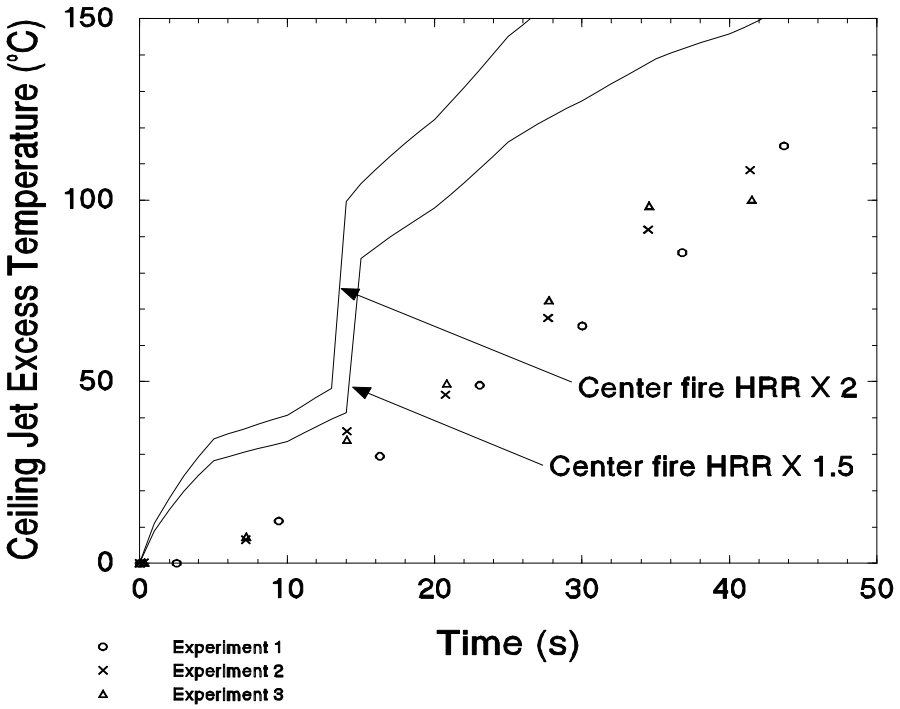

Figure 59 - Ceiling jet temperature increase - fast fire - burner against wall - vent open

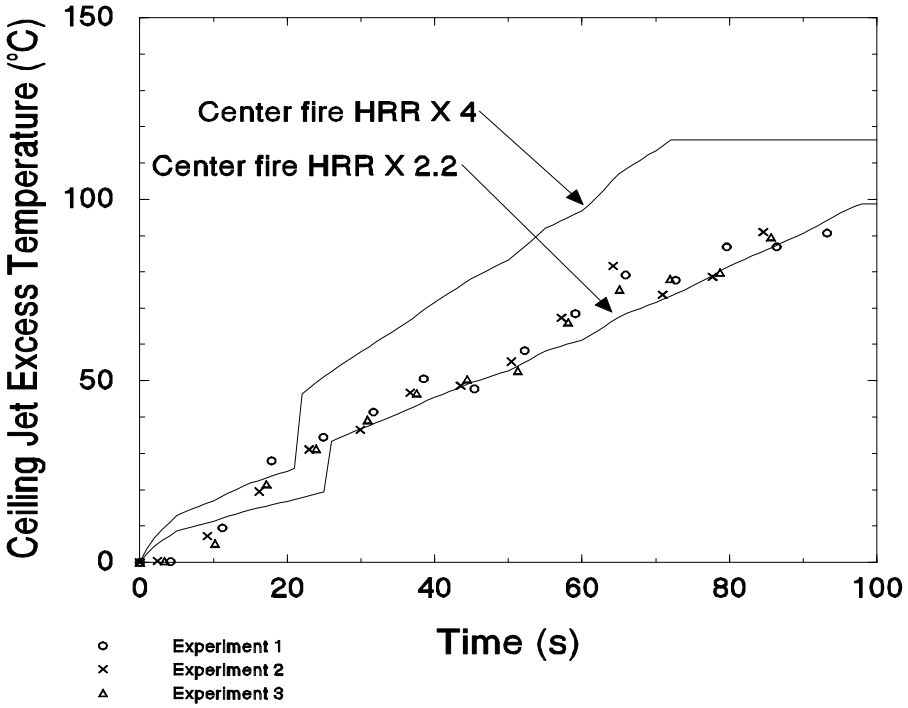

Figure 60 - Ceiling jet temperature increase - slow fire - burner in corner - vent open

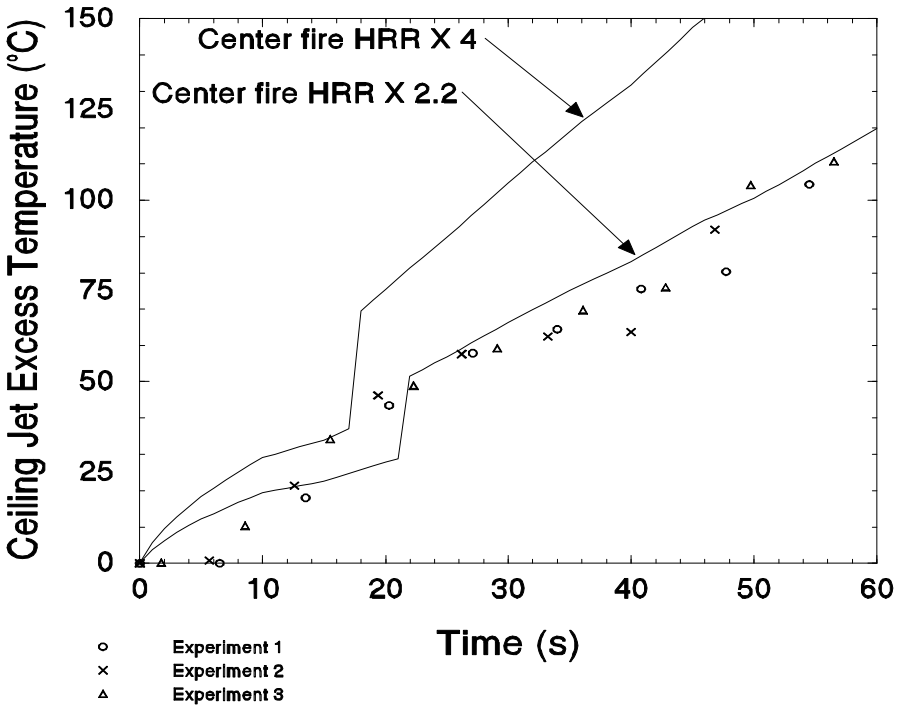

Figure 61 - Ceiling jet temperature increase - medium fire - burner in corner - vent open

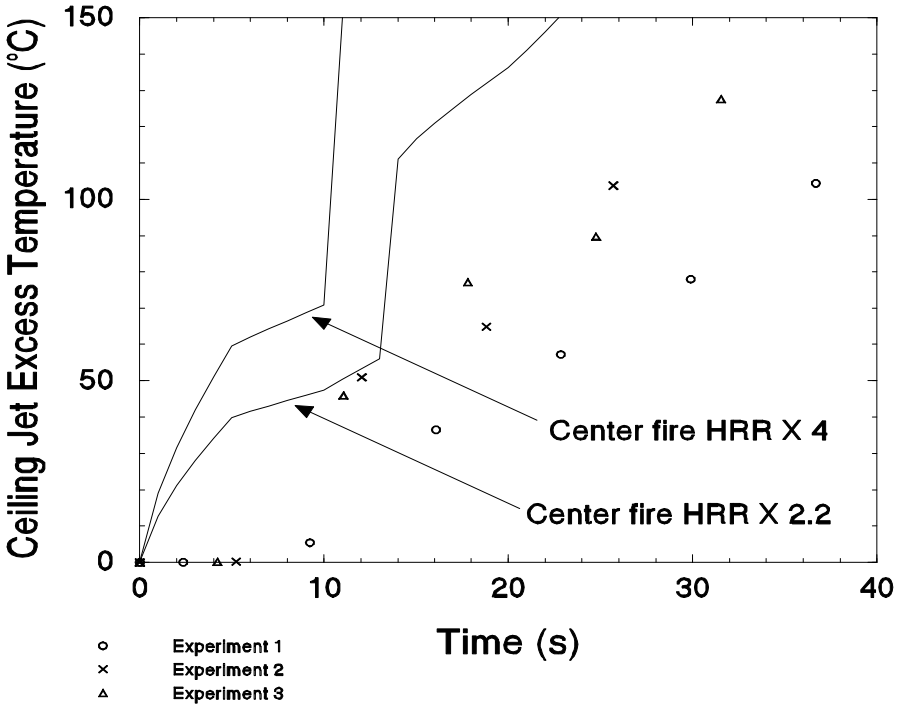

Figure 62 - Ceiling jet temperature increase - fast fire - burner in corner - vent open